International Scientific-Technical and Production Journal

The Paton WELDING JOURNAL

February 2004 # 2

English translation of the monthly «Avtomaticheskaya Svarka» (Automatic Welding) journal published in Russian since 1948

Founders: *E.O. Paton Electric Welding Institute of the NAS of Ukraine*
International Association «Welding»

Publisher: *International Association «Welding»*

Address:
E.O. Paton Electric Welding Institute,
International Association «Welding»,
11, Bozhenko str., 03680, Kyiv, Ukraine
Tel.: (38044) 227 67 57
Fax: (38044) 268 04 86
E-mail: journal@paton.kiev.ua
http://www.nas.gov.ua/pwj

State Registration Certificate
KV 4790 of 09.01.2001

Subscriptions:
$460, 12 issues per year,
postage and packaging included.
Back issues available.

CONTENTS

MATHEMATICAL MODELLING OF THE PROCESS OF MANUFACTURE OF SPHERICAL FUSED TUNGSTEN CARBIDE GRANULES

V.I. MAKHNENKO, A.P. ZHUDRA, E.A. VELIKOIVANENKO, V.I. DZYKOVICH and A.I. BELY
E.O. Paton Electric Welding Institute, NASU, Kiev, Ukraine

Possibility of developing mathematical dependencies relating basic parameters of the process of manufacture of spherical tungsten carbide granules by melting of the tip of a tungsten carbide rod rotating at a high speed is considered.

Keywords: *tungsten carbide, plasma heating model, conditions of initiation, evolution and detachment of droplets, droplet size, size distribution density, process productivity*

Introduction. Fused tungsten carbides are an efficient component of hard-facing consumables for the cases where the challenge is to produce a highly resistant surface for special conditions under which rock crushing tools and, primarily, cone drill bits operate.

Tungsten carbide is an eutectic tungsten-carbon alloy consisting of about 20 % of tungsten carbides of the type of WC and 80 % of the type of W_2C [1–5]. The total content of carbon in it is 3.9 wt.%, and its melting temperature is 2780 °C.

The E.O. Paton Electric Welding Institute developed a unique technology for manufacture of spherical tungsten carbide granules by melting a tungsten carbide rod of a required composition: the rod is heated from the tip, rotated at an angular speed of v_{rot} = = 2000–4000 rpm, and, as the tip is melted, the axial feeding of this material is provided at speed v_{feed} (Figure 1). The rod is heated by a plasma heat source with a power of W = 24 kW. At this thermal power and at v_{rot} = 3900 rpm, for the rod with a diameter of 28 mm and length of L_r = 200 mm the formation of droplets begins approximately 1 s after the beginning of heating. Then, at v_{feed} = 0.5 m/h = = 0.139 mm/s, the process reaches the quasi-stationary state.

The experimental results (Figure 2) can give an idea of sizes of the spherical particles ejected from the molten tip of the rotating rod. Figure 3 shows the data on density of distribution, Q, of particles with size d_d at a rotation speed of v_{rot} = 2200 and 3900 rpm. In this case helium and argon were used as the plasma gas. It can be seen from the Figure that the mathematical expectation of size of a droplet, $\overline{d}_d$, grows with decrease in the rotation speed and just slightly depends upon the type of the plasma gas.

The task of mathematical modelling is to derive mathematical dependencies to relate basic parameters (geometric sizes and speed of rotation of the rod, thermal characteristics of heat source) to productivity of the process (v_{feed}) and size of the formed tungsten carbide granules, $\overline{d}_d$.

Physical phenomena determining the process under consideration can be conditionally subdivided into two groups: phenomena of group I are associated with heating of the rotating tungsten carbide rod by a fixed plasma heat source (see Figure 1), and phenomena of group II cause formation, evolution and detachment of molten metal droplets from the tip surface of the rotating rod.

Heating model. Mathematical description of the process of heating of the rapidly rotating spindle with tungsten carbide rod *1*, graphite sleeve *2* and pusher *3* (see Figure 1) in the system of co-ordinates r, z, assuming that contact between the sleeve (pusher) and rod is ideal, can be made in a traditional way using the theory of unsteady thermal conductivity, i.e. temperature $T(r, z, t)$ is determined by solving the following differential equation:

$$\frac{\partial}{\partial r}\left(r\lambda\frac{\partial T}{\partial r}\right)+r\frac{\partial}{\partial z}\left(\lambda\frac{\partial T}{\partial z}\right)=rc\gamma\frac{\partial T}{\partial t} \quad (1)$$

under the corresponding initial conditions

$$T(r, z, 0) = T_0 \approx 20\ ^\circ\text{C} \quad (2)$$

and boundary conditions:

$$z = z_{tip} = L_p + L_r$$

$$\lambda(z)\frac{\partial T}{\partial z} = q_f(r, t) - B\varepsilon^{(1)}[(T + 273)^4 - (T_m + 273)^4]; \quad (3)$$

$$z = 0 \quad -\lambda(z)\frac{\partial T}{\partial z} = \alpha^{(1)}_{h.e}(T - T_m);$$

$$r = R \quad 0 < z < L_r + L_p - L_s$$

$$-\lambda(z)\frac{\partial T}{\partial z} = \alpha^{(2)}_{h.e}(T - T_m); \quad (4)$$

$$r = R_s \quad L_r + L_p - L_s < z < L_r + L_p$$

$$-\lambda(r)\frac{\partial T}{\partial r} = B\varepsilon^{(2)}[(T_s + 273)^4 - (T_m + 273)^4]; \quad (5)$$

$$L_r = L_r^0 \text{ at } 0 < t < t_h,$$
$$L_r = L_r^0 - v^{(t)}_{feed}(t - t_h) \text{ at } t > t_h, \quad (6)$$

where $\lambda(t)$ is the coefficient of thermal conductivity of the rod or graphite sleeve and pusher; $c\gamma = c\gamma(T)$

is the heat capacity of the same parts per unit volume; $z = z_{tip}$ is the heated surface of the tip of the rod and sleeve with an assigned heat flow $q_f(r, t)$ from the plasma heat source and heat transfer to the surrounding medium with temperature T_m, following the Stefan–Boltzmann law; B is the corresponding constant, $B = 5.67 \cdot 10^8$ W/(m^2·K^4); $\varepsilon^{(1)}$ and $\varepsilon^{(2)}$ are the emissivity factors of the emitting surface and outside surface of the sleeve, respectively; $\alpha^{(1)}_{h.e}$ is the coefficient of heat exchange, following the Newton's law, between the graphite pusher tip and surrounding medium; $\alpha^{(2)}_{h.e}$ is the same between the surface of the rod (pusher), $r = R$, and water cooling the spindle; r_0 is the displacement of axis of the plasma torch relative to axis of rotation of the rod melted; and t_h is the time of heating.

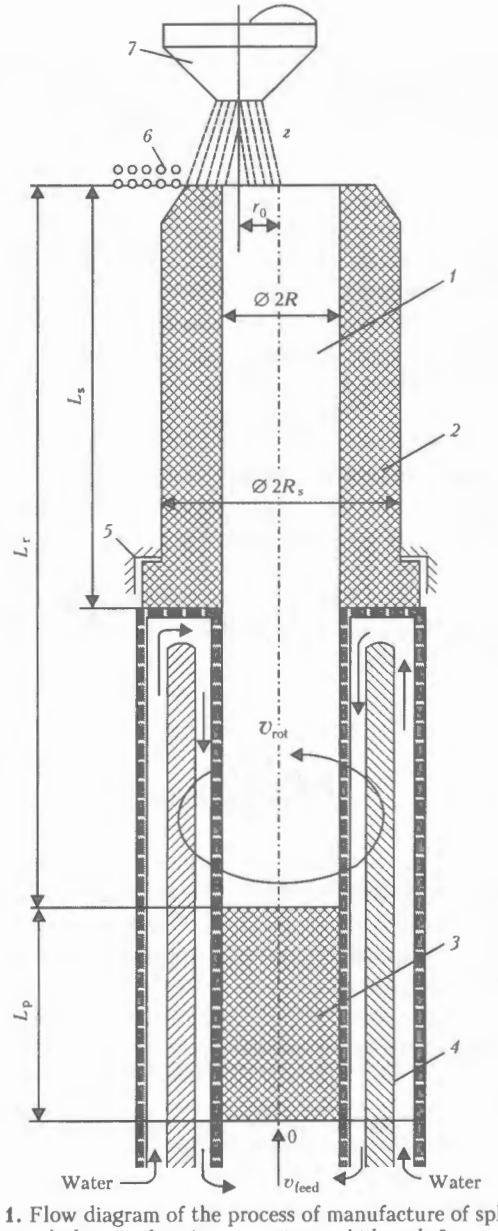

Figure 1. Flow diagram of the process of manufacture of spherical tungsten carbide granules: *1* — tungsten carbide rod; *2* — graphite sleeve; *3* — graphite pusher; *4* — water-cooled spindle shaft; *5* — spindle support; *6* — tungsten carbide droplets; *7* — plasma torch; L_r — length of the rod; L_s — length of the sleeve; L_p — length of the pusher; $2R$ — diameter of the rod; $2R_s$ — diameter of the sleeve

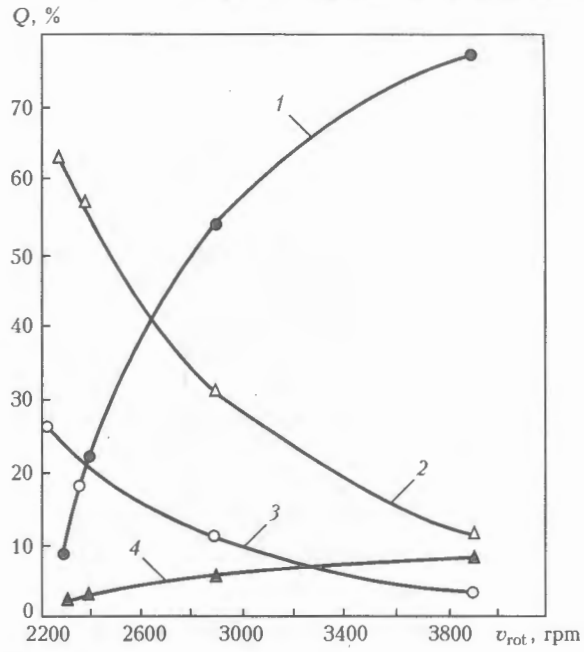

Figure 2. Dependence of granulometric composition of spherical particles with size d_d upon the spindle rotation speed v_{rot}: *1* — d_d = 0.28–0.45; *2* — 0.45–0.63; *3* — 0.63–0.80; *4* — less than 0.28 mm

Value $q_f = q_f(r, t)$ is related to power input W at its Gaussian distribution [6–8] through the following relationship:

$$q_f(r, t) = \frac{W\eta_w(t)}{K} \pi \exp(-Kr^2) \ldots , \qquad (7)$$

where K is the coefficient of concentration of the heat flow from the plasma torch.

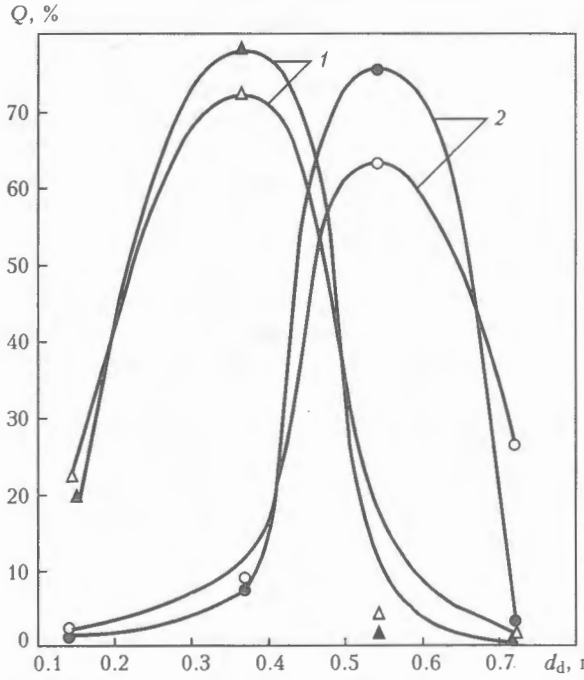

Figure 3. Effect of the plasma gas kind and rod rotation speed v_{rot} on granulometric composition of spherical particles: *1* — v_{rot} = 3900; *2* — 2200 rpm; ●, ▲ — helium; ○, Δ — argon

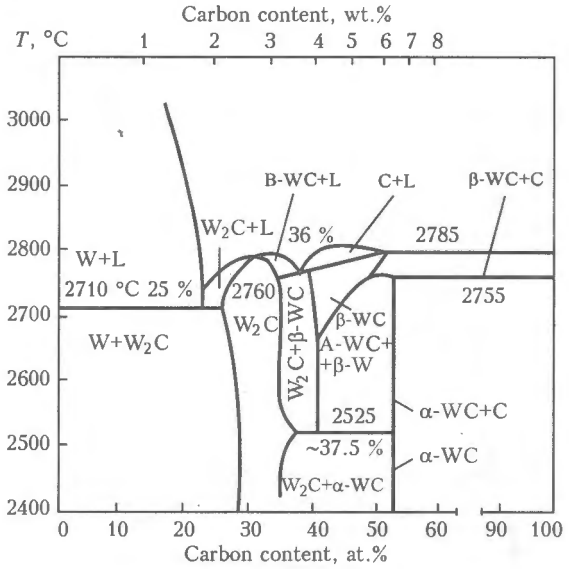

Figure 4. W–C constitutional diagram

According to the data of [6–8], K = 1.5–4.0 1/cm^2. For the process under consideration, K is determined on the basis of experimental data. The second unknown value in relationship (7) is the coefficient of efficiency of heating of a workpiece, $\eta_w(t)$. According to the data of [6–8], the value of η_w for a direct-action plasmatron depends upon many factors, including temperature of the surface heated. Usually the latter is appreciable only at the initial stage of heating, whereas in the steady-state processes of welding, surfacing and cutting it shows up very insignificantly.

However, for the given technology of melting of the tip, where the time of heating, t_h, to formation of the first droplets of tungsten carbide (melting out of the rod tip) is comparatively short, to make the model adequate, one should allow for the fact that values of $\eta_w(t)$ vary with time from 1 at $t = 0$ to η_w^d, i.e. the steady-state value, at $t > t_h$. The values of η_w^d depend upon a number of parameters of the plasma jet, and at a normal operation of the plasmatron with a power of 24 kW they may vary from 0.55 to 0.70 [6] in a case of welding of steel at a heating temperature of the rod tip surface equal to about 2000 °C. For tungsten carbide at a heating temperature of the rod tip surface equal to about 3000 °C, one might expect these values to be at a level of $\eta_w^d \cong$ $\cong$ 0.4–0.5. In this case the mean value of η_w^{mean} at a heating stage of $0 < t < t_h$ is about 0.8–0.9.

Unfortunately, difficulties arising during experiments did not allow the authors to obtain the actual values of parameters of the heat source, i.e. mean efficiency of heating of a workpiece, η_w^{mean}, and coefficient of concentration of the heat flow, K, as well as such surface temperature T_d at which the droplet formation process begins. The authors had the data on values of power input W, time of heating to the beginning of droplet formation, t_h, and thermal-physical properties of tungsten carbides as given in Table 1 [1–5].

The value of latent melting heat q_l for tungsten was assumed to be equal to 183 J/g. Specific weight of the tungsten carbide components was: γ_{WC} = = 15.6 g/cm^3 and γ_{W_2C} = 17.2 g/cm^3. Accordingly, for tungsten carbide $\gamma_{t.c}$ = 0.8·17.2 + 0.2·15.6 = = 16.88 g/cm^3. The latent melting heat per unit volume of tungsten carbide is $q_l\gamma_{t.c}$ = 3089 J/cm^3.

Allowing for the latent melting heat, the value of $c\gamma(T)$ was adjusted within a temperature range of $T_S \le T \le T_L$, where T_L, i.e. the liquidus temperature, was about 2735 °C, and T_S, i.e. the solidus temperature, was about 2525 °C (see Figure 4 for alloy with a carbon content of 3.9 wt.%).

Considering the above-said, numerical calculations of the stage of heating were made at different values of parameters η_w^{mean}, K and T_d.

Figures 5–7 show some results of these calculations. It follows from them that the most satisfactory conditions are $t_h \approx 1$ s and $T_d \approx T_L + 200$ °C, and at a sufficiently uniform heating of the rod tip surface, $\eta_w^{mean} \approx 0.9$, K = 1.5 1/cm^2 and T_d = 3000 °C.

Droplet formation model. Formation of droplets occurs at $t > t_h$. Having the data on granulometric composition of droplets (see Figure 2), the quantity of the tungsten carbide droplets, N_d, formed per unit time can be determined for the assigned values of v_{feed} and diameter of the rod melted, $2R$, using the following relationship:

$$N_d = \frac{v_{feed}\pi R^2}{\int_{d_d^{min}}^{d_d^{max}} \frac{\pi d_d^3}{6}\frac{Q(d_d)}{100}\,d(d_d)}, \quad \frac{1}{s}.$$

Results of these calculations are given in Table 2. This Table also gives data on the values of $\overline{d}_d$ (according to Figure 2) and d_{eq} obtained from the following condition:

Table 1. Variations in thermal-physical properties of tungsten carbides depending upon the temperature

Thermal-physical properties	*T*, °C												
	20	*100*	*300*	*500*	*700*	*900*	*1100*	*1300*	*1500*	*1700*	*2000*	*2400*	*2600*
$c\gamma_{WC}$, J/cm^3	2.86	2.93	3.07	3.22	3.33	3.51	3.65	3.80	3.94	4.09	–	–	–
$c\gamma_{W_2C}$, J/cm^3	3.15	3.08	3.38	3.54	3.67	3.86	4.02	4.17	4.33	4.50	–	–	–
$\frac{\lambda(T)}{\lambda(20\ °C)}$	1.00	0.90	0.80	0.70	0.66	0.64	0.62	0.60	0,58	0.56	0.55	0.53	0.52

Note. Thermal conductivity coefficient λ_{WC} (20 °C) = 1.79 W/(cm·°C); λ_{W_2C}(20 °C) = 0.29 W/(cm·°C).

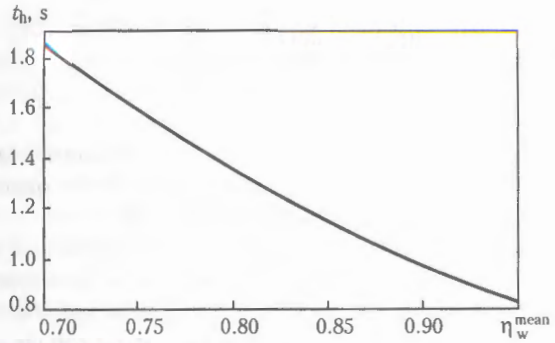

Figure 5. Dependence of the time of heating, t_h, of the rod tip surface to the temperature of formation of droplets, T_d = 3000 °C, upon η_w^{mean}

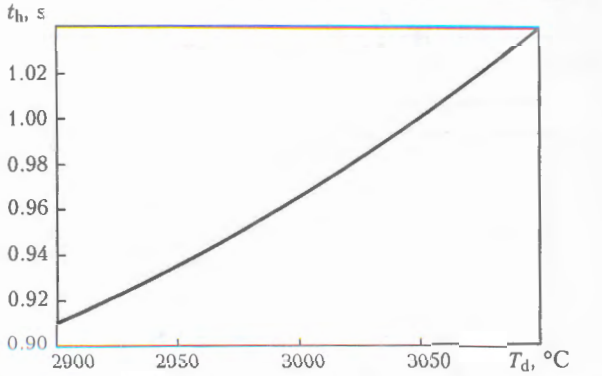

Figure 6. Dependence of the time of heating, t_h, of the rod tip surface upon the assigned temperature of formation of droplets, T_d, at η_w^{mean} = 0.9

$$N_d \frac{\pi d_{eq}^2}{6} = v_{feed} \pi R^2.$$

It can be seen from Table 2 that the quantity of the droplets dramatically grows and they decrease in size with increase in v_{rot}. The values of d_{eq} are very close to the mathematical expectation of $\overline{d}_d$ (see Figure 2).

Three stages can be distinguished in evolution of each droplet: initiation, growth and detachment. The process of initiation of a droplet (Figure 8) is caused by excessive pressure P that develops under the effect of centrifugal forces in the molten layer at the rod tip.

At the moment of the beginning of melting, when the speed of movement in the surface layer is low, the following Navier–Stokes dependence of movement can be derived for excessive pressure P:

$$\frac{\partial P}{\partial r} = -\rho\omega^2 r, \qquad (8)$$

where ρ is the material density, $\rho = \gamma_{t.c}/g = 16.9 \cdot 10^{-5}$ N·s^2/cm^4 (g is the acceleration of the gravity force); and ω is the angular speed of rotation of the rod, $\omega = v_{rot} 2\pi/60$.

(8) yields:

$$P(r) - P_0 = \rho\omega^2 \frac{r^2}{2}. \qquad (9)$$

Accordingly, the maximum excessive pressure is $P_{max} - P_0 = 0.27$ MPa at v_{rot} = 3900 rpm and 0.07 MPa at v_{rot} = 2000 rpm.

As the surface layer is overheated, increase in the speed of rotation results in certain redistribution of pressure along r. However, its values remain approximately at the same level. This is quite enough for the flat shape of the surface to become less rational at a certain temperature proceeding from the energy conditions. These conditions have the following form:

$$P > \sigma(T) \frac{F_d}{V_d}, \qquad (10)$$

where $\sigma(T)$ is the surface tension of a material at temperature T; F_d is the surface area of the forming droplet; and V_d is the volume of the droplet.

In the case of a spherical shape of a droplet at a wetting angle of $\theta = 0$ (Figure 8), it follows from (10) that $P > \sigma(T) 6/d_d$, i.e. the higher the pressure, the smaller the size of the formed droplets. If a droplet with size d_d detaches not completely from the molten layer, i.e. there exists a wetting surface of $F_{wet} = (\pi d_d^2/4) \sin^2 \theta$ (see Figure 8), then

$$V_d = \frac{\pi d_d^3}{6} \xi_V; \quad F_d = \pi d_d^2 \xi_F,$$

where $\xi_V = \frac{1 + \cos\theta}{2} + \frac{1}{4} \sin^2\theta \cos\theta$ and $\xi_F = \frac{1 + \cos\theta}{2}$.

Then, instead of (10), the following can be written down:

Table 2. Results of calculation of N_d, d_{eq} and v_{feed}

Plasma gas	v_{rot}, *rpm*	$\overline{d}_d$, *mm*	N_d, *1/s*	d_{eq}	v_{feed}, *mm/s*
Argon	3900	0.37	2001	0.43	0.14
	2200	0.55	813	0.56	0.12
Helium	3900	0.37	2143	0.42	0.14
	2200	0.55	700	0.57	0.12

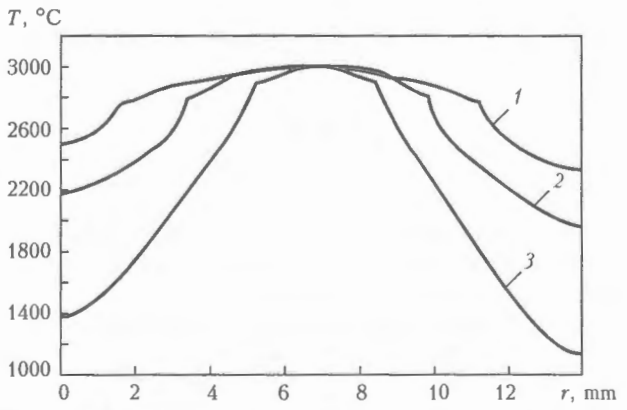

Figure 7. Distribution of temperature over the rod tip surface at the moment of formation of the first droplets, $t = t_h$: 1 — K = 1.0, t_h = 1.52 s; 2 — K = 1.5, t_h = 0.97 s; 3 — K = 3.0, t_h = 0.45 s

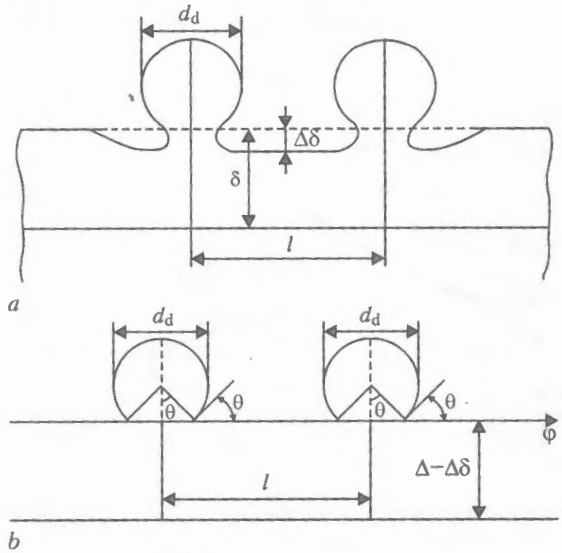

Figure 8. Schematic of formation of droplets in circumferential section r = cost (a) and corresponding calculation idealisation in the system of co-ordinates r, φ, z (b); δ – liquid layer thickness

$$P > \sigma(T)\frac{6\xi}{d_d},$$

where $\xi = \dfrac{\xi_F}{\xi_V} = \dfrac{1}{1 + \dfrac{1-\cos\theta}{2}\cos\theta}$ is the value close to 1 at $0 < \theta < \pi/2$, i.e. the imperfection of shape of a droplet at its initiation does not have a significant effect on pressure P.

The energy condition of evolution of the droplet can be written down as follows:

$$dE > 0, \qquad (11)$$

where $E = PV_d - \sigma(T)F_d = P\dfrac{\pi d_d^3}{6}\xi_V - \sigma(T)\pi d_d^2\xi_F$,

i.e. $dE = \dfrac{\partial E}{\partial d_d}d(d_d) + \dfrac{\partial E}{\partial P}dP + \dfrac{\partial E}{\partial T}dT + \dfrac{\partial E}{\partial\theta}d\theta$.

At $d\theta = dP = dT = 0$ and a free access of liquid to the droplet

$$dE = \left(P\frac{\pi d_d^2}{2}\xi_V - 2\sigma(T)\pi d_d\xi_F\right)d(d_d)$$

condition (11), accordingly, is kept to under isothermal conditions at

$$P > \frac{4\sigma(T)}{d_d}\xi, \qquad (12)$$

which corresponds at $\xi = 1$ to the known Laplace equation of existence and evolution of the droplet under the isothermal conditions.

With a change in the droplet temperature

$$dE = \left(P\frac{\pi d_d^2}{2}\xi_V - 2\sigma(T)\pi d_d\xi_F\right)d(d_d) - \frac{\partial\sigma(T)}{\partial T}dT\pi d_d^2\xi_F > 0.$$

Accordingly, if $dE > 0$, then

$$\frac{d(d_d)}{dT} \geq -\frac{\partial\sigma(T)}{\partial T}\frac{2\xi}{P - \dfrac{4\sigma(T)}{d_d}\xi}.$$

Therefore, in the case of increase in temperature ($dT > 0$) and keeping to condition (12) the growth of a droplet is guaranteed at $\partial\sigma(T)/\partial T < 0$.

These estimates show that initiation and evolution of each particular droplet is the process developing with time, which is caused by a temperature state of the molten layer at the tip of the rotating rod. It can be shown that the condition of detachment of the formed droplets is also determined by temperature of the molten layer.

The droplet formed is affected by centrifugal force Q_c generated by rotation of the rod

$$Q_c = \rho\omega^2 r\frac{\pi d_d^3}{6}\xi_V.$$

The wetting force that keeps the droplet is

$$Q_{wet} = \tau_{wet}S_{wet} = \tau_{wet}\frac{\pi d_d^2}{4}\sin^2\theta,$$

where $\tau_{wet}(T)$ is the ability of a molten material to resist detachment at temperature T, and S_{wet} is the wetting area.

Condition of detachment of the droplet is

$$d_d r > \tau_{wet}(T)\frac{3}{2}\frac{\sin^2\theta}{\rho\omega^2\xi_V} = \tau_{wet}(T)\frac{3\xi(1-\cos\theta)}{\rho\omega^2}. \qquad (13)$$

If the left and right parts of equation (13) are multiplied by v_{feed}, the flow of mass of metal, $v_{feed}d_d r$ in zone r will be determined approximately by the same value of $3\tau_{wet}(T)v_{feed}\dfrac{1-\cos\theta}{\rho\omega^2}$ over the entire surface of the molten layer, and will depend mostly upon the temperature at assigned $v_{feed}/\rho\omega^2$. Note that at $\xi_V < 1$ the true diameter of the detached droplet is smaller than d_d and equal to $d_d\sqrt[3]{\xi_V}$, which in general is close to the d_d value.

Therefore, for the entire molten surface layer, heating of a corresponding zone of this layer to temperature $T_d > T_L$ can be assumed to be a condition of removal of metal in the form of droplets.

Also, it is apparent that the process of droplet formation at a particular point of the layer occurs with a certain periodicity, rather than continuously.

Designate the time of the droplet formation period as Δt_p. Divide conditionally this value into two summands

$$\Delta t_p = \Delta t_d + \Delta t_i,$$

where Δt_d is the time of initiation, evolution and detachment of the droplet, and Δt_i is the incubation period during which restoration at a corresponding point of the molten layer and its preparation for the droplet formation occur.

During the Δt_d period the heat flow from an external heat source in a given place and to a given degree is screened by the formed droplet (see Figure 8), i.e. according to (7), the intensity of the heat flow, $q_f(r, t)$, in a given place during the Δt_d period should be decreased, assuming that difference of the heat flow goes to overheating of the droplet.

It follows from Table 2 that as v_{rot} increases, increase in the quantity of the droplets at a relatively small change in v_{feed} should be accompanied by decrease in the droplet formation time Δt_p caused by decrease both in Δt_d and Δt_i.

In this connection, it is convenient to operate with the $\eta_{sc}(\Delta t_d/\Delta t_i)$ relationship (here η_{sc} is the relative time of screening of a given point of the rod tip surface during the droplet formation time), assuming that this value changes but slightly during the process studied.

Accordingly, upon estimating the time of the incubation period of heating, Δt_i, at a given point by solving the above temperature problem (from the moment of detachment of the droplet and reaching temperature T_d on the newly formed volume surface), we have that $\Delta t_p = \Delta t_i/(1 - \eta_{sc})$ and $\Delta t_d = \Delta t_i[\eta_{sc}/(1 - \eta_{sc})]$.

Therefore, it was necessary to determine η_w^d and η_{sc} by considering the process of formation of a droplet according to (1)–(7) on the basis of numerical experiments. For this, first a series of numerical experiments was conducted at $\eta_{sc} = 0$ and different values of η_w^d within $0.50 > \eta_w^d > 0.25$.

The results of numerical modelling of the process of heating and ejection of the material volumes from the surface, when their temperature reaches T_d = = 3000 °C at η_w^d = 0.4–0.5 show that this process occurs without substantial interruptions. However, in this case the process productivity exceeds several times the one which is experimentally observed, i.e. v_{feed} = 0.14 mm/s at v_{rot} = 3900 rpm.

Sizes of finite elements that approximate the rod heated are assumed to be such that the volume of one cell, h^3, corresponds to the mathematical expectation of the volume of one droplet, $\pi\overline{d}_d^3/6 = 0.0265$ mm^3, i.e. h = 0.3 mm. In this case approximately $2\pi r/h$ droplets ($h \le r \le R$) are simultaneously formed in the surface layer with co-ordinate r.

Figure 9 shows some results of calculations of the process productivity at $\eta_{sc} = 0$ and different η_w^d values ranging from 0.45 to 0.35. Characteristically, in this case the productivity decreases with decrease in η_w^d. However, it remains at a much higher level than that experimentally observed, while at $\eta_w^d < 0.35$ the heat equilibrium without droplet formation begins, i.e. temperature of the surface does not reach T_d = = 3000 °C.

Therefore, the model of η_{sc} = 0, i.e. with no allowance for local screening of the heat flow within the zone of a formed droplet, showed no promise. So, it was necessary to choose the value of η_{sc} from a range of $0 < \eta_{sc} < 1$ at η_w^d = 0.4–0.5 from a condition

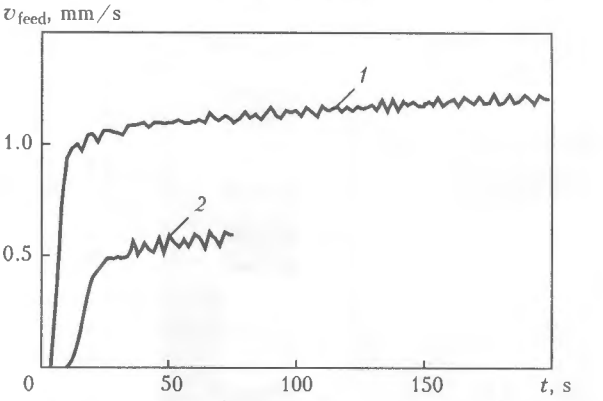

Figure 9. Effect of the η_w^d values on productivity of the droplet formation process v_{feed} at $\eta_{sc} = 0$: *1* — η_w^d = 0.45; *2* — 0.35

of achieving the experimentally observed productivity v_{feed} and sufficiently uniform melting of the rod tip surface.

Good results were achieved after a number of experiments at η_w^d = 0.45 and η_{sc} = 0.31.

The data shown in Figures 10 and 11 prove the above-said. As seen, the process productivity is close to 0.14 mm/s (Figure 10), and non-uniformity of melting of the rod surface is moderate (Figure 11).

Now the question is what the thermal energy screened by a droplet is spent for. At η_w^d = 0.45 and η_{sc} = 0.31 the thermal power screened by all the droplets is $Q_{sc} = W \cdot 0.45 \cdot 0.31 = 3348$ W. Accordingly, the power per one droplet is Q_{sc}/N_d on the average. This heat is consumed during time Δt_d for increase in temperature of a droplet and emission into the surrounding medium. The calculation results shown in Figure 12 for $\overline{d}_d$ = 0.37 mm (at v_{rot} = 3900 rpm) and corresponding mean values of Δt_d = 0.66 s (Δt_i = 2.0 s, Δt_p = 2.66 s) indicate that the heat of screening leads to overheating of a droplet not in excess of 40–50 °C, which fits the existing concepts.

Variants of v_{rot} = 2200 rpm at $\overline{d}_d$ = 0.55 mm were considered allowing for the obtained values of the η_w^d and η_{sc} parameters. The results of modelling of this process at finite elements h = 0.45 mm in size are indicative of the fact that the period of formation of a droplet increases in such a way that Δt_d = 1.0 s, Δt_i = 3.2 s and Δt_p = 4.2 s. The process productivity in this case is v_{feed} = 0.14 mm/s, which is sufficiently close to the experimental data (0.12 mm/s). Never-

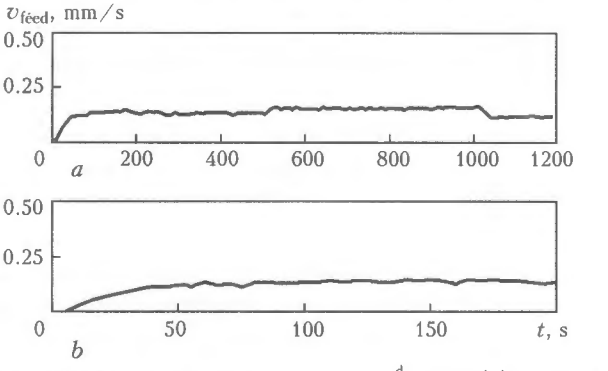

Figure 10. Kinetics of variations in v_{feed} at η_w^d = 0.45 (*a*) and η_{sc} = = 0.31 (*b*) (*a* and *b* differ in scale along *t*)

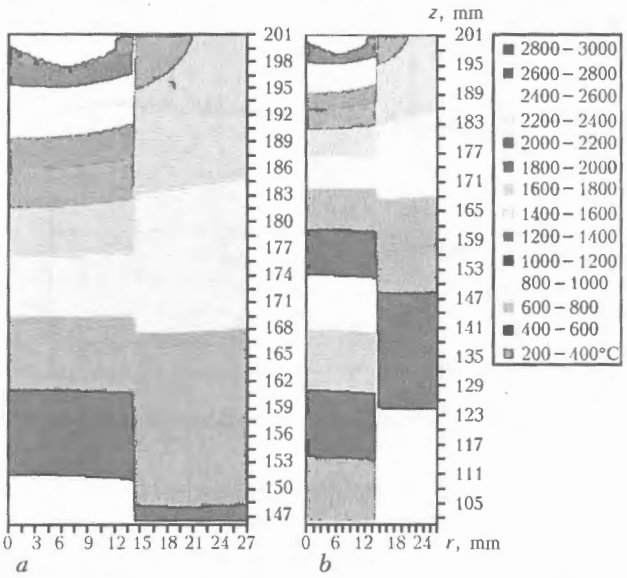

Figure 11. Results of calculation of temperature fields and profile of the tip surface of the rod (*a*) and sleeve (*b*) for the steady state at $\eta_w^d = 0.45$ and $\eta_{sc} = 0.31$

theless, this shows that increase in $\overline{d}_d$ with this variant requires increase in η_{sc}. However, the $\Delta\eta_{sc}$ value can be considered constant at approximate estimations.

Based on this assumption, consider the possibility of prediction of conditions for formation of smaller droplets with $\overline{d}_d = 0.25$ mm for the given set-up (see Figure 1) at $W = 24$ kW.

Modelling of this process at finite elements of $h = 0.2$ mm shows that the productivity of the process of rod melting is $v_{feed} \approx 0.14$ mm/s at $\eta_{sc} = 0.31$, $\Delta t_d = 0.22$ s, $\Delta t_i = 0.7$ s and $\Delta t_p = 0.92$ s.

The required quantity of revolutions to produce such droplets can be estimated only very approximately by extrapolating the available experimental results (see Table 2).

Equations (9) and (12) can be used as a basis to derive the extrapolation dependence, i.e.

$$\overline{d}_d \approx \frac{\sigma(T)4}{P_0 + \rho\omega^2 r^2/2} = \frac{C}{\omega^2 + A^2},$$

where C and A are certain constants for the given process.

Accordingly,

$$\frac{d_d^{(1)}}{d_d^{(2)}} = \frac{\omega_2^2 + A^2}{\omega_1^2 + A^2}. \qquad (14)$$

Using the data of Table 2, we have that $A = \sqrt{1590 \cdot 10^2}$ (rpm).

For $d_d^{(2)} = 0.25$ mm from (14) at $d_d^{(1)} = 0.55$ mm and $\omega_1 = 2200$ rpm, it yields that $\omega_2 = 5350$ rpm.

CONCLUSIONS

1. The efficiency of utilisation of power of plasma heating in melting of the tip of a tungsten carbide rod in a quasi-stationary steady state is $\eta_w^d(1 - \eta_{sc}) \approx 0.3$.

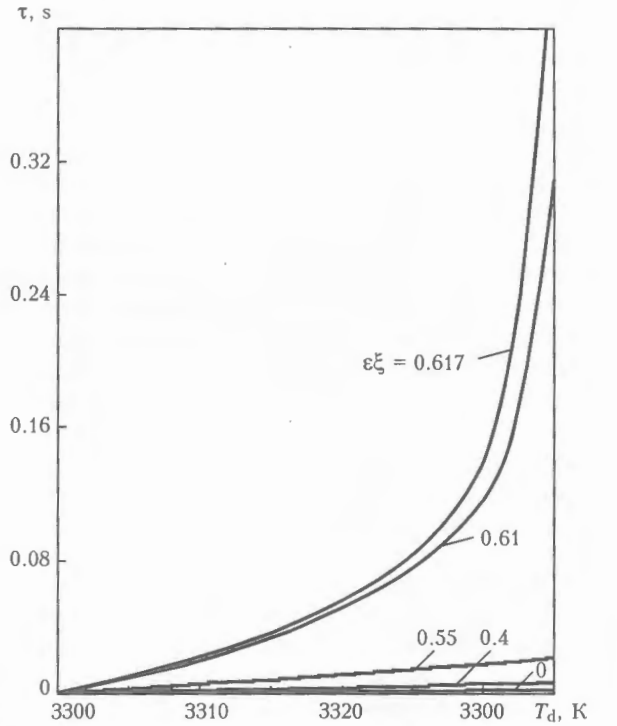

Figure 12. Relationship between droplet temperature T_d and overheating time τ at $\overline{d}_d = 0.37$ mm, $\Delta t_d = 0.66$ s and different values of $\varepsilon\xi$

2. Two stages can be distinguished in the droplet formation process. The first stage is initiation, evolution and detachment of a droplet with time, Δd_d. The second stage is the incubation period, Δd_i, which includes restoration of a molten layer in a corresponding place and its preparation for droplet formation.

3. The larger the diameter of a formed droplet, the higher the values of Δd_d and Δd_i.

4. Size d_d of the formed droplets at a given speed of rotation of the rod melted may vary within wide ranges. However, the mathematical expectation of $\overline{d}_d$ and the distribution density are determined mostly by the rotation speed v_{rot}.

5. Productivity of the process of melting of the rod, v_{feed}, depends primarily upon the electric power input W. However, increase in v_{rot} and decrease in $\overline{d}_d$ lead to a partial decrease in $\eta_{sc} = \Delta d_d / \Delta d_i$, which provides some increase in the value of v_{feed}.

1. Samsonov, G.V., Umansky, Ya.S. (1957) *Hard joints in refractory metals*. Moscow: Metallurgizdat.
2. Samsonov, G.V. (1963) *Refractory joints*. Moscow: Metallurgizdat.
3. (1967) *Refractory materials in mechanical engineering*. Refer. Book. Ed. by A.T. Tumanov, K.I. Portnoj. Moscow: Metallurgizdat.
4. Chirkin, V.S. (1959) T*hermal-physical properties of materials*. Moscow: Fizmatgiz.
5. Krzhizhanovsky, R.E., Shtern, Z.Yu. (1977) *Thermal-physical properties of nonmetallic materials (carbides)*. Refer. Book. Leningrad: Energiya.
6. Rykalin, N.N., Kulagin, I.D., Nikolaev, A.V. (1963) Thermal characteristics of interaction of plasma jet with heated body. *Avtomatich. Svarka*, **6**, 3–13.
7. Gladky, P.V. (1999) Thermal characteristics of surfacing plasmatron arcs. *Ibid.*, **6**, 13–17.
8. Demin, E.A., Klopov, A.I., Khramushin, V.A. (1974) Influence of process parameters and shielding atmosphere composition on thermal efficiency of plasma-arc welding of steel. *Svarochn. Proizvodstvo*, **4**, 15–17.

INCREASE IN STABILITY OF ARC, BURNING UNDER WATER, IN FLUX-CORED WIRE WELDING

Yu.Ya. GRETSKY and **S.Yu. MAKSIMOV**
E.O. Paton Electric Welding Institute, NASU, Kiev, Ukraine

The results of studies conducted in a special chamber to simulate deep-water flux-cored wire welding conditions are given. The efficiency of introducing activating additions to the wire composition to stabilize the arc operating at high depths is shown.

Keywords: *underwater welding, flux-cored wire, arc burning, hydrostatic pressure, stability of process, activating additions*

The problem of increasing the arc stability in wet welding is associated with unfavourable conditions of existence of arc discharge in a water medium, whose effect is greatly manifested with increase in a hydrostatic pressure (operating depth). The causes of this phenomenon were studied in work [1]. In the same work the initial statements were also formulated for conductance of investigations on increasing the stability of unprotected arc as regards to the research problem of widening the technological capabilities of the mechanized flux-cored wire welding using a wet method. Authors came to the conclusion that among two possible ways of solution, i.e. energy and metallurgical, the second way, based on control of the electrode wire composition, is seemed to be more rational. It is advantageously differed from an alternative variant by eliminating the need in creation of conditions of existence of a high-current arc, that could require the development of specialized powerful supply sources with a high value of open-circuit voltage (up to 250 V). In addition, the safety of a diver-welder working is decreased under these technological conditions due to violation of safety rules established for underwater jobs.

The aim of the present work was to obtain results of evaluation of effectiveness of effect of easily-ionising and gas-forming additions into a flux-cored wire charge on stabilization of arc under the conditions of an increased pressure of the surrounding water on the arc. The investigations were carried out using experimental flux-cored wires of two series.

The first series is characterized by a simultaneous adding of two compounds into a wire charge composition, sodium silicate Na_2SiO_3 and marble $CaCO_3$, which should create conditions for ionising the arc gap in atmosphere of vapour-gas bubble consisting mainly of hydrogen and counteraction to hydrostatic pressure, decreasing the volume of this bubble as a space for the arc existence. In this series, the wire charge includes a half of iron powder and a half of the above-mentioned mixture by mass. Here, the ratio between amounts of silicate and marble was regulated so, that with increase in share of one of them from 0 up to 50 % the share of the another one in each 10 % was reduced from 50 % down to 0 also in each 10 %. Table 1 gives the composition of experimental wires of the first series calculated with allowance for the degree of their filling with the charge.

The second series of wires was manufactured for evaluating the effect of compounds of alkali metals only. It is characterized by that the sodium silicate Na_2SiO_3 or cesium nitrite $CsNO_3$ were added additionally to the charge of the known wire PPS-AN1 [2]. Amount of these compounds was 5, 10 and 20 % of the wire charge mass. Table 2 shows a calculated content of additions of the above-mentioned elements as regards to a total mass of the wire.

Welding with above-said experimental wires, and also with standard wire PPS-AN1 (for comparison) was made by a wet method using automatic machines under the water layer sufficient to avoid the contact of arc with air, and also in a special high-pressure

Table 1. Content of components in experimental wires with charge of Fe–Na_2SiO_3–$CaCO_3$ system, %

No. of wire	*Iron powder*	*Sodium silicate*	*Marble*
1	12	–	12.0
2	12	2.4	9.6
3	12	4.8	7.2
4	12	7.2	4.8
5	12	9.6	2.4
6	12	12.0	–

Table 2. Share of charge components of experimental wires from total its mass, %

No. of wire	*Charge PPS-AN1*	*Sodium silicate*	*Cesium nitrite*
7	29.45	1.55	–
8	26.55	2.95	–
9	22.40	5.60	–
10	29.45	–	1.55
11	26.55	–	2.95
12	22.40	–	5.60

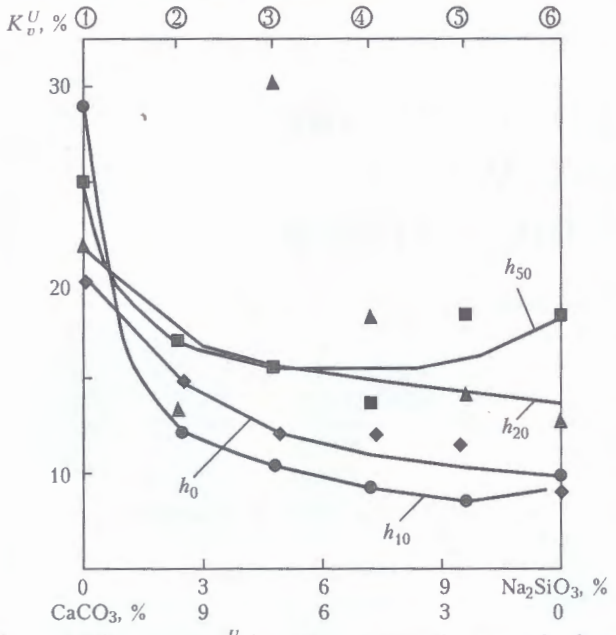

Figure 1. Mean values K_v^U depending on ratio of content of sodium silicate and marble in the composition of experimental wires and test depth (numbers in circles — wire numbers)

chamber filled with water. Immersion for different depths up to 200 m was simulated by changing the pressure in this chamber. In all cases the welding was made with open arc at direct current of reverse polarity. The power source was a special unit ASUM-400 with a flat-rising volt-ampere characteristic. Arc voltage in all experiments was within 28–30 V, welding current was slightly changed (170–190 A).

The study of electrical parameters of the underwater welding was carried out using of information-monitoring system (IMS) on the base of a personal computer having a feedback with an object [3]. Designers of IMS took into account the previous experience of construction and use of specialized IMS with high rates of processing and input of information, including that for the assessment of processes of the underwater welding [4–6]. The IMS, used in the present work, consists of a module of technological interface, a board of analog input-output RSL-718 and a personal computer, into which this board is built-in. Acquisition of experimental data with their subsequent amplitude-time processing is realized in an integrated program medium «Analyzer V4.0». IMS allows recording paramaters of the process with their accumulation and next processing after the completion of the whole cycle of experiments.

To evaluate the specifics of the wet welding process using the experimental wires, the following electric and time parameters were measured: arc voltage and welding current, U_a and I_w; voltage and current of arc burning, $U_{b.a}$ and $I_{b.a}$; voltage and current of short circuit, $U_{sh.c}$ and $I_{sh.c}$; interval between short circuits of electrode gap by a molten metal drop, $T_{sh.c}$. Nature of metal transfer was evaluated by the duration of short circuits $\tau_{sh.c}$ and their frequency $f_{sh.c}$. Analysis of features of arc burning was performed by histograms of arc voltage and welding current using the method of a stage-by-stage processing of multimodal distributions. In this case an amount of events (measurements) n, mean value of parameter $\bar{x}$, dispersion σ and coefficient of variation K_v were determined for each separate area:

$$\bar{x} = \frac{x_1 + x_2 + \ldots + x_n}{n}; \quad \sigma = \sqrt{\frac{\sum_{i=1}^{n} (\bar{x} - x_i)^2}{n}};$$

$$K_v = (\sigma/\bar{x})100\ \%.$$

These data can evaluate completely enough the nature of proceeding of arc process and electrode metal transfer through an arc gap without conductance of a high-speed filming. According to [5] the arc process is recommended to be considered stable enough for welding under the conventional conditions, if the coefficient of voltage variation K_v^U does not exceed 20 %. The reduction in K_v^U value means the increase in stability of arc process voltage and, consequently, the tendency to the constancy in the welding arc length. The same recommendations are accepted for the evaluation of results obtained also under the conditions of wet underwater welding. Below the results of experiments are given and analyzed.

Combined effect of Na_2SiO_3 and $CaCO_3$. The results obtained are generalised in Figure 1. Designation of wires in it corresponds to Table 1; h_0–h_{50} is the simulated depth of welding from near-surface layer h_0 to 50 m (h_{50}). It is possible to see the usefulness of adding the sodium silicate into the wire charge: almost within the entire range of its content (2–12 %) the coefficient of voltage variation does not exceed 20 %. With increase in depth the effectiveness of Na_2SiO_3 effect is reduced, but negligibly. There is no sufficient grounds to state from this series of experiments that the presence of marble influences greatly the process stability: at ratio of $CaCO_3/Na_2SiO_3 > 5$, when the sodium silicate content in wire compositions is less than 2 %, the value K_v^U has a tendency to the intensive increase even at small depths. The ratio of these components, corresponding to the content of silicate in the 6–7 % ranges (Table 1, wire No.4) can be considered promising enough. At such ratio the combination of low values of duration and frequency of short circuits is observed (Figures 2 and 3), that proves the increase in a net time of arc burning.

Composition, giving the best results (wire No.4), was tested additionally at 80–200 m depths. The data obtained are given in Table 3.

The challenging fact of preserving the values of the coefficient of variations at the 19–20 % level can be outlined. The values of duration of short circuits and their frequency, as compared with similar data of experiments at smaller depths, are somewhat higher that corresponds to a negligible decrease in time of arc burning. However, as a whole, the data of Table 3 show that the presence in wire of compounds, increasing the ability of components of atmosphere of a vapour-gas bubble to ionising and transformation to the plasma, is quite necessary to provide the stable proceeding of the arc welding process.

Table 3. Results of tests of wire No.4 at up to 200 m depths

File in IMS	*Depth, m*	K_v^U, %	$\tau_{sh.c}$, *ms*	$f_{sh.c}$, *Hz*
R36	80	20	3.05	4.04
R37	100	20	3.08	4.30
R38	150	19	3.89	3.45
R39	200	20	1.57	7.99

Under the conditions of simulation of 200 m depth (Table 3, experiment R39) the reduction in $\tau_{sh.c}$ and increase in $f_{sh.c}$ is noted by more than 2 times as compared with the same characteristics for 150 m depth. However, there is no grounds to consider this fact as a result of an abrupt decrease in arc stability as the value of coefficient of voltage variation is preserved. In addition, at a clear instability of arc process of underwater welding with experimental wires of the same series, when values K_v^U were 30–40 %, the values $\tau_{sh.c}$ and $f_{sh.c}$ were much higher and located in the ranges of 4–5 ms and 17–22 Hz, respectively. Explanation of nature of some decrease in duration of short circuits and increase in their frequency in experiment R39 can be found in authors of work [6]. The main cause of a growth in number of short circuits and arc breaks with a depth growth is the decrease in sizes of vapour-gas bubble. The arc, more compressed in this case, should have also the higher gradient of voltage in the column. At increased voltage gradient in arc column the arc length should be smaller, providing the arc voltage constant (28–30 V) by volt-ampere characteristic of the power source. This, in its turn, should lead to the decrease in mean value of duration of short circuits after exceeding some critical depth of immersion that is also confirmed by comparison of results of experiments R38 and R39 (Table 3).

When analyzing the data about the effect of ratio of amount of silicate and marble in charge of experimental wires on characteristics of stability of arc burning, it seems that $CaCO_3$ has a negligible role as compared to Na_2SiO_3. Probably, the hope for arc stabilization at the expense of gas formation in marble dissociation is rather little. It is due to the fact that the excessive gas formation does not lead to the bubble inflation around the arc beyond the limits of sizes of dynamic equilibrium at a certain hydrostatic pressure. It only increases the frequency of gas bubbles escape. Moreover, each this collapse of the bubble should be an additional factor of the arc destabilizing.

As to the ionising action of the marble, then here it is necessary to take into account the nature of effect of alkali (sodium, potassium) and alkali-earth (calcium, strontium, barium) metals [7]. Physical properties of salts, used as activating coatings are such that salts and oxides of alkali metals have low temperatures of melting and decomposition, not exceeding 1173 K. Therefore, even at some distance from the electrode wire end the evaporation of activating compound is occurred and the vapours, entered the arc, reduce the effective potential and change positively the degree of ionising in it. However, the salts of alkali-earth metals, though are melting at relatively low temperatures for arc (close to 875 K), are decomposed at a further heating with the formation of oxides

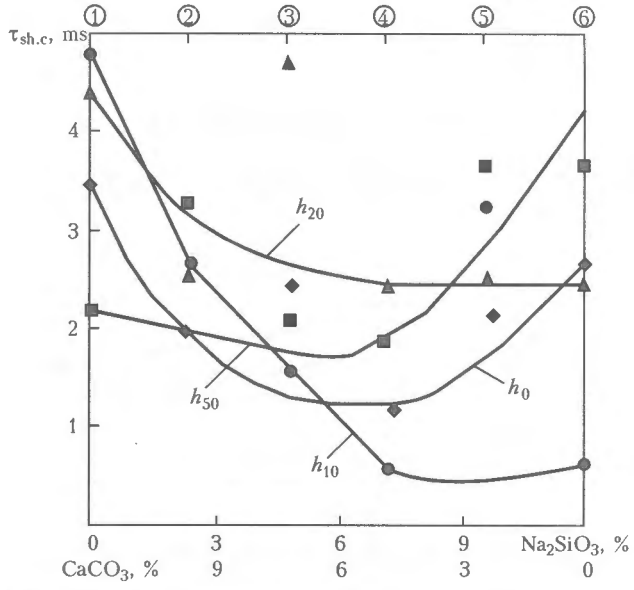

Figure 2. Mean values $\tau_{sh.c}$ depending on ratio of content $Na_2SiO_3/CaCO_3$ and test depth

which are characterized by exclusive refractoriness (3000–3770 K) in parallel with a low work function of electrons. In this connection, their stabilizing effect is manifested due to arc localizing at areas of consumable electrode tip, covered with this oxide. Consequently, the activating coatings, containing salt of alkali metals, have an influence both on the processes in arc column and also on the cathode processes, while activating components in the form of salts of alkali-earth metals influence only the cathode processes.

Effect of Na_2SiO_3 and $CsNO_3$, added separately. Data of Figure 4 confirm the high capability of alkali metals to stabilize the underwater arc in wet welding with the flux-cored wire. They were obtained in testing the second series of experimental wires, whose compositions on the base of known of wire PPS-AN1 are given in Table 2. These results allow us to evaluate the possibility of radical effect on properties of real electrode materials, tested comprehensively under the industrial conditions. With increase in content of ac-

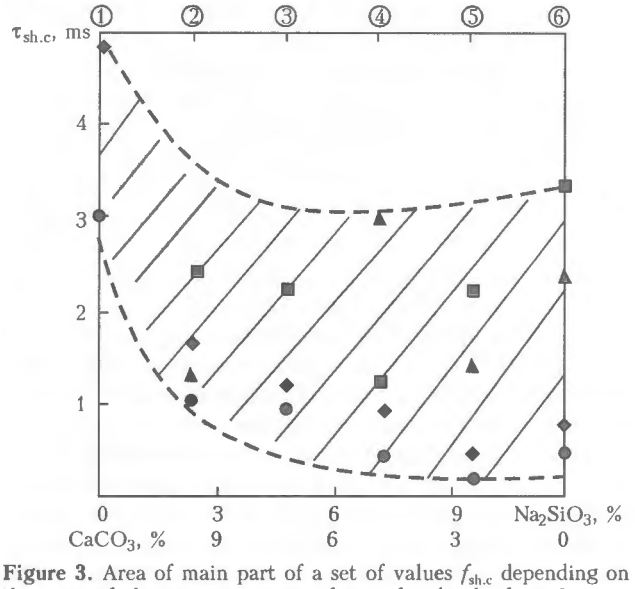

Figure 3. Area of main part of a set of values $f_{sh.c}$ depending on the ratio of charge components of wire for depths from 0 up to 50 m (designation of conditional marks corresponds to Figure 2)

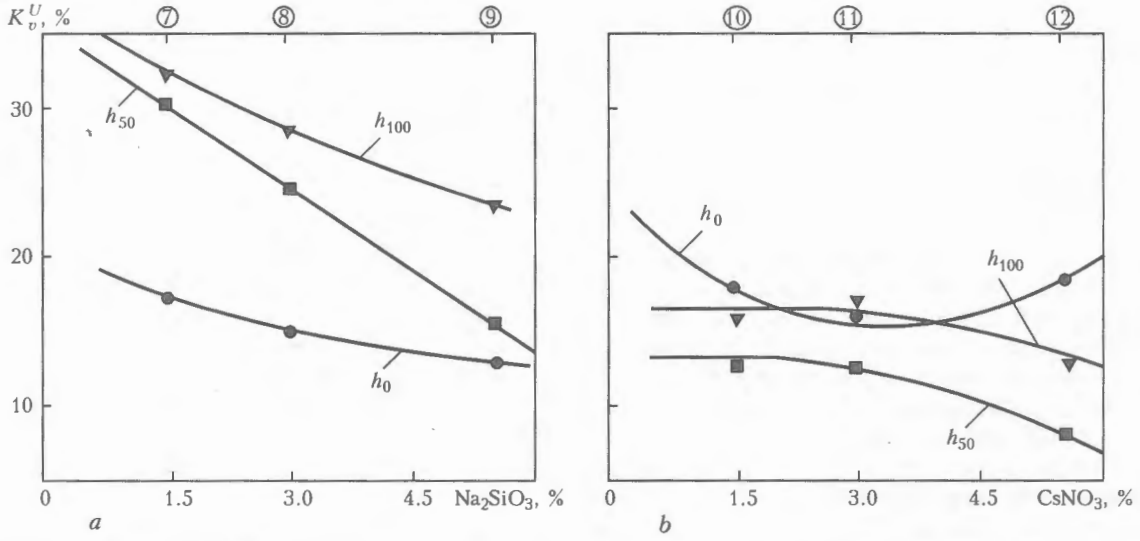

Figure 4. Effect of Na_2SiO_3 (*a*) and $CsNO_3$ (*b*) content in wire composition and test depth on coefficient of arc voltage variation

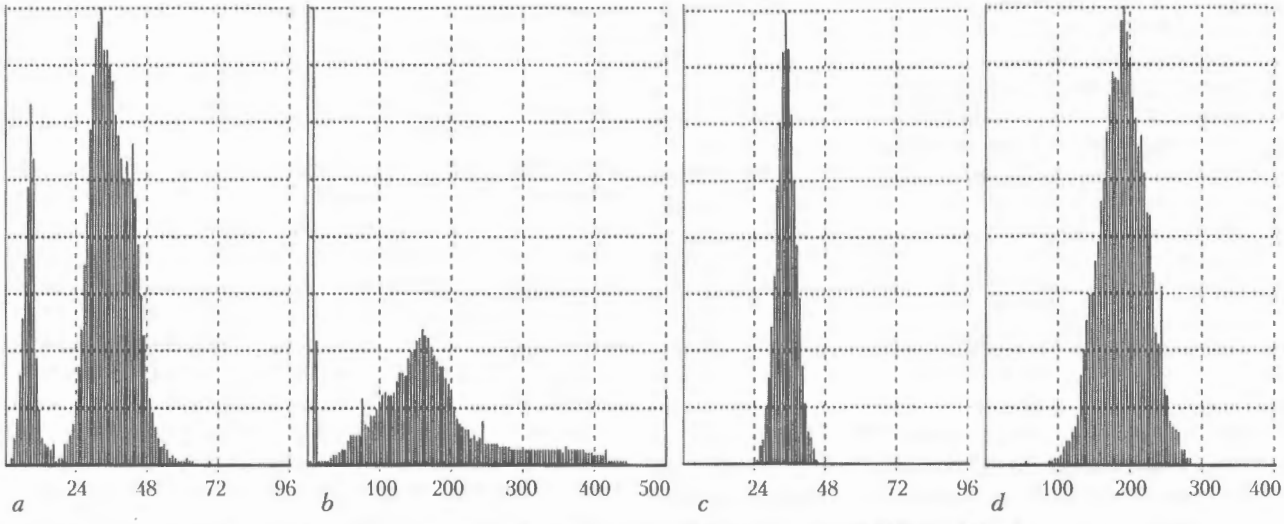

Figure 5. Histograms of arc voltage (*a, c*) and welding current (*b, d*) at testing wire PPS-AN1 (*a, b*) and experimental wire on base of PPS-AN1 with 9 % $CsNO_3$ (see Table 3, R37) (*c, d*)

tivating additions into the wire charge the degree of their action is greatly increased. In addition, the positive effect of cesium salt is more effective as compared with that of the sodium silicate.

It is interesting to compare these results with data of testing the PPS-AN1 wire [1], where there is no additions. It occurred that in case of use of a standard wire the coefficient of variation of voltage even at the 20 m depth exceeds 40 %. At the same time the experimental wires with additions of salts of sodium and cesium at 50–100 m depth give value $K_v^U < 35$ %. A significant difference is observed especially in adding cesium salt, which gives result, quite acceptable for practical application. Histograms of welding under conditions of 100 m depth simulation (Figure 5) reflect clearly the sufficiently positive effect of flux-cored wire activation with cesium salt.

Thus, the adding of alkali metals into the composition of wires and dilution of vapour-gas bubble atmosphere with products of their decomposition, made it possible to decrease greatly the variation of values of electrical parameters of the arc and to preserve the stability of wet welding within the range of depths up to 100 m. Evidently, the presence of elements with a low potential of ionising has led to the increase in electric conductivity of «cold» periphery areas of arc column, as a result of which the arc constriction was decreased providing the compensation of action of the increased hydrostatic pressure.

1. Gretsky, Yu.Ya., Maksimov, S.Yu. (2003) Effect of hydrostatic pressure on arc stability in underwater welding (Review). *The Paton Welding J.*, **12**, 10–12.
2. (1980) *Flux-cored wires for arc welding*. Kiev: Naukova Dumka.
3. Korotynsky, A.E., Kunitsa, I.I., Maksimov, S.Yu. (1992) Computer system of control of underwater welding processes. In: *Abstr. of pap. of School-Seminar*, Slavskoe, June 2–4, 2002.
4. Rehfeldt, D., Bollman, A., Koerbe, T. (1989) Statistical analysis for monitoring underwater arc welding processes. In: *Proc. of Int. Conf. on Welding under Extreme Conditions*, Helsinki, Sept. 4–5, 1989. Pergamon Press.
5. Pokhodnya, I.K., Gorpenyuk, V.N., Ponomaryov, V.E. et al. (1985) Statistical methods of measurement of electric and time parameters of DC arc welding circuit. In: *CMEA inf. materials*. Issue 2.
6. Pokhodnya, I.K., Gorpenyuk, V.N., Kononenko, V.Ya. et al. (1990) Some peculiarities of arc burning and metal transfer in self-shielded underwater welding. *Avtomatich. Svarka*, **9**, 1–4.
7. Lenivkin, V.Kh., Dyurgerov, N.G., Sagirov, Kh.N. (1989) *Technological properties of shielded welding arc*. Moscow: Mashinostroenie.

FORMATION OF STRUCTURE OF JOINTS IN RESISTANCE AND FLASH-BUTT WELDING

S.I. KUCHUK-YATSENKO[1], G.K. KHARCHENKO[1], V.F. ZAGADARCHUK[1], Yu.V. FALCHENKO[1] and V.F. MAZANKO[2]
[1]E.O. Paton Electric Welding Institute, NASU, Kiev, Ukraine
[2]G.V. Kurdyumov Institute of Metal Physics, NASU, Kiev, Ukraine

Comparative analysis of peculiarities of formation of pipe steel joints made by flash and resistance butt welding was made. It is shown by the investigations performed that the presence of a melt layer in a butt joint leads during upsetting to the development of an extensive zone of volumetric interaction, minimum distortion of leneage structure and insignificant decrease in metal density in the butt.

Keywords: *flash-butt welding, resistance welding, melt, isotope, deformation*

Formation of metal bonds in resistance welding (RW) and flash-butt welding (FBW) occurs at the final stage of the process as a result of deformation of heated edges of pieces. In both cases, the processes, proceeding in near-contact zones and leading to the formation of common structures for materials structures, have a dominating influence on the formation of joints. Here, the condition of surfaces being joined in the period, preceding the deformation, greatly influences the formation of these structures.

In RW of components of a large area of cross section (more than 500 mm^2) the metal in the contact zone is not finalized by melting and the joining is occurred in a solid phase at temperature of near-contact layers, close to the temperature of melting.

In FBW, there is always a layer of molten metal of thickness from 0.1 to 0.8 mm before upsetting. In both cases the quality of joints is determined by the structure and properties of a thin layer of metal, revealed in butt on macrosections of the joints made by RW and FBW, in the form of a light band of melting.

Investigations carried out during recently at the E.O. Paton Electric Welding Institute showed that in joints, made by FBW, the melt of the molten metal is not extruded completely from the butt, its part is remained in butt and influences greatly the structure of surfaces welded. It was established in particular, that the formation of different microdefects and microimperfections in the surfaces welded can be caused by the presence of structures in the butt, which are formed after the deep deformation of the melt. An indirect confirmation of structure change is the reduction in the metal density in the zone of surfaces welded [1].

In this connection, the assumption was made about the effect of microimperfections on characteristics of ductility at low temperature tests. However, the distribution of melt in surfaces welded and mode of its interaction with a solid phase were not managed to be determined using the standard methods of metallographic investigations and spectral analysis. In addition, the presence of different microimperfections of structure can be caused not only by the presence of the melt, but also by the peculiarities of deformation of near-contact layers of metal and redistribution of impurities in the parent metal. The comparison of metal structure in the zone of surfaces welded in RW and FBW makes it possible to evaluate the melt role in the formation of joints in pressure welding.

The aim of investigations was to make a comparison analysis of peculiar features of formation of the structure of joints, made by FBW and RW, under similar conditions using procedures allowing determination of the mass transfer in near-contact volumes of the metal.

The investigations were performed on welded joints from pipe steels of class X70 of 14 mm thickness and up to 100 mm width. Steels of this class, produced by using a controllable rolling, are characterized by a clearly expressed segregation of impurities, oriented along the rolling bands. In welding of these steels, the chemical inhomogeneity of the metal of joints, made by the RW is most clearly manifested. FBW of plates of the above-mentioned section was made at the conditions optimum for the given category of steels [2]. In RW of samples the welding conditions were selected so that the common zone of heating and upsetting for RW and FBW joints was approximately equal. Upsetting in RW and FBW was about 0.5δ (δ — sheet thickness). Upsetting in RW was performed under the conditions of a free formation in accordance with the generally-accepted technology. In this case, the distribution of temperature in HAZ in RW and FBW cannot be identical due to physical specifics of heating. In both cases the accepted welding conditions provided the mechanical properties of the joints specified by standard API 1104.

It should be noted that the mechanical tensile and bend tests of standard specimens did not reveal significant differences between the specimens produced by FBW and RW methods. Values of ultimate strength, yield strength, bend angle were very close to similar characteristics of the parent metal. At impact bend tests the mean values of a_n were 50–60 %

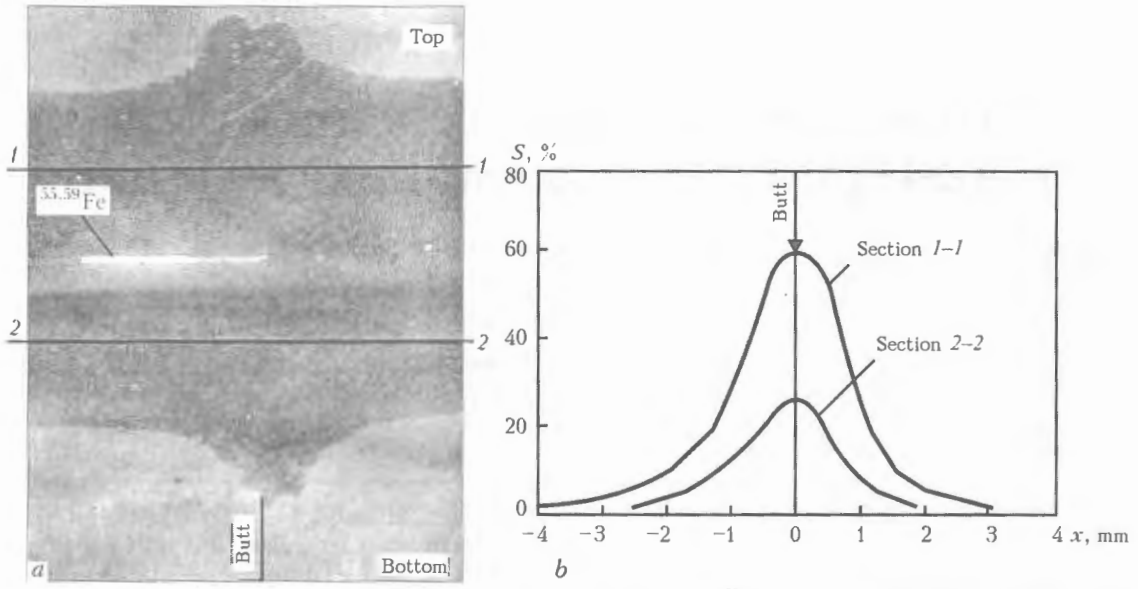

Figure 1. Autoradiogram (*a*) and concentration curves (*b*) of distribution of isotope $^{55.59}$Fe in sections *1*, *2* of the welded joint produced by FBW (x – distance from butt; S – degree of blacking of X-ray film)

of similar value of the parent metal. However, the scattering of these a_n values in RW was much higher than in FBW.

Comparative investigations of processes of mass transfer using radioactive isotopes in RW and FBW were carried out at the E.O. Paton Electric Welding Institute with participation of the representatives of the Institute of Metal Physics.

In RW the radioactive iron (isotope $^{55.59}$Fe) was deposited by a layer of 0.5–1.0 μm thickness on an edge of one of the specimens being welded. In case of FBW the isotope was placed inside of a two-layer specimen or on its surface from the side of arrangement of the welding transformer.

In FBW the contacting surfaces are renewed continuously in the process of flashing and as a result of melt migration at the flashing surface to the side opposite to the welding transformer [3, 4]. Isotope arrangement at the specimen surface from the side of welding transformer allows its continuous introducing into melt during flashing. Figures 1 and 2 present diagrams of distribution and displacement of iron isotope, and also concentration curves of its distribution in different areas of the welded joint.

Analysis of nature of this distribution showed the following. If the isotope was placed initially inside the composite specimen (Figure 1), then it was moving in the composition of a liquid phase more to the upper edge of butt than to the lower edge under the action of the electrodynamic force. The depth of isotope penetration to the parent metal was several millimeters, moreover, this penetration in the area of the upper edge was more intensive than in the lower edge. In this connection it is possible to assume that during FBW of rolled metal the concentration of inclusions transferred by a liquid phase in migration in the spark gap will be higher in the weld area, removed at a larger distance from the transformer.

Figure 3 presents the concentration curves of iron isotope distribution in RW and FBW. In the first case the width of the zone of a volumetric interaction is approximately 0.4 mm [5], while in the second case it increases by more than 2 orders. Undoubtedly, we cannot divide at present the mechanical intrusion of liquid phase into microcracks of the parent metal and mass transfer of atoms as a result of proceeding the intensive diffusion processes. Probably, the transfer of iron isotope for such a large distance into near-contact layers of metal at FBW is stipulated by interaction of the liquid phase (melt) and fusible structures

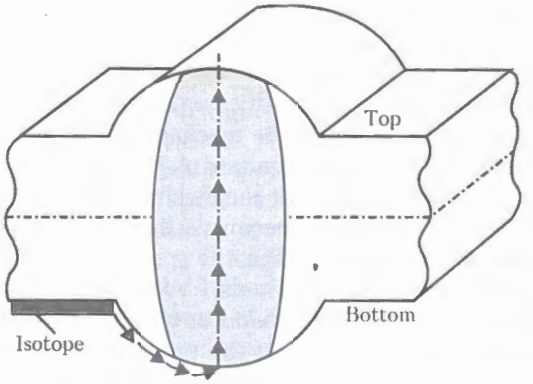

Figure 2. Scheme of distribution of iron isotope in butt of joint produced by FBW

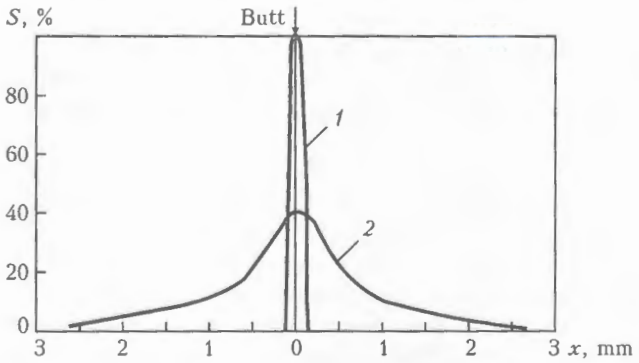

Figure 3. Typical form of concentration curves of distribution of iron isotope in welded joints made by RW (*1*) and FBW (*2*)

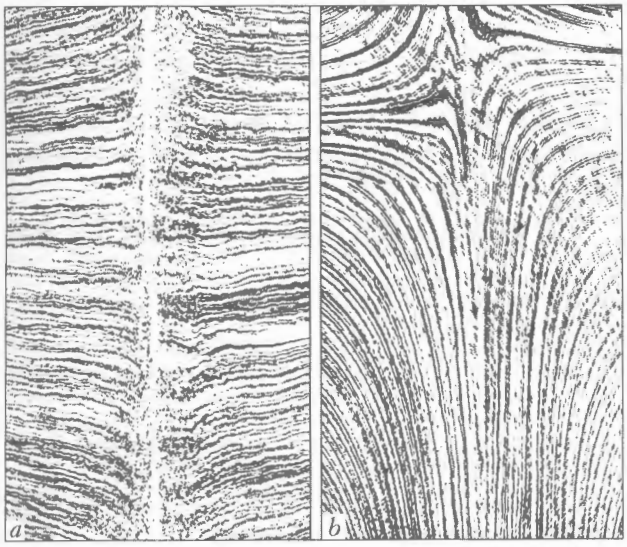

Figure 4. Macrostructure of butt joints produced by FBW (*a*) and RW (*b*) after heat treatment (×25)

of segregation bands. It can be stated that the presence of a liquid phase at the stage of upsetting causes the increase in mass transfer and depth of displacement of chemical elements by several orders from the butt to the solid metal as compared with welding without flashing, that leads to the formation of an extensive zone of volumetric interaction in FBW.

Metal structure in the region of surfaces welded was examined in optical and scanning electron microscopes on sections after their chemical or ion etching. The latter was conducted in JEOL unit Ionsputter JFC-1100. To evaluate the metal density in surfaces welded, a method of hydrostatic weighing was used. Samples for density measurement were made according to recommendations of work [1].

A positive effect of melt, located in butt at the stage of upsetting, on the steel structure in the zone of contact was established. Procedure of investigations was as follows. Welded joints were annealed in furnace at 950–1000 °C temperature, then they were cooled at the 120–150 °C/h rate [1, 6]. Non-metallic inclusions after changing their initial location as a result of upsetting are the centers of the ferrite recrystallization during joint cooling. The precipitating pearlite is arranged in accordance with a ferrite shape. The presence of a lineage structure, recovered as a result of heat treatment, in the zone of contact testifies to its negligible distortion in joints made by FBW as compared with joints made by RW (Figure 4).

One more convincing prove of the positive effect of melt in the butt on the quality of the joint is the results of measurement of metal density in the region of the surfaces welded location. Figure 5 gives curves, characterizing the change in metal density in FBW and RW for the case of formation of joint with an equal upsetting. It can be concluded from the Figure that the density of metal in the area of surfaces welded in specimens of RW is lower than that in FBW that proves the presence of microimperfections of structure in RW (microcracks, porosity). The use of ion etching allowed revealing the microcracks, which are arranged

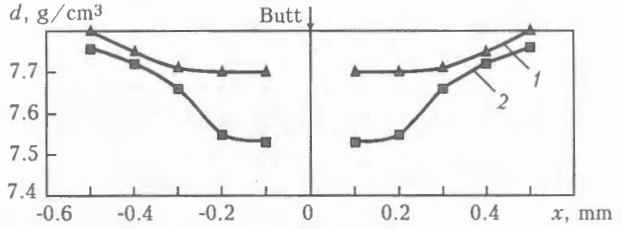

Figure 5. Change in density *d* of butt metal produced by FBW (*1*) and RW (*2*)

mainly in a lineage structure, in the butt of joint, made by RW (Figure 6).

In specimens made by FBW, microcracks in the zone of contact were not revealed, the bending of fibres in the butt is much smaller than that in RW. During FBW the extrusion of a part of melt from the butt into the flash is occurred, while the remained melt takes part in the joint formation. The microimperfections, formed in the process of deformation, are filled with a melt, which behaves as a brazing alloy, filling the microcavities in brazing at pressure applying [7, 8]. It should be noted that it was not managed to reveal the location of a layer of the former liquid interlayer on sections by a metallographic method. Absence of the cast structure in the butt at optimum parameters of upsetting is explained by the fact that a thin band of melt, being crystallized on the grains of solid metal, repeats its structure [1].

As follows from the given data, the presence of melt on edges in FBW contributes to the formation of a monolithic structure in the butt. This is manifested in particular in welding steels with an increased content of oriented liquation structures. Therefore, all the technological procedures, allowing us to produce melt distributed uniformly over the surface of edges in the butt, will promote the increase in the quality of joints.

Selection of upsetting at RW and FBW is a subject of discussions until now, that was reflected in existing instructions accepted in different countries. In most cases the tolerances for upsetting, amounting to 1.0–1.5δ, that is 2–3 times exceeds the tolerances for upsetting accepted by us, are recommended in welding of sheet steels. It is not difficult to prove that the

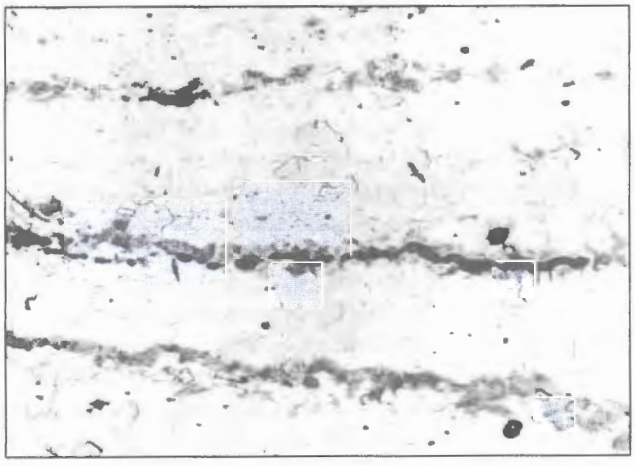

Figure 6. Microstructure with a microcrack in joint made by RW (×100)

degree of deformation of fibres in near-contact area at these conditions will be much higher than in our investigations, and the probability of formation of microcracks and other imperfections of the structure in HAZ is larger.

The data obtained confirm the recommendations developed at the E.O. Paton Electric Welding Institute for technologies of FBW of pipes and rolled metal where the upsetting is set minimum within the limits, not exceeding $1.2\Delta_{gap}$ (Δ_{gap} – maximum spark gap in flashing).

Probably, the limitation of upsetting in RW will promote the increase in stability of characteristics of mechanical properties of joints if to perform welding under the conditions of a forced formation of the welded joint [9].

CONCLUSIONS

1. It was established that the nature of formation of joints in RW depends on the presence of melt at the edges in the period preceding the upsetting.

2. In RW the intensive deformation of near-contact volumes of metal promotes the formation of microimperfections that is especially manifested in welding rolled metal with a clearly expressed segregation of impurities.

3. It was determined that the presence of melt in FBW at the stage of upsetting provides the development of the extensive zone of volumetric interaction, minimum distortion of a lineage structure and negligible decrease in metal density of metal in the butt.

1. Kuchuk-Yatsenko, S.I., Kharchenko, G.K., Grigorenko, G.M. et al. (2002) Heterogeneity of pipe steel joints made by flash-butt welding. *The Paton Welding J.*, **2**, 2–5.
2. Kuchuk-Yatsenko, S.I. (1992) *Flash-butt welding*. Kiev: Naukova Dumka.
3. Kuchuk-Yatsenko, S.I., Nikitin, A.S., Kazymov, B.I. (1986) Some peculiarities of control of flashing process in resistance welding with use of external magnetic field. *Avtomatich. Svarka*, **9**, 24–26.
4. Nikitin, A.S., Kuchuk-Yatsenko, S.I. (1996) Formation of structure of joint in flash-butt welding. *Ibid.*, **2**, 3–5.
5. Kuchuk-Yatsenko, S.I., Kharchenko, G.K., Nikitin, A.S. et al. (1996) Investigation of peculiarities of mass transfer in solid phase welding. *Ibid.*, **12**, 14–17.
6. Polosukhin, N.A. (1952) *Structure and strength of pressure-gas welded joints*. Kiev: Mashgiz.
7. Lebedev, V.K., Tabelev, V.D., Pismenny, A.S. (1983) Butt pressure brazing of steel pipelines. *Avtomatich. Svarka*, **9**, 25–27.
8. Tabelev, V.D., Kareta, N.L., Panasenko, A.I. et al. (1985) Structure and phase composition of seams made by capillary and pressure brazing. *Ibid.*, **11**, 26–29.
9. Lebedev, V.K., Sakhatsky, G.P., Shirokovsky, R.M. (1986) Resistance welding with joint formation. Principle of method and its possibilities. In: *Transact. on Resistance Welding with Joint Formation*. Kiev: PWI.

EFFECT OF PRIMARY STRUCTURE OF CAST HEAT-RESISTANT NICKEL ALLOYS ON FORMATION OF HOT CRACKS DURING WELDING

N.I. PINCHUK[1] and **N.K. RYAZANTSEV**[2]
[1]E.O. Paton Electric Welding Institute, NASU, Kiev, Ukraine
[2]Kharkov Design Bureau for Engine Construction, Kharkov, Ukraine

Effect of primary structure and phase composition on weldability of cast nickel alloys containing up to 6 % aluminium is considered. The positive effect of two-phase primary structure containing an increased amount of aluminium eutectic with the γ'-phase (Ni_3Al) is shown. Investigation data on alloy JS6-U of conventional casting and oriented solidification, as well as on new alloy LJ1-I, used for manufacture of welded gas turbine rotors are presented.

Keywords: *nickel alloy, fusion welding, hot cracks, primary structure, crystalline grain boundaries, eutectic, second phase*

Cast heat-resistant nickel alloys are extensively applied for the manufacture of gas turbine and other types of engines. They are used to make cast structures or structures with mechanical mounting. As a rule, there is no possibility of making welded structures from these alloys, especially from alloys with a high level of heat resistance. This is attributable to a high sensitivity of the majority of heat-resistant nickel alloys to cracking during welding, i.e. formation of hot intercrystalline cracks in the weld and weld zone metal. At the same time, it is necessary to improve weldability of these alloys, as their use in welded structures can make the fabrication simpler and provide a substantial economical benefits. The problem of hot cracking in welding heat-resistant nickel alloys is topical and has been discussed in literature for many years.

The article gives some results of investigations of weldability of nickel alloys conducted under the project of fabrication of a welded gas turbine rotor for the highly augmented turbopiston engine by the Kharkov Design Bureau for Engine Construction (KhDBEC) in collaboration with the E.O. Paton Electric Welding Institute*. Alloys for the project were produced by the Joint-Stock Company «NII-Stali» (Moscow). The new approach developed on the basis of analysis of primary structure of casting alloys aimed at improvement of their weldability became one of the key points in building of a welded rotor. The new technology was applied for mass production of high-temperature welded rotors at the V.O. Malyshev Factory in Kharkov [1].

Hot cracks in the weld zone or weld metal are formed under the effect of tensile welding stresses that separate crystalline grains. This is caused to a large extent by formation of liquid metal films on the crystalline grain boundaries. These boundaries, containing liquid, may «open» at the presence of very low stresses, and even at the absence of stresses. Figure 1, *a* shows a typical pattern of hot intercrystalline cracks formed in the weld zone of heat-resistant nickel alloy JS6-U. Fine intercrystalline layers are seen near the line of fusion with the weld (Figure 1, *b*).

Formation of hot cracks in welding of single-phase nickel alloys is favoured also by the so-called «harmful» impurities of metallurgical production origin, such as sulphur, phosphorus, carbon and silicon, or impurities of low-melting point non-ferrous metals, such as antimony, arsenic and lead [2, 3], which form eutectics with nickel at their relatively low concentrations. The lowest-temperature eutectics are formed by sulphur, phosphorus and boron. Hot cracks in the weld zone are often formed in regions of accumulation of liquating elements and non-metallic inclusions [4]. Therefore, different methods are used in practice to limit the content of impurities in nickel alloys to a level below which they exert no marked effect.

Cracking of nickel alloys in welding is usually related to the presence of alloying elements that form low-melting point eutectics (boron, cerium, hafnium, zirconium) [2, 5]. Some of them, present even in an insignificant amount (hundredths or thousandths of a percent), may cause formation of films of the eutectic liquid and cracks in the weld zone. First of all, these are boron and zirconium. For example, sensitivity of alloy Ni–10Al–10Fe to hot cracking dramatically grows at a boron content equal to as low as 0.005 % [6].

It is thought that cracks in the weld zone are formed in cooling after the welding heating in a temperature range close to solidus. In this range the bonds between crystalline grains become dramatically weakened, alloys lose their plastic deformation ability and fracture by a brittle mechanism (plastic deformation is equal to zero). The method for evaluation of weldability on the basis of width of the brittle temperature

*Participating in the investigations were K.A. Yushchenko, A.A. Nakonechny (PWI), I.L. Rovensky (KhDBEC), V.F. Kotov and G.A. Makhneva (NIIStali).

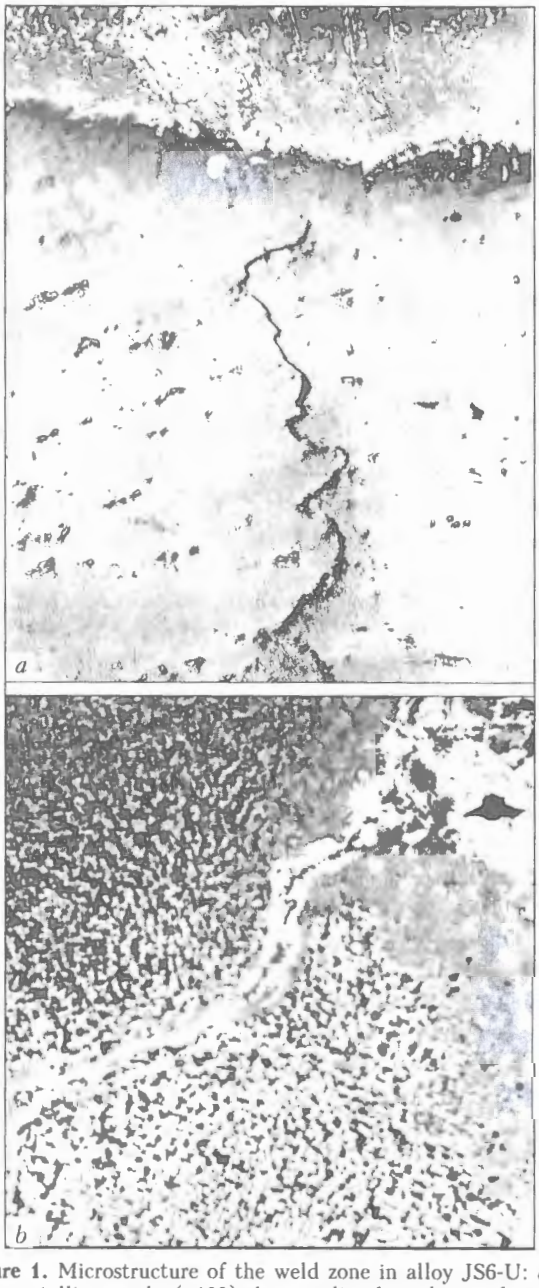

Figure 1. Microstructure of the weld zone in alloy JS6-U: *a* — intercrystalline cracks (×100); *b* — molten boundaries of crystalline grains (×1000)

range (BTR) in cooling after the welding heating simulation is suggested in [7]. Alloys sensitive to cracking in the weld zone, e.g. heat-resistant steel Kh15N24V4T2 [8] and alloy JS6-U (Figure 2, *a, c*), have a wide BTR, i.e. in cooling after the welding heating simulation they fracture by the brittle mechanism in a temperature range that is much lower than solidus. Zero ductility of alloy JS6-U (solidus temperature is 1290 °C) in cooling after heating to 1260 °C persists to a temperature of 1120 °C. And vice versa, a high rate of restoration of plastic properties and a narrow BTR are characteristic of alloys with a two-phase primary structure, which are resistant to hot cracking in the weld zone [8] (Figure 2, *b*).

Brittle fracture in BTR can be caused by eutectic interlayers. In addition to the elements indicated above, eutectics with nickel can be formed also by the γ′-formers, such as aluminium, titanium and niobium. Weldability is usually evaluated on the basis of the content of these elements, particularly on the basis of the total content of aluminium and titanium [3, 9].

One of the possible mechanisms of the effect of aluminium, titanium and niobium on weldability of heat-resistant nickel alloys can be their presence in the eutectic phases and intercrystalline layers. The negative effect of aluminium and niobium on resistance to hot cracking of the welds in binary nickel alloys is shown in [10]. Increase in the content of each of them to 5 % leads to a continuous decrease in critical strain rate v_{cr} (Figure 3) and, accordingly, decrease in hot crack resistance. Comparison of both elements at the same atomic concentration (3 %) shows that niobium decreases v_{cr} to a larger extent. Increasing the niobium content to 2 % leads to a continuous widening of BTR in alloy 20Cr–32Ni–Nb [11], in which the lower bound of BTR decreases from 1275 (at 0.03 % Nb) to 1125 °C (at 2.05 % Nb).

Sensitivity of cast nickel alloys to hot cracking is related to their high microchemical heterogeneity. It shows up as segregation of liquating elements. The segregation is evaluated from the ratio of the content of a given element in individual zones of crystalline grains, i.e. axes, spaces between axes and boundary zones, to its content of the melt. In solidification of nickel alloys, the first to form are crystals of a solid solution enriched with refractory elements (tungsten, cobalt, iron). Principal axes of dendrites are formed from these crystals. Elements that greatly differ from nickel in atomic diameter (boron, carbon, yttrium, zirconium, hafnium) enrich the remaining portions of liquid to a still higher extent and decrease the melting point. The second-order axes and spaces between the axes are formed from this liquid. Liquation and, accordingly, segregation of elements is most pronounced in the boundary zones of crystalline grains. Microchemical heterogeneity is typical of the single-phase nickel welds (3 % Al) (Figure 4, *a*) and nickel alloys of oriented solidification (5 % Al, 8 % Nb) (Figure 4, *b*), where skeletons of axes, spaces between the axes and boundary zones of crystalline grains are revealed (secondary boundaries in the weld results from polygonisation). The microchemical heterogeneity of an alloy can be estimated also from the depth of penetration into the weld metal of principal axes of its dendrites.

According to the diagram shown in Figure 5, alloys Ni–Al with 10 % Fe may contain the γ + γ′ eutectic with the primary γ′-phase (Ni_3Al). In multi-component nickel alloys the intermetallic γ′-phase has a more complex composition, which is reflected by the Ni_3(Al, Ti, Nb) formula. Temperature of the γ + γ′ eutectic in such alloys is much lower than in binary alloy Ni–Al (1385 °C) and alloys with 10 % Fe (1345 °C). Temperature of the γ + γ′ eutectic in heat-resistant alloy B1914 (5.5Al and 5.2Ti) is not higher than 1220 °C, and in alloy MAR-M-200 it is equal to

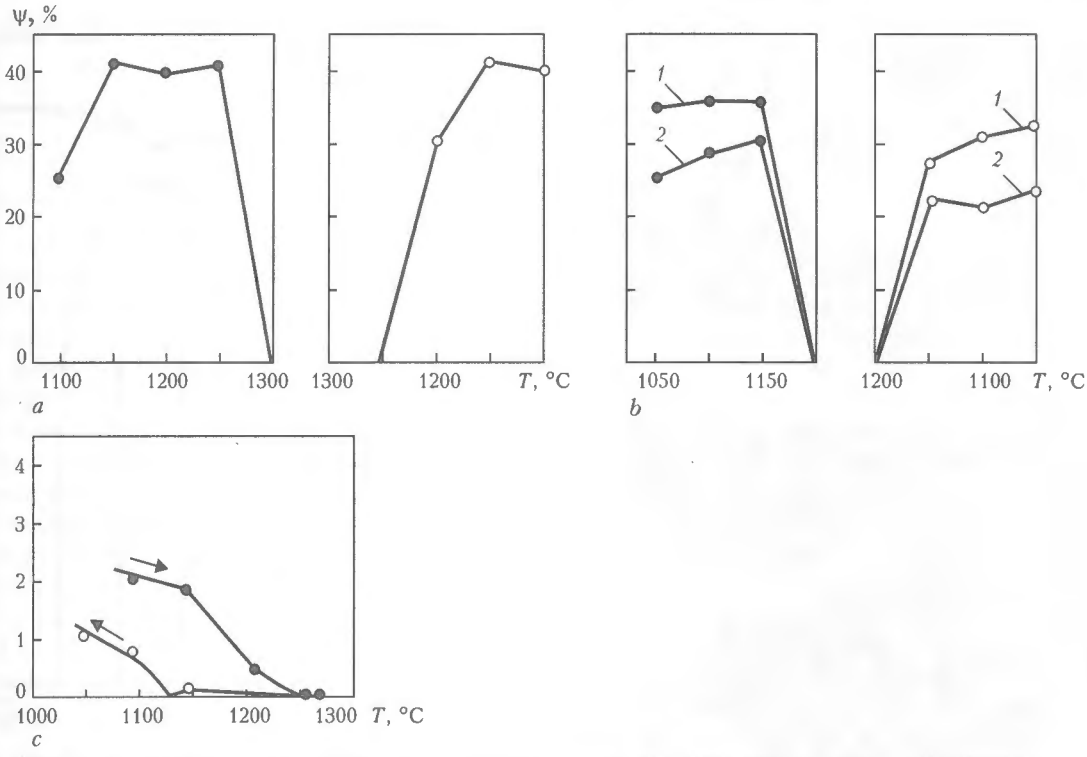

Figure 2. Hot ductility in heating by the thermal cycle of welding of steels Kh15N24V4T2 (*a*) and Kh15N24V4T2R1 (*b*) with 0.47 (*1*) and 0.70 (*2*) % B [8] and alloy JS6-U of conventional vacuum casting (*c*): ● – heating; ○ – cooling; ψ – reduction in area

1214 °C [12]. Eutectic in these alloys is formed at a much lower aluminium content than in the binary alloy (12.2 % Al). In alloy Inconel 939 the γ + γ′ eutectic (1 vol.% of the primary γ′-phase) is present even at 2 % Al [13].

The fact that boundary zones of crystalline grains in cast nickel alloys have a lower melting temperature than the matrix solid solution is important for properties of the weld zone. The γ′-formers, i.e. titanium and niobium [10, 12, 14], also belong to the elements that enrich the crystalline grain boundaries. In addition, segregation of the γ′-forming elements in the weld zone may grow due to diffusion of the liquating elements, especially if the liquid phase is present at the boundaries. Thus, melting of the crystalline grain boundaries in the weld zone of alloys Inconel 718 and Waspalloy [14] begins as low as at 1150–1200 °C. As experimentally found, fracture in welding of alloy Inconel 718 (5.5 % Ta/Nb, 1 % Ti) [14] and alloy Udimet 700 (4.3 % Al, 3.3 % Ti) [15] occurs in liquid intercrystalline films enriched with niobium and titanium, respectively. The last portions of the melt in Inconel 100 solidify to form the γ + γ′ eutectic (Ni_3Al) [12]. Very fine intercrystalline films of this eutectic may, with a high degree of probability, cause cracks. However, explanations of the effect of aluminium, titanium or niobium on sensitivity of alloys to welding cracks are ambiguous and require solution.

Of interest is investigation of weldability of alloys containing a considerable amount of the γ + γ′ eutectic, corresponding to the second primary phase. An example of structure of a binary nickel alloy with the γ + + γ′ eutectic (Ni_3Al) is shown in Figure 6, *a*. The eutectic is located on the crystalline grain boundaries along the principal axes. No cracks were found in microplasma welding of thin strips of this alloy (δ = = 2.5 mm) in a direction across the crystals. In wrought alloy Ni–9Al, the γ + γ′ eutectic is formed in the weld zone (Figure 6, *b*) and helps to eliminate cracks.

Improved weldability of B-alloyed nickel alloys and welds is reported in [8, 16]. It is shown that the eutectic liquid at the boundaries of crystals can be

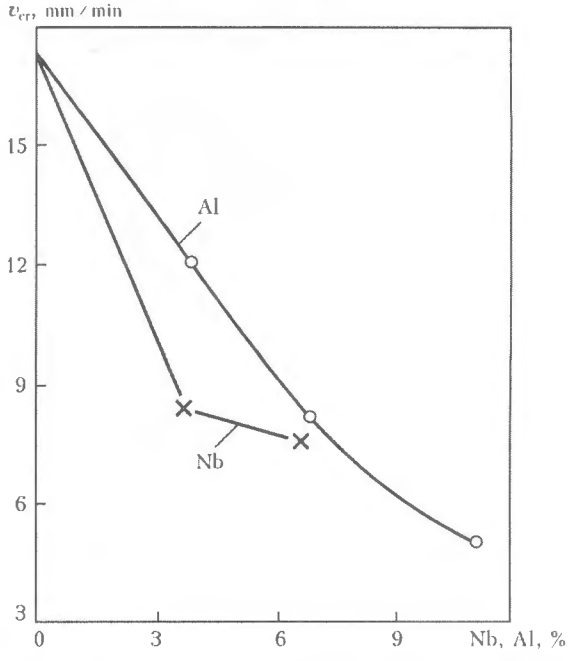

Figure 3. Effect of aluminium (*1*) and niobium (*2*) on critical strain rate v_{cr} in nickel [10]

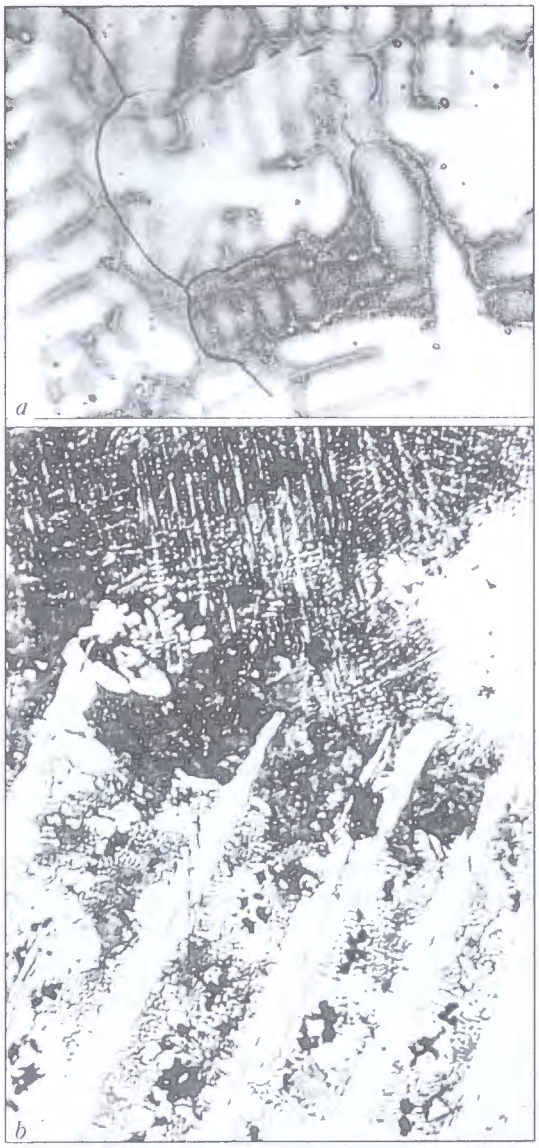

Figure 4. Microchemical heterogeneity in cast nickel alloys: *a* — Ni–Cr–3Al weld (×600); *b* — weld zone in oriented-solidification alloy Ni–Cr–8Nb–5Al (×100)

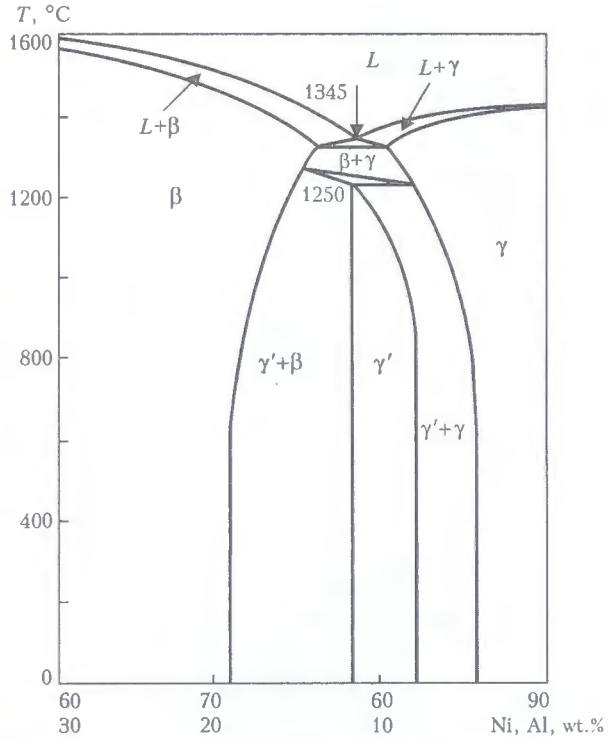

Figure 5. Vertical section of the constitutional diagram for alloys Ni–Al–10Fe [6]; *L* — liquid phase

beneficial. «Harm» and «benefit» depend only upon its content. At its low content, the eutectic liquid forms intermittent films along the crystalline grain boundaries, thus leading to cracking. At its content above a certain limit, the eutectic liquid envelopes crystalline grains, providing relaxation of welding stresses. As a result, resistance to hot cracking of the weld zone grows. Decrease in the width of BTR is noted in the case of heat-resistant steel Kh15N24V4T2 (EP164) alloyed with boron (0.47 and 0.72 %) (see Figure 2, *a, b*). Also noted is improvement in weldability of cast heat-resistant alloys KhN60MVTYu and KhN77TYu. The fact that the eutectic liquid at the boundaries of crystals can be beneficial is proved in [17]. Increase in a boron content of heat-resistant nickel welds of the type of KhN60MVBYu from 0.01 to 0.3 % leads to a continuous decrease in v_{cr}, whereas further increase in the boron content to more than 0.3 % causes increase in v_{cr} and improvement of hot crack resistance. In analogy with boron, a «beneficial»

range of the concentration of elements that form the γ + γ′ eutectic (Ni_3Al) can also be used for welding nickel alloys.

Alloy JS6-U produced by conventional vacuum casting (Table 1), which is sensitive to hot cracking,

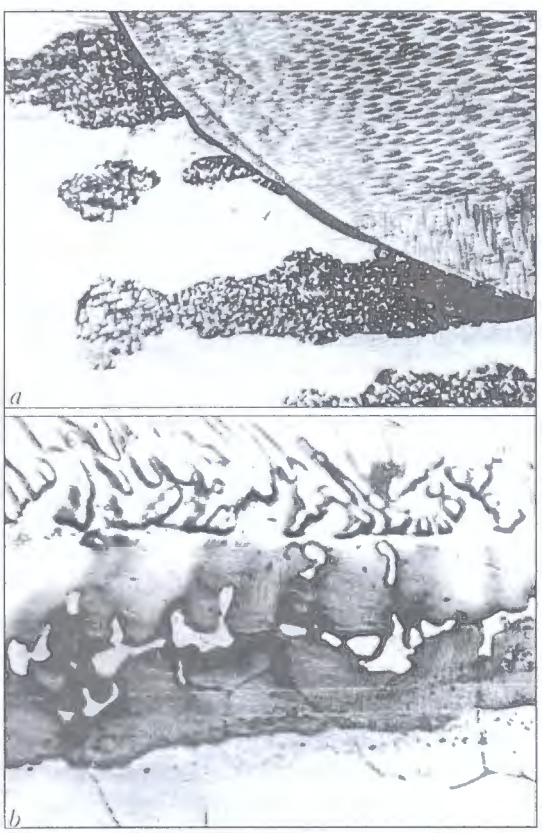

Figure 6. Microstructure of the weld zone in nickel alloys containing the γ + γ′ eutectic (Ni_3Al): *a* — oriented-solidification alloy Ni–12Al; *b* — wrought alloy Ni–9Al (×100)

Table 1. Content of alloying elements in nickel alloys, wt.%

Alloy	*C*	*Cr*	*Co*	*Mo*	*W*	*Nb*	*Ti*	*Al*	*Fe*	*Other*
JS6-U	0.14	9.2	9.0	1.5	10.2	0.95	2.4	5.9	1.0	B, Zr
OS JS6-U	0.12	9.5	9.0	1.8	9.6	1.0	2.5	5.5	2.0	B, Zr
LJ1-I	0.18	6.4	–	5.0	3.6	6.5	–	6.2	2.0	B, Zr, Y

has a structure of equiaxed crystalline grains (see Figure 1, *a*). Its structure comprises the γ-solid solution of alloying elements in nickel (matrix), inclusions of primary carbides of the MC type and a small amount of the γ + γ′ eutectic with the primary γ′-phase (Ni_3Al) located along the crystalline grain boundaries in the form of light globules in optical microscope images and dark globules in electron microscope images, as well as the hardening γ′-phase in the form of dispersed precipitates in the matrix γ-phase (in electron microscope images).

Earlier we noted increase in the degree of segregation of molybdenum, niobium, chromium and tungsten in oriented-solidification (OS) alloy JS6-U [18]. This increase is accompanied by growth in the amount of the γ + γ′ eutectic.

According to the X-ray microanalysis data, the OS alloy JS6-U (Table 1) is characterised by growth of the nickel content in spaces between the axes, the molybdenum content increasing to a lesser degree, and the tungsten content decreasing. The higher content of the γ + γ′ eutectic achieved in OS (Figure 7, *c*) moves the OS alloy JS6-U to a category of alloys with a two-phase primary structure. As proved by welding of restrained specimens under laboratory conditions at the E.O. Paton Electric Welding Institute, and by welding of models of rotors in experimental production at KhDBEC, this change in phase composition of the alloy provides improvement in its weldability. Cracks do not form during welding. Increase in crack resistance of the weld zone in OS alloys can be achieved by performing welding across the crystals (due to decrease in length of the crystalline grain boundaries) and owing to higher ductile properties of the OS metal in this direction. The investigations that followed, as well as the practice of welding of alloys of the JS6-U type, show that of primary importance for improvement of weldability is an increase in the γ + γ′ eutectic content.

Differential thermal analysis (heating at a rate of 80 °C/min in helium) of alloys JS6-U produced by conventional casting and the OS alloy JS6-U showed changes in a thermal effect, evidencing changes in structure (Figure 8). Change in the thermal effect

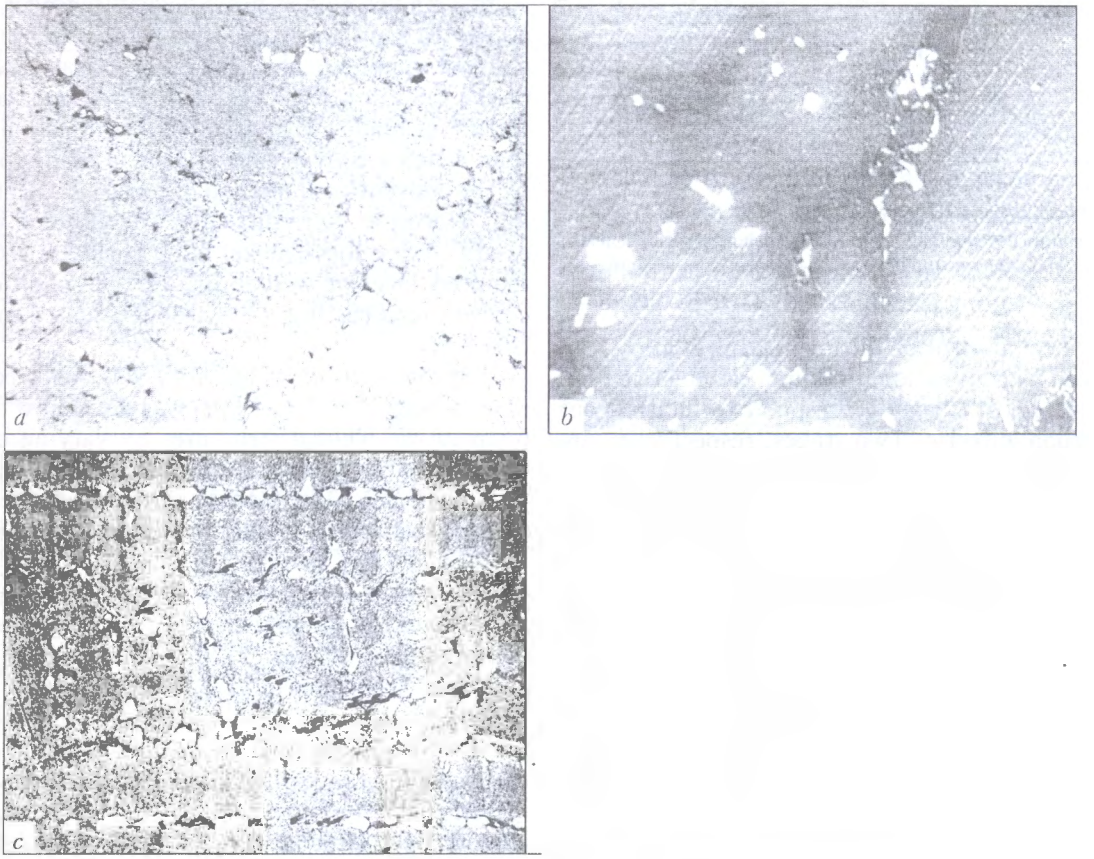

Figure 7. Microstructure of alloy JS6-U: *a*, *b* – conventional solidification (precision vacuum casting); *c* – oriented solidification; *a*, *c* – optical microscope (×100); *b* – electron microscope (×1300)

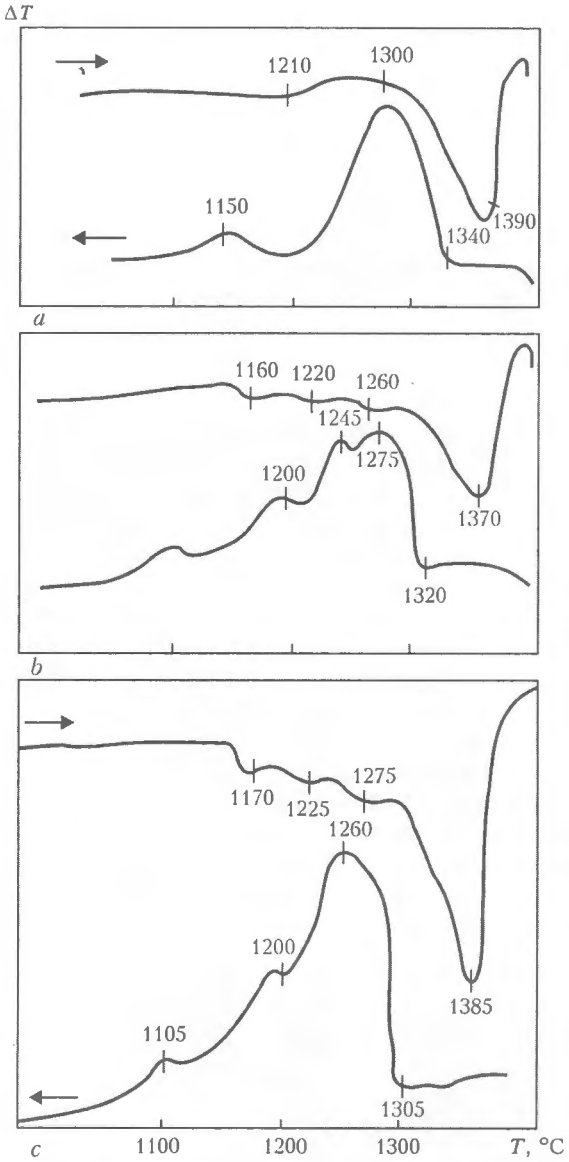

Figure 8. Differential thermal curves for alloy JS6-U: *a* — conventional vacuum casting; *b* — casting with oriented solidification; *c* — alloy LJ1-I, conventional vacuum casting; ΔT — change in thermal effect

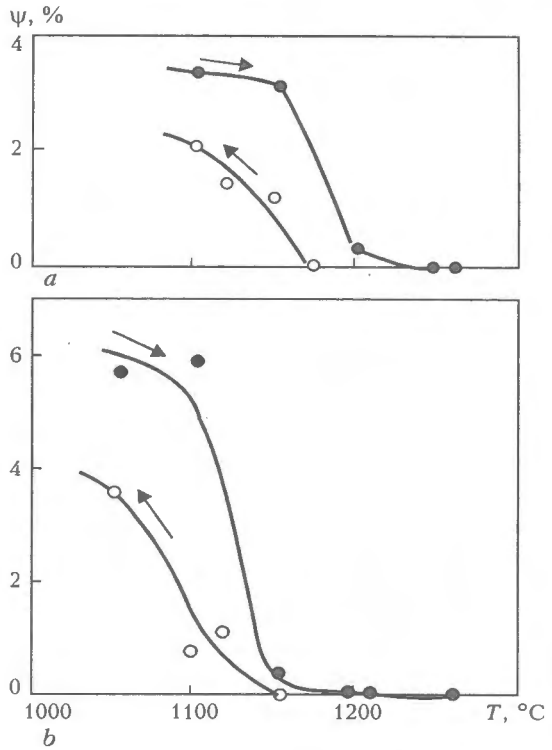

Figure 9. Hot ductility in heating following the thermal cycle of welding of the oriented-solidification alloy JS6-U (*a*) and alloy LJ1-I of conventional vacuum casting (*b*); ● — heating at a rate of 10 °C/s; ○ — cooling from 1260 °C

involving heat absorption during heating of alloy JS6-U produced by conventional vacuum casting to a temperature of 1210 °C may correspond to melting out of the carbon eutectic. Two stages, respectively, are fixed in solidification. In heating the OS alloy JS6-U, a change in the thermal effect is fixed at temperatures of 1160, 1220 and 1260 °C. It is likely that a temperature of 1260 °C corresponds to the $\gamma + \gamma'$ eutectic of aluminium (NiAl), and temperatures of 1220 and 1160 °C correspond to the eutectics of carbon and boron. Solidification occurs in four stages.

Figure 9, *a* shows the data of evaluation of BTR for the OS alloy JS6-U. In cooling from 1260 °C (solidus 1290 °C), BTR is limited to a temperature of 1175 °C. This temperature is 1120 °C for alloy JS6-U of conventional vacuum casting (see Figure 2, *c*). Decrease in the width of BTR is indicative of an increased resistance of the OS alloy JS6-U to cracking in the weld zone, which is proved by practice.

Using casting with oriented solidification, where the content of the second primary phase ($\gamma + \gamma'$ eutectic) is much higher, provided improvement in weldability to such an extent that it allowed welding of the first samples of the gas turbine rotors with blades of the OS alloy JS6-U [1, 18]. However, the manufacture of blades with oriented solidification is more than 4 times as expensive as that of blades produced by the conventional method of precision vacuum casting, as well as more difficult. Therefore, it was necessary to develop a nickel alloy characterised by the required level of weldability in the condition after conventional casting, i.e. without oriented solidification.

Improvement of weldability was achieved, and a new casting alloy LJ1-I [19] was developed for high-temperature welded structures by varying chemical composition of the heat-resistant nickel alloy LJ 1 (6 % Al, 6 % Nb) in order to form a stable two-phase primary structure (γ-solid solution of elements in nickel and $\gamma + \gamma'$ eutectic).

Thermal analysis of alloy LJ1-I (Table 1) showed a change of the thermal effect (with heat absorption) at three temperatures: 1170, 1225 and 1275 °C (Figure 8, *c*). The value of 1275 °C is likely to correspond to the $\gamma + \gamma'$ eutectic of aluminium (Ni_3Al), while two other values seem to correspond to the eutectics of carbon and boron. Solidification occurs in four stages.

Alloy LJ1-I of conventional vacuum casting has a narrow BTR after heating to 1260 °C following the thermal welding cycle (Figure 9, *b*). Similarly to the two-phase austenitic-boride alloys (see Figure 2, *b*),

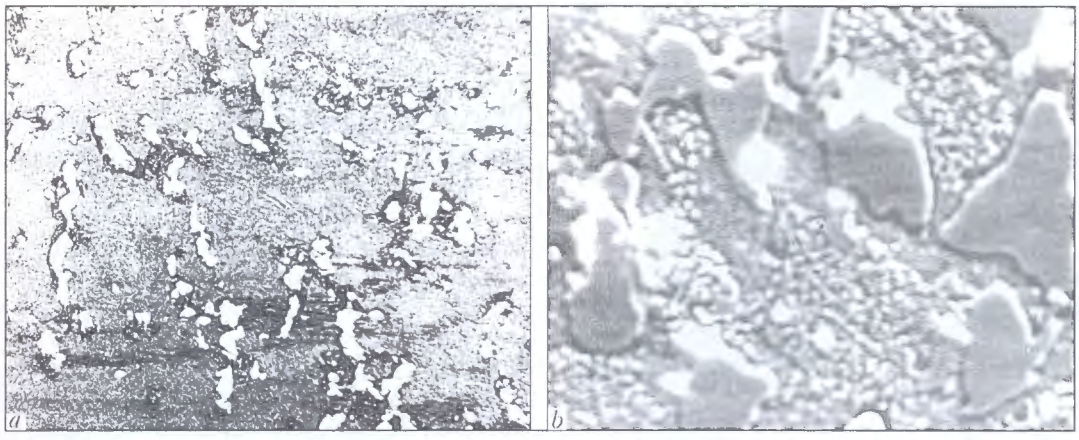

Figure 10. Microstructure of alloy LJ1-I revealed by optical (*a* — ×100) and electron (*b* — ×1000) microscopy

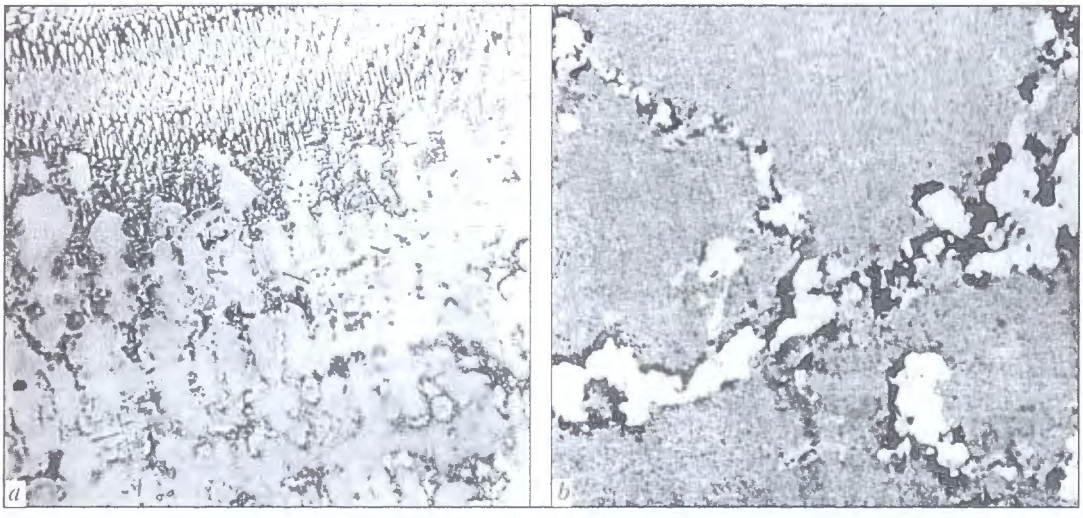

Figure 11. Microstructure of the weld zone in alloy LJ1-I: *a* — remelted regions of the γ + γ′ eutectic near the fusion line (×100); *b* — molten crystalline grain boundaries (×1000)

it is characterised by a high rate of restoration of ductile properties, compared also with OS alloy JS6-U.

Structure of alloy LJ1-I (Figure 10) in the as-cast condition consists of equiaxed crystalline grains with two types of inclusions located along the boundaries. These chains of relatively coarse globular inclusions of the γ + γ′ eutectic look light in optical microscopy and dark in electron microscopy. Finer inclusions (dark and light, respectively) are the inclusions of carbides and borides.

Structure of the alloy changes under the thermal effect of welding. Skeletons of dendrites are more pronounced in an overheated region of the weld zone (Figure 11, *a*). Regions of the newly formed eutectic are located near the fusion line in spaces between the axes and at the molten crystalline grain boundaries. These regions look light in optical microscopy. Because of a high cooling rate (compared with the rate of solidification of a casting) the intercrystalline layers of the melt in the weld zone solidify to form eutectics of a finer structure than that of the base metal (Figure 11, *b*). The new γ + γ′ eutectic is formed from the melt that joins low-melting point boride and carbide eutectics with the γ + γ′ eutectic of the base metal. The melt at the crystalline grain boundaries becomes additionally enriched with elements that dif-

Table 2. Distribution of alloying elements in structure of a welded joint in alloy LJ1-I

Specimen No.	*Specimen*		*Content of elements, wt.%*					*Relative content of elements* C_n/C_m*				
	Region	*Object*	*Al*	*Nb*	*W*	*Mo*	*Cr*	*Al*	*Nb*	*W*	*Mo*	*Cr*
1	Base metal	Crystalline grain axes	6.09	5.52	4.24	3.31	4.95			C_2/C_1		
2		Spaces between axes	6.40	6.05	3.80	5.02	6.42	1.05	1.09	0.90	1.52	1.34
3		γ + γ′ eutectic inclusions	7.81	7.62	0.72	1.10	2.11			C_5/C_3		
4	Weld zone	Spaces between axes	6.58	6.10	3.17	5.74	6.50	0.77	1.73	1.11	14.72	1.27
5		Phase at molten boundaries	6.00	13.19	0.80	16.20	2.69					

*Here C_1–C_3, C_5 is the content of elements in specimens 1–3 and 5.

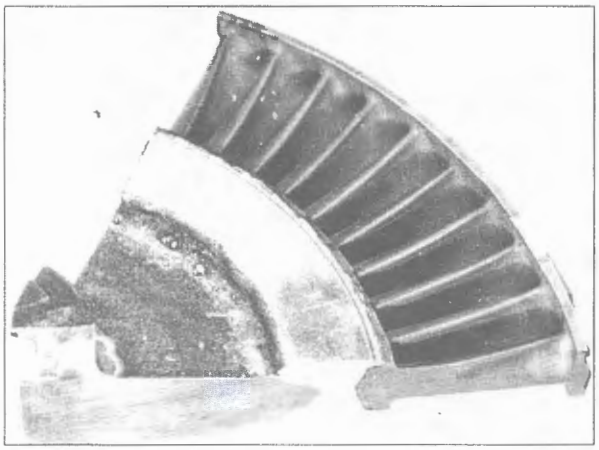

Figure 12. Appearance and macrostructure of specimen of a welded joint between the rotor with blades of alloy LJ1-I and disk of alloy EI698

fused into the liquid from the solid phase. Change in a composition of the eutectic results in a substantial increase in its molybdenum and niobium contents (Table 2).

Change in a composition of the melt results in change in temperatures of the eutectics. According to the data of [12, 14, 15], the melt enriched with aluminium, titanium and niobium, and the $\gamma + \gamma'$ eutectic are contained in intercrystalline layers of the weld zone in nickel alloys of the above type at 1150–1220 °C [12]. Therefore, temperature of the $\gamma + \gamma'$ eutectic may be lower than 1214 °C. This can explain the effect exerted by the γ'-forming elements (aluminium, titanium and niobium) on sensitivity to hot cracking of the weld zone, particularly by participation of these elements in formation of the low-melting point $\gamma + \gamma'$ eutectic of aluminium (Ni_3Al). According to our estimation, the range with a zero ductility of alloy JS6-U reaches a temperature of 1120 °C. In the OS alloys JS6-U and LJ1-I characterised by a high content of the $\gamma + \gamma'$ eutectic, the lower bound of BTR is higher and equals 1175 and 1150 °C, respectively. A high temperature gradient in the weld zone may change proportion of the eutectics formed from the intercrystalline melt. The first to solidify is the $\gamma + \gamma'$ eutectic. Under non-equilibrium conditions (high cooling rate), its composition can be close to that of the melt. By dissolving impurities, the $\gamma + \gamma'$ eutectic can prevent subsequent precipitation of lower-melting point eutectics. By enveloping the crystalline grain boundaries and promoting relaxation of stresses, it prevents hot cracking in the weld zone. However, in alloys with a low content of the $\gamma + \gamma'$ eutectic (alloy JS6-U etc.), it creates conditions for initiation of cracks by forming intermittent films, similarly to other eutectics.

Therefore, peculiarities of structure of alloy LJ1-I, i.e. presence of the second primary phase, the role of which is played by the eutectic of aluminium with the primary γ'-phase, determine its increased resistance to hot cracking in the weld zone, compared with unweldable alloys JS6-U and Inconel 738 close to it in composition.

Alloy LJ1-I is close to alloy JS6-U in content of the hardening γ'-phase and level of mechanical properties at room temperature and at a temperature of up to 900 °C [1].

The development of alloy LJ1-I made it possible to avoid the manufacture of blades with oriented solidification. Gas turbine blades of alloy LJ1-I are manufactured by a conventional technology of precision vacuum casting at the Zaporozhie Factory «Motor Sich». They are used for the manufacture of high-temperature welded gas turbine rotors for turbopiston engines (Figure 12) at the V.O. Malyshev Factory in Kharkov [1, 20].

1. Rovensky, I.L., Pinchuk, N.I., Yushchenko, K.A. (2001) Development of all-welded high-temperature turbine rotor for augmented turbopiston engines. *Dvigatelestroenie*, **3**, 11–13.
2. Medovar, B.I. (1966) *Welding of refractory austenitic steels and alloys*. Moscow: Mashinostroenie.
3. Eniskevich, V. (1976) Joining of parts from refractory alloys. In: *Refractory alloys*. Moscow: Metallurgiya.
4. Stephenson, N., Symonds, C.H., Thorneycroft, D.R. (1962) Welding of nickel alloys in heavy sections for power generating plant. *British Welding J.*, 9(**5**), 301–310.
5. Medovar, B.I., Chekotilo, L.V., Pinchuk, N.I. et al. (1964) Prevention of near-weld hot crack formation in arc welding of refractory alloy EI437B. *Aviats. Promyshlennost*, **5**, 77–79.
6. Santella, M.L., David, S.A. (1986) A study of heat-affected zone cracking in Fe-containing Ni_3Al alloys. *Welding J.*, **5**, 129–137.
7. Shorshorov, M.Kh., Klebanov, G.N., Gushchin, L.S. (1956) Study of kinetics of grain growth and changes in structure and mechanical properties of low-alloy steel in the weld zone. *Svarochn. Proizvodstvo*, **9**, 1–4.
8. Medovar, B.I., Pinchuk, N.I., Chekotilo, L.V. (1971) *Austenitic-boride steels and alloys for welded structures*. Kiev: Naukova Dumka.
9. Sorokin, L.I., Tupikin, V.I. (1985) Classification of refractory nickel alloys on the basis of their crack resistance. *Avtomatich. Svarka*, **5**, 23–25.
10. Bulatov, Yu.V., Loseva, G.I. (1977) Segregation of niobium and aluminium in nickel alloy welds. *Svarochn. Proizvodstvo*, **5**, 6–7.
11. Schmidtman, E., Eckel, W. (1983) An investigation into the tendency to hot cracking when X10NiCrAlTi 32 20 material is manual arc welded using electrodes of the X15NiCrNb 32 21 type of varying composition. *Welding and Cutting*, **6**, 92–94.
12. Bachle, E., Lesou, J. (1981) Quality of refractory alloy castings. In: *Refractory steels for gas turbines*. Moscow: Metallurgiya.
13. van Maaren, P.W. (1984) Polarisation and scanning electron microscopic investigation of corrosion and oxidation layers in IN 939 stator blades in a natural gas-driven turbine. *Practical Metallography*, **21**, 215–240.
14. Adam, P. (1981) Welding of high-strength alloys for gas turbines. In: *Refractory steels for gas turbines*. Moscow: Metallurgiya.
15. Owczarski, W.A., Duwall, D.S., Sillivan, C.P. (1962) A model for affected zone cracking in nickel-base superalloys. *Welding J.*, 45(**4**), 145–155.
16. Pinchuk, N.I., Ryazantsev, N.K., Rovensky, I.L. (2002) Welded joints of austenitic steel 25Cr–20Ni–2Si in augmented turbopiston engines. *The Paton Welding J.*, **6**, 13–18.
17. Zimina, L.N. (1977) Weldable refractory nickel alloys and principles of their alloying. *Metallovedenie i Term. Obrab. Materialov*, **11**, 2–7.
18. Yushchenko, K.A., Pinchuk, N.I., Nakonechny, A.A. et al. (1985) Investigation of weldability of cast refractory nickel alloys with 6 % aluminium. *Avtomatich. Svarka*, **10**, 18–24.
19. Kotov, V.F., Makhneva, G.A., Shvarts, V.I. et al. *Weldable blade alloy*. Pat. 8163 Ukraine. Int. Cl. C 22 C 19/03. Publ. 16.12.95.
20. (2001) High-temperature welded rotors of gas turbines. *Avtomatich. Svarka*, **4**, 32.

FATIGUE RESISTANCE OF WELDED JOINTS OF EXPERIMENTAL TITANIUM ALLOY T-110

S.L. ANTONYUK[1], V.N. KOROL[1], A.G. MOLYAR[1], V.N. ZAMKOV[2] and V.F. TOPOLSKY[2]
[1]Antonov ANTK, Kiev, Ukraine
[2]E.O. Paton Electric Welding Institute, NASU, Kiev, Ukraine

Strength and fatigue characteristics of TIG and EB welded joints in experimental ($\alpha + \beta$) titanium alloy T-110 of the Ti–Al–Mo–V–Nb–Fe–Zr system have been evaluated. TIG welding has been performed with an edge preparation and through penetration of plates with and without use of filler wire of the SP15 grade. Values of mechanical properties were compared with respective characteristics and also the life of welded joints of commercial alloy VT22.

Keywords: *arc welding, electron beam welding, titanium alloy, welded joint, heat treatment, fatigue strength*

Titanium alloys are characterized by a high specific strength, heat resistance at moderate temperatures and corrosion resistance in most aggressive media. Owing to these properties they are used widely in aircraft industry. Welding is one of the most widely spread and effective methods of joining allowing manufacturing intricate components, sub-assemblies and structures of different functional purposes. Aircraft welded structures from high-strength titanium alloys are used mainly under conditions of low-cycle loads which are characterized by a low frequency of loading (5–200 cycle/min), smooth change in load and fatigue mode of fracture. The life of the welded joint, made from high-strength alloy, depends on peculiar features of its structure, phase composition and degree of weld defectness. At testing the defect-free welded joints for a low-cycle fatigue, a linear dependence of their life on characteristics of strength and ductility was recorded [1].

Welding of titanium alloys in aircraft industry is performed, as a rule, by arc method with tungsten electrode in argon or by electron beam [2]. Each of these methods of welding has a specific effect on structure and phase composition of metal in different areas of the welded joint depending on the nature of its thermal cycle [3, 4]. The aim of the present work was to define the method of welding providing the highest fatigue life of welded joints at cyclic loading of the experimental high-strength titanium alloy T-110.

As parent metal, the 10 mm thick plates of alloy T-110 (chemical composition is as follows, %: Ti – base, 5.35Al; 1.1Mo; 1.37V; 5.04Nb; 1.6Fe; 0.35Zr; $0.09O_2$; $0.02N_2$; $0.003H_2$), produced by rolling of forging billets, were used (Table 1). Initial ingot of 380 mm diameter and 1000 mm length was melted in

Table 1. Mechanical properties of plates from alloy T-110

Metal condition	σ_t, *MPa*	$\sigma_{0.2}$, *MPa*	δ, %	ψ, %	*KCV, J/cm²*
As-rolled	1220	1190	17	54	21
Annealing (750 °C, 1 h, air cooling) – condition 1	1100	1080	20	55	46
Hardening heat treatment – condition 2	1165	1090	18	48	28

Note. Mean values from results of testing five specimens are given.

Table 2. Conditions of welding specimens from alloy T-110

Method of welding	*Number of passes*	*Welding current, A*	*Voltage, V*	*Welding speed, m/h*	*Wire feed speed, m/h*
Argon arc welding without filler wire (I)	1	450	12	15	–
EBW (II)	1	0.08	60,000	24	–
Argon arc welding with filler wire (III)	1	100	11	18	–
	2	180	10	9	9
	3	200	10	12	9

Notes. 1. Diameter of filler wire is 2.5 mm. 2. Figures I–III – welding methods.

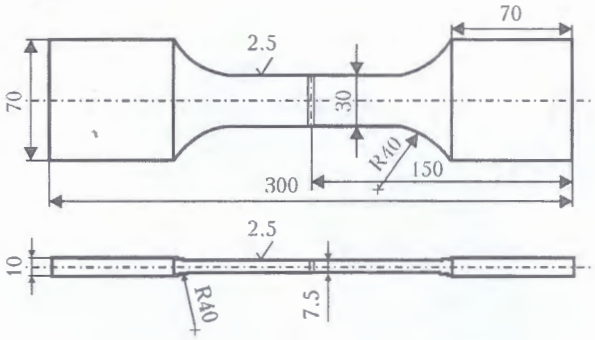

Figure 1. Sketch of specimen for fatigue test of welded joints

the cold hearth electron beam installation UE-121 (double remelting) and then subjected to forging and rolling for plates of 50 mm thickness. Forging was started in β-region (1180–1050 °C) and completed in (α + β)-region at 850 °C temperature. Then, the produced billets were rolled in (α + β)-region for 10 mm thick plates and subjected to shot-blasting treatment and etching.

Table 3. Conditions of testing welded specimens for low-cycle fatigue

Number of group of specimens	*Main loading*		*Marking block*	
	σ_{max}, *MPa*	P_{max}, *kN*	σ_{max}, *MPa*	P_{max}, *kN*
I	500	110	400	88
II	300	66	200	44

As-rolled alloy possesses a high strength and satisfactory ductility and impact strength. Annealing of alloy from two-phase (α + β)-region leads to the reduction in strength and increase in ductility due to elimination of the cold working deformation. The hardening heat treatment contributes to the increase in strength of the alloy after annealing. Here, the high level of ductility is preserved, whereas the impact strength of the alloy exceeds the level of its impact strength in as-rolled state.

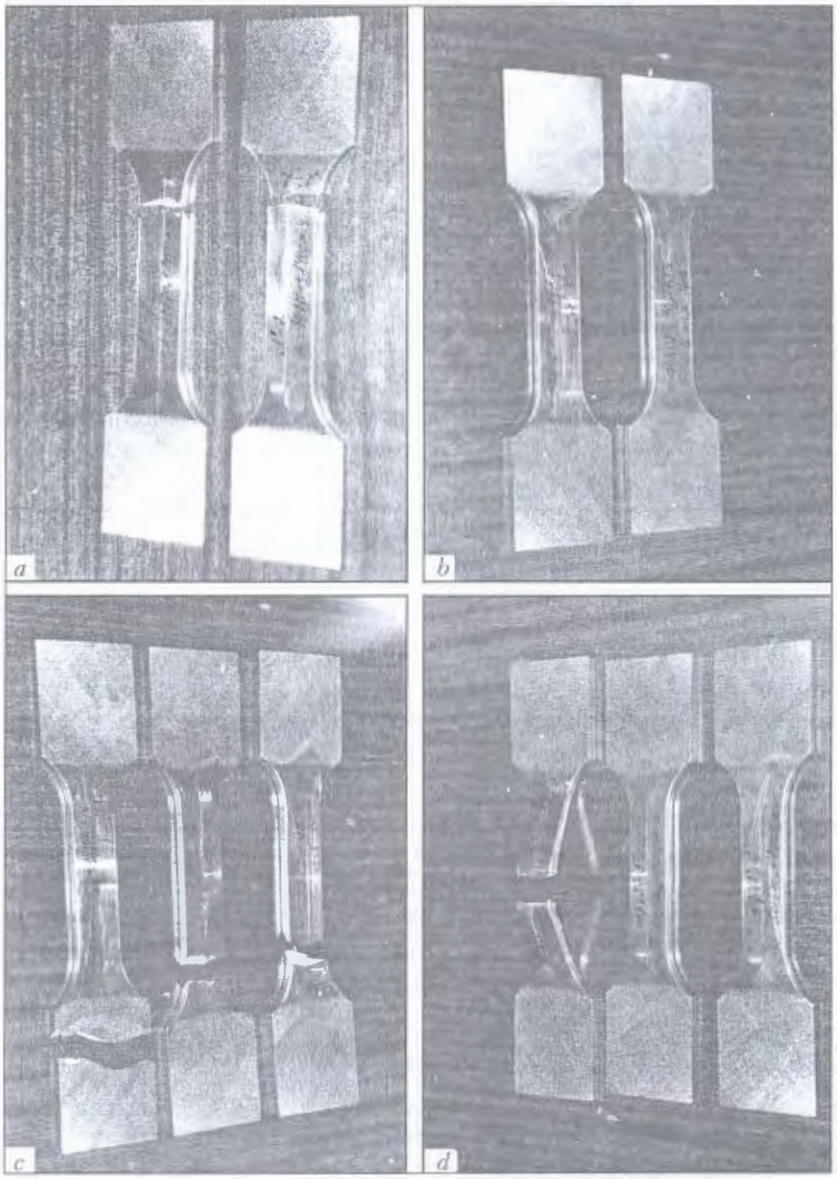

Figure 2. Appearance of specimens from T-110 alloy after tests: *a*, *b* — single-pass arc welding; *c*, *d* — EBW; σ_{max} = 500 (*a*, *c*) and 300 (*b*, *d*) MPa

Table 4. Mechanical properties of welded joints of alloy T-110

Method of welding	Heat treatment	σ_t, MPa	KCV, J/cm²		Place of fracture
			Weld	HAZ	
I	Annealing by condition 1	1070*	43	23	Weld
II	Quenching and ageing, condition 2	1150	27	22	HAZ
III	Annealing by condition 1	1030	35	38	Weld

*Mean values of properties from results of testing five specimens are given.

The butt joints were made by the automatic TIG welding for one pass without edge preparation and without the filler wire [5] and for three passes with an edge preparation. In this case a root weld was welded along the layer of flux ANT-23A without a filler wire. The second and third passes for filling a groove and producing a full size of the weld were made with the filler wire of SP15 grade [6]. A part of plates was welded using an electron beam. Welding conditions are presented in Table 2.

After welding the specimens were subjected to heat treatment. According to the results of preliminary investigations, the joints made by argon arc method (condition 1) had optimum mechanical characteristics after annealing at 750 °C temperature for 1 h and subsequent air cooling. Specimens, welded by electron beam (condition 2), were quenched in air from 870 °C temperature after holding at quench temperature for 30 min. Then, the specimens were subjected to two-stage ageing: holding at 380 °C for 8 h and at 550 °C for 2 h and air cooling [7].

Mechanical properties of welded joints were determined, such as fatigue resistance, impact strength of weld and HAZ metal. For fatigue tests the flat specimens of 300×70×10 mm size with 7.5 mm thickness of test part were manufactured (Figure 1). Specimens under cyclic loads were tested until fracture in universal servohydralic machines UIM-25 and UIM-40-2. 500,000 cycles were taken as reference operating time under the conditions of the given experiment and then the test was interrupted. Two groups of specimens by seven in each group were tested (by two specimens from each arc method and three specimens from the joints made by EBW). Loading was made from zero cycle ($R = 0$) at 3 Hz frequency. After each 5000 cycles a marking block, consisting of hundred from-zero cycles, was applied to the specimen. Maximum loads of from-zero cycles are given in Table 3.

As is seen from data of Table 4, the strength of metal of welded joints made by arc welding is close to that of parent metal after the heat treatment (see Table 1), and metal of joints made by EBW is actually similar to it. Values of impact strength of weld and parent metal are also close. Some reduction in characteristics *KCV* was observed in HAZ metal of joints made for one pass. Reduction in strength of metal of welded joints, made with a filler wire, as compared to those produced by the method of a single-pass weld-

Table 5. Fatigue properties of welded joints of alloy T-110

Method of welding	Number of specimen	Operating time, cycle	Place of fracture
		σ_{max} = 500 MPa, P_{max} = 110 kN	
I	I-1	74070 + (1400)	Radius transition
	I-2	74220 + (1400)	Same
II	II-1	451960 + (9000)	In machine clamp
	II-2	452960 + (9000)	Dent on specimen
	II-3	67000 + (1300)	Radius transition
III	III-1	49090 + (900)	Defect in weld metal
	III-2	91290 + (1800)	Radius transition
		σ_{max} = 300 MPa, P_{max} = 66 kN	
I	I-3	524150 + (10400)	Not fractured
	I-4	525550 + (10500)	Same
II	II-4	432720 + (8600)	Machine disconnection
	II-5	510840 + (10200)	Not fractured
	II-6	501570 + (10000)	Same
III	III-3	466930 + (9300)	Defect in weld metal
	III-4	503790 + (10000)	Not fractured

Note. In brackets the number of marking cycles is indicated.

ing, is due to the decrease in degree of weld metal alloying. The multipass welding influences favourably the impact strength of metal in HAZ and, therefore, the results obtained make it possible to recommend the wire SP15 for T-110 alloy welding.

It should be also noted that the values of strength and impact strength of welded joints of T-110 alloy correspond to those of welded joints from VT22 alloy [8] even after a simple annealing using condition 1. At the same time, the alloy VT22 joints require a multi-stage long-time heat treatment at a regulated rate of cooling. If the welded joints of alloy T-110, made by EBW, to subject to hardening heat treatment, then the level of values of their mechanical properties will exceed those of joints made from alloy VT22.

Appearance of specimens after fatigue tests is given in Figure 2, and the results obtained are given in Table 5.

As is seen from data, given in the Table, almost all the specimens tested at load of the second level (300 MPa) were not fractured after reference 500,000 cycles, except two specimens. One of them (No.II-4) withstood 432720 + (8600) cycles and fractured as a result of emergency disconnection of the test machine. The fracture of the second (No.III-3) specimen after 466930 + (9300) cycles was caused by the presence of a technological defect in weld metal. In both cases the premature fracture of specimens was not due to method of welding or peculiarities of phase composition and microstructure of welded joints. Quality of manufacture of specimens made a determinant influence on the results of testing specimens of welded joints at the load of the first level (500 MPa). Thus, four specimens of joints made by different methods of welding were fractured in a parent metal at the far distance from weld in an area of a radius transition at load from 67000 + (1300) up to 91290 + (1800) cycles. Two specimens made by EBW were fractures at load of 451960 + (9000) and 452960 + (9000) cycles in clamps of test machine and due to a dent at the specimen surface, respectively. Only one specimen (No.III-3) fractured in weld due to the presence of a technological defect in it. These results do not show the objective values of operating time of specimens before their fracture and, consequently, they are not true values of life of the welded joints. Nevertheless, they can state that at the absence of the technological defects the performance of welded joints of alloy T-110 at cyclic loading (σ_{max} = 500 MPa) does not depend on the method of welding.

CONCLUSIONS

1. Strength properties of T-110 alloy joints made by arc welding are 0.93–0.97 of those of the parent metal, and in EBW this characteristic reaches a unity. Here, all the joints are characterized by high values of impact strength, most typical of welds made by arc methods for one pass and HAZ of joints made for several passes.

2. It is recommended to use wire of SP15 grade as a filler wire for multipass arc welding of T-110 alloy.

3. Results of fatigue tests of welded joints of T-110 alloy at 500 MPa load showed the similar operating time as the typical welded specimens of VT22 alloy.

4. At 300 MPa load the life of specimens reached the reference operating time and then they were removed from tests without fracture.

1. Gurevich, S.M., Kulikov, F.R., Zamkov, V.N. et al. (1975) *Welding of high-strength titanium alloys*. Moscow: Mashinostroenie.
2. Krivov, G.A., Ryabov, V.R., Ishchenko, A.Ya. et al. (1998) *Welding in aircraft industry*. Kiev: MIIVTs.
3. Antonyuk, S.L., Molyar, A.G., Kalinyuk, A.N. et al. (2003) Titanium alloys for aircraft industry of Ukraine. *Advances in Electrometallurgy*, **1**, 9–13.
4. Antonyuk, S.L., Molyar, A.G. (2002) Composition and properties of high-strength titanium alloys of electron beam remelting. In: *Proc. of Interbranch Sci.-Pract. Conf. on Problems of Development of New Materials for Aerospace Industry for the 21st Century*, Moscow, June 25, 2002. Moscow: VIAM.
5. Gurevich, S.M., Zamkov, V.N., Blashchuk, V.E. et al. (1986) *Metallurgy and technology of welding of titanium and its alloys*. Kiev: Naukova Dumka.
6. Zamkov, V.N., Topolsky, V.F., Tyapko, I.K. (1996) Wire for welding of titanium ($\alpha + \beta$)-alloys. *Avtomatich. Svarka*, **7**, 51–52.
7. Topolsky, V.F., Kishkina, S.I., Stronina, L.A. et al. (1983) Strength of welded joints of VT23 alloy in repeated-static load. *Ibid.*, **7**, 42–44.
8. Zamkov, V.N., Shevelyov, A.D., Tyapko, I.K. (1989) Peculiarities of electron beam welding of tubular billets from titanium alloy VT22. *Ibid.*, **2**, 40–44.

APPLICATION OF PSh107 TYPE SEMI-AUTOMATIC MACHINES OF A MODULAR DESIGN FOR WELDING, SURFACING AND CUTTING OF STEELS AND ALUMINIUM*

B.E. PATON[1], V.A. LEBEDEV[1], V.G. PICHAK[1], B.Ya. URUMBAEV[2], A.A. KHUDOJNAZAROV[2] and A.N. SAIDOV[2]
[1]E.O. Paton Electric Welding Institute, NASU, Kiev, Ukraine
[2]Tajik Aluminium Plant, Tursunzade, Tajikistan

The paper deals with the main aspects of application of a broad series of various-purpose semi-automatic machines of a unified modular design, developed from the basic model of semi-automatic machines of PSh107 type and designed for welding, surfacing and cutting. These machines were put into operation at the Tajik Aluminium Plant. Typical processes, using new semi-automatic machines, as well as their service conditions, are described. Rationality of integrated implementation of the semi-automatic machines, developed using common basic components, is substantiated and confirmed. These machines are shown to have wide capabilities in terms of technological application and further upgrading.

Keywords: *arc welding, welding modes, surfacing, cutting, semi-automatic machine. operating cycle, production, introduction, operation, reliability, repairability*

PWI developed a series of semi-automatic machines of a unified modular design, proceeding from the basic model of PSh-107V semi-automatic machine [1, 2]. Engineering solution realized in the semi-automatic machines envisages fitting them with all the required additional components and modules, which allows performance of various processes of welding steels and aluminium alloys, as well as their surfacing and cutting. The developed semi-automatic machines have already become applied in industry [3, 4]. Both solid and self-shielded flux-cored electrode wires are used in them, and various welding current sources are applied, which is one of the conceptual solutions in development of this kind of mechanized equipment. When evaluating its capabilities and taking into account the experience of industrial application of individual semi-automatic machine designs, developers came to the conclusion that it is rational to analyze the results of integrated application of various-purpose semi-automatic machines in one plant. Moreover, this would allow evaluation of the actual effectiveness of modular semi-automatic machines in terms of simplifying their setting-up and readjustment, service, repair and provision of spare parts and consumable materials, reliability of equipment operation, its loading, which ultimately determines the engineering excellence of the semi-automatic machines.

Over the recent years PWI and Tajik Aluminium Plant (TAP) started joint work to improve the elements of current-carrying parts of electrolyzers. PWI specialists noted the large scope of work, performed by TAP technical services to maintain the operating condition of plant equipment and prepare the electrolyzers for operation. Most of the work, conducted in this plant, is related to welding, surfacing and cutting of steels, cast iron and aluminium alloys. In this case, most of the welding and surfacing processes were based on the use of stick electrodes. TAP employs several hundred manual arc welders, and a much smaller number of semi-automatic machine operators, which perform just the current repair of the main (electrolyzers) and auxiliary (cranes, mills, vehicles, etc.) equipment. Based on the gained experience, very often it was possible to simplify the welding and surfacing work, and well as increase its effectiveness and quality. Considering the specifics of TAP operation as a high-capacity non-ferrous metallurgy plant, special features of its location and the related logistic and scientific support problems, it may be stated that practically ideal conditions and possibilities are in place for introducing a series of various-purpose semi-automatic machines of a modular design to solve the problems of welding, surfacing and cutting of steels, cast iron, and aluminium alloys.

To simplify service and provision of spare parts, as well as to enable application of various sources of welding current, available at the plant (VDU-504, VDU-506, VDU-300, VDS-600, VDG-303), all the types of semi-automatic machines should have the same basic components. Design of semi-automatic machines of PSh107 type, developed at PWI, fully satisfies these requirements. It includes a feed mechanism with systems of control and adjustment, as well as a self-sufficient power unit. However, such a design of the semi-automatic machine requires certain retrofitting, taking into account the special conditions of machine operation at TAP (high temperatures in the

*I.S. Kuzmin and V.D. Fyodorov participated in introduction of the series of semi-automatic machines at TAP.

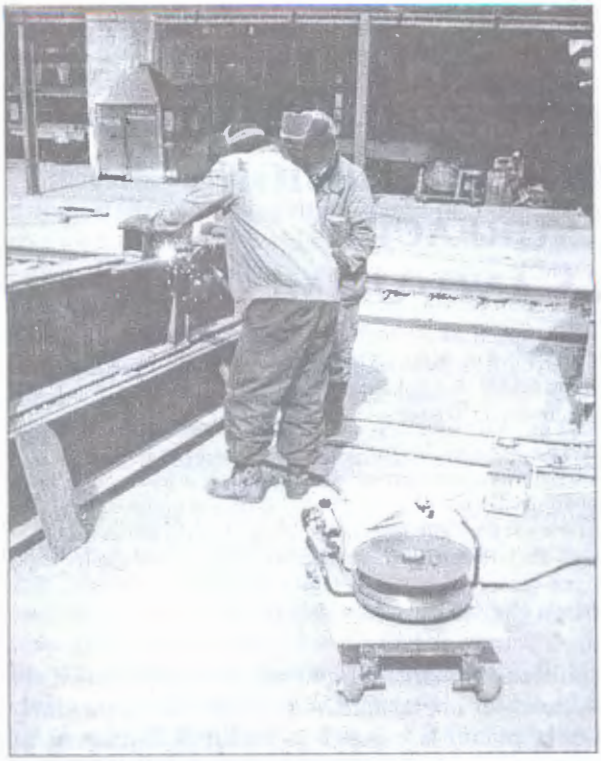

Figure 1. Performance of welding of horizontal welds on a vertical plane of the skin of an electrolyzer case with PSh-107V semi-automatic machine

operating zone of electrolyzers, where repair welding should be performed, high load during welding and surfacing, long duty cycles). It is also necessary to take into account the qualification of technologists, welders and repair personnel.

During performance of joint work with TAP nine modifications of semi-automatic machines were adapted to plant conditions. Theses machine cover practically the entire range of operations on welding, surfacing and cutting. The scope of delivery included the following semi-automatic machines:

- PSh-107V — two modifications, including the one with power supply from arc voltage for self-shielded flux-cored electrode wire welding in site;
- PSh-107VA — two modifications for welding aluminium with electrode wires of different diameters;
- PSh-107VN — two modifications for surfacing with self-shielded flux-cored surfacing electrode wires of different diameters;
- PSh-107G — two modifications for gas-shielded welding with thin solid electrode wires;
- PSh-107R — one modification for submerged-arc welding and surfacing with solid electrode wires.

Alongside the above equipment, also the electrode wires and fluxes required for operation were selected, taking into account the technological requirements to solve the problems of welding, surfacing and cutting at TAP, as well as the capabilities of semi-automatic machines.

Let us consider specific objects and conditions, where certain modifications of modular semi-automatic machines were used.

During scheduled repair of components and cases of electrolyzers, welding was performed with self-shielded flux-cored electrode wires of PP-AN1 type. Basic model of PSh-107V semi-automatic machine with VDU-506 and VS-300 welding current sources was used. This work done earlier with semi-automatic machines of A765 type, which perform welding with self-shielded flux-cored electrode wire of PP-10 grade.

Application of semi-automatic machines PSh-107V with smooth adjustment of welding modes and availability of process feedbacks, as well as PP-AN1 electrode wire allowed considerably simplifying the welding process, in particular on a vertical plane and in the semi-overhead position, improving the welding efficiency, specifically due to greater deposition coefficient, and, above all, significantly improving the quality of the weld (reducing the number of defects, metal losses for spatter, improving formation, etc.).

Figures 1 and 2 show welding stations for welding an electrolyzer case (horizontal and vertical welds are made on a vertical plane of steel sheets 10 to 20 mm thick under the conditions of open repair sites) and welding of a steel boss of 104 mm diameter to the anode-holder rod in the shop. Characteristic features of flux-cored electrode wire welding are the large scope of work performed and high requirements to the mechanical properties of welded joints. So, for instance, several hundred anode-holders are repaired in the plant every day, each of which should stand a load of 1–10 kN.

In addition to welding with flux-cored self-shielded wires, the plant further performs cutting of various structural elements, using special cutting electrode wire. This, for instance, is cutting off the worn bosses of anode-holders (Figure 3), cutting technological holes in steel structures of electrolyzer cases (Figure 4), and cutting out worn sections of electrolyzer cases. At cutting of bosses (diameter of worn section is up to 100 mm, which is greater than the guaranteed values of semi-automatic machine operation in the cutting mode) power source of VS-600 type was used, and when technological holes were cut out VDU-506 type power source was used. It is important to note that only manual gas-cutting de-

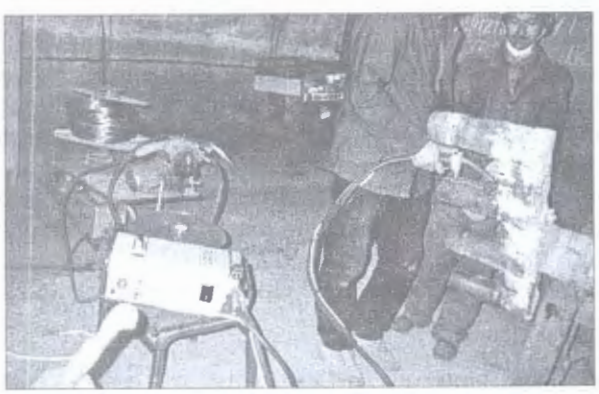

Figure 2. Welding of a boss to anode-holder (circumferential welds) with PSh-107V semi-automatic machine

Figure 3. Cutting of anode-holder bosses with PSh-107R semi-automatic machine

vices had earlier been used at TAP. These devices have such disadvantages as low manoeuvrability, use of quite dangerous energy carriers, etc. Performance of arc cutting with PSh-107R semi-automatic machines allows in a number of cases significantly simplifying this process and improving safety. This, in particular, goes for repair of electrolyzer cases, where cutting efficiency can also be increased.

During repair of electrolyzer cases semi-automatic machines PSh-107V (for welding) and PSh-107R (for cutting) often replaced each other, when required. In this case a cassette with the appropriate wire was mounted, current conduit was changed, and some adjustments were made. All these operations took not more than 5–7 min. Figure 5 gives an idea of the scope of repair work, performed on anode-holders.

The process of welding a kiln case turned out to be quite complicated (diameter of the steel structure was 3 m). To make welds of the required quality and improve the efficiency of operations, it was necessary to perform CO_2 welding of inner circumferential welds with solid electrode wire of 1 or 2 mm diameter into an X-shaped groove, and self-shield flux-cored wire welding of outer welds. This required application of two types of semi-automatic machines, namely the above PSh-107V semi-automatic machine and PSh-107G semi-automatic machine for CO_2 welding. Figures 6 and 7 show fragments of welded joints of a

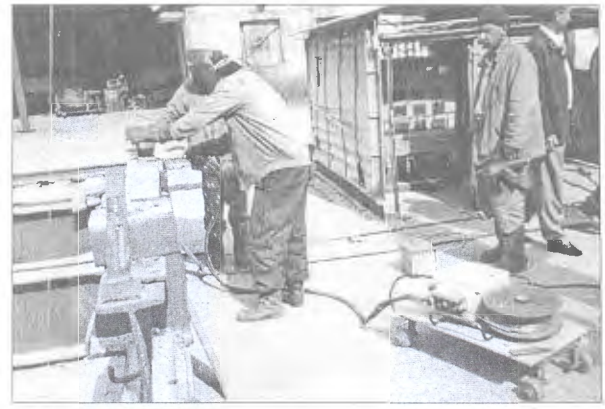

Figure 4. Use of PSh-107R semi-automatic machine for cutting out a technological hole in an electrolyzer case

kiln, made with two types of semi-automatic machines.

A large number of cast iron products (reduction gear cases, process equipment beds, electric motors, etc.) has accumulated at the plant, which require repair. Previously, cast iron metal structures were seldom repaired at TAP. If the components or parts could not be replaced, but needed repair, manual arc welding with special electrodes was used. This is a labour-consuming and not always successful process. Therefore, welding of steel began to be performed with PSh-107G semi-automatic machine, using PANCh-11 electrode wire, which allowed solving most of the problems in performance of repair operations under the conditions of TAP. Welding of different components to be repaired was performed both in CO_2 and argon. Figure 8 shows welding with PSh-107G semi-automatic machine of a crack in the case of a powerful reduction gear. It should be noted that some large-sized components and parts of cast iron also require preheating with subsequent cooling, as well as cutting out the crack location and certain sequence of weld deposition.

In a number of cases the main scope of the work consisted of different variants of welding the aluminium structures of electrolyzers, namely elements of the bus system and contact pads. The task was made more complicated by the need to perform welding in the operating electrolyzers, which were under load (current of 160–220 kA). Here two problems

Figure 5. Storage of anode-holders to be repaired, using welding and cutting

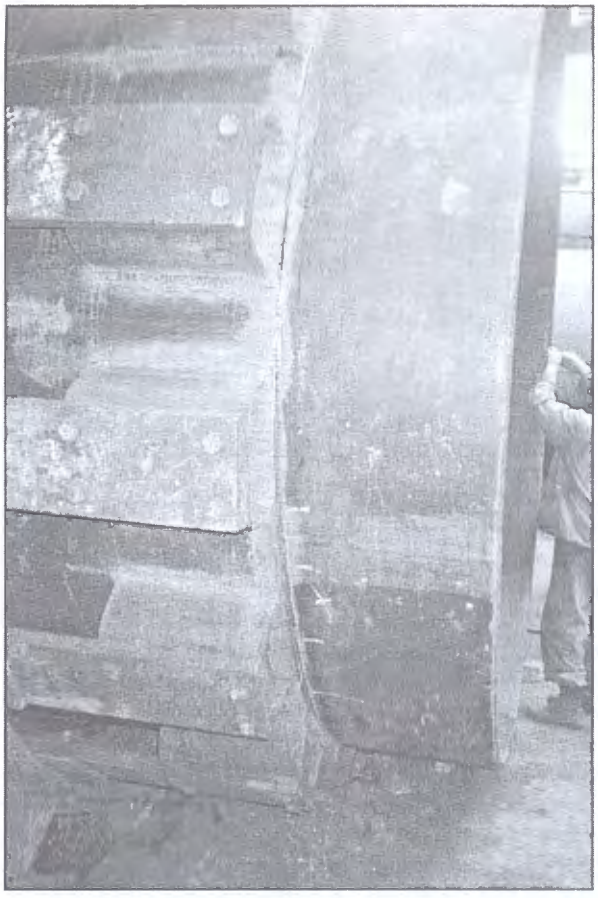

Figure 6. Fragment of a kiln with grooving for making a circumferential weld

had to be solved simultaneously, namely following the safety rules and ensuring a stable arc process in strong magnetic fields (external relative to welding location).

Welding of elements of aluminium structures of electrolyzers without load did not run into any serious problems. In this case we used PSh-107VA semi-automatic machine with a gun-type holder of a novel design in a set with welding power source VDU-506, which performs welding with electrode wire of 2 mm diameter in argon. Aluminium contact pads welded by PSh-107VA semi-automatic machine are shown in Figure 9.

This work was earlier performed with PRM-2 semi-automatic machine, using aluminium electrode

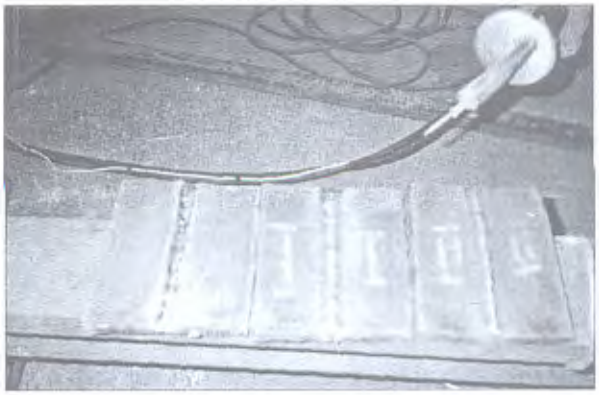

Figure 7. Welded joints of a kiln made with PSh-107V and PSh-107G semi-automatic machines in different positions

Figure 8. Welding up a crack in the case of a reduction gear using PSh-107G semi-automatic machine

wire of 1.2 mm diameter. Application of PSh-107VA semi-automatic machines in welding of aluminium contact pads allowed a 2 to 3 times increase of the efficiency of welding operations, and, this being particularly important, significantly improving the welded joint quality in terms of its mechanical properties and transient electric resistance. Measurement of voltage drop across this current conduit section leads to the conclusion that in this case the voltage decreased by 10–15 %.

It should be noted that the scope of this kind of work is quite large, and in our opinion, small-scale mechanization systems can be used here in the form of mechanized transportation device developed at PWI, for hose semi-automatic machine PSh-107VA. It turned out to be very complicated to achieve a stable welding process and satisfactory formation of the welded joint on an electrolyzer in the working condition.

We suggested and put into practice a set of devices, allowing a significant simplification of welding in strong magnetic fields. These devices, conditionally called magnetic shields, combined with a highly stable feed of electrode wire and a certain set of feedbacks, enabled producing a stable arcing and satisfactory formation of the welded joint at this stage under specific conditions. However, results of subsequent application of magnetic shields, made to have the same geometrical dimensions and of the same materials as for test welding, showed that in the welding location

Figure 9. Aluminium contact pads for fastening electrolyzer anodes welded with PSh-107VA semi-automatic machines

Figure 10. Repair welding of elements of an aluminium busbar in an operating electrolyzer with semi-automatic machine PSh-107VA using magnetic shields

it was possible to weaken the field by 30 to 50 times, whereas proceeding from the calculations, these fields should be reduced 100 to 150 times to achieve the necessary quality of welding. This work is currently being carried on. Figure 10 shows welding of elements of a powerful aluminium busbar in an operating electrolyzer, using PSh-107VA semi-automatic machine.

It is appropriate to mention here those difficulties, which have to be overcome in welding of aluminium structures in those locations, which have already been welded many times, also using outdated technologies, namely carbon electrode welding. As shown by analysis, the metal in many regions of these welds cannot be identified by its composition. It is impossible to perform sound welding of such metal, and still less feasible to produce a joint with minimum electric resistance. When doing the repair, it is recommended to cut out this metal and deposit a new layer of aluminium. All these operations should be performed using the above semi-automatic machines, as for instance on contact pads of electrolyzers (see Figure 9).

One of major problems at TAP is reconditioning and strengthening of a broad range of components and parts. These are seats of reduction gears, mill hammers, wheel pairs of intraplant vehicles, tractor and bulldozer components, and crane wheels (Figure 11). About one thousand of the latter are currently in operation and repair. In order to solve the problems of their surfacing, we also proposed PSh-107VN semi-automatic machines with the appropriate set of components with special adjustment of process feedbacks, using the appropriate types of self-shielded flux-cored wires, developed at PWI.

Surfacing of the bodies of revolution (shaft axes, crane wheels) was performed at rotation in a special machine tool. In this case the hose holder of the semi-automatic machine is held by the welder or fastened with a special cleat on the machine-tool carriage. Such surfacing was earlier performed at TAP with the above-mentioned electrode wires of PP-10 type by submerged-arc process. However, such a simple and relatively inexpensive technology and materials permitted just reconditioning the parts and components.

We suggested using special self-shielded electrode wires of PP-Np-80Kh20RZT-S (PP-AN170), PP-Np-30Kh5G2SM-S (PP-AN122), PP-Np-200Kh15S1GRT-S (PP-AN125) type. Their application makes the process of reconditioning of the components and parts somewhat simpler, and one more task is solved, namely that of strengthening of the working surfaces of the above products.

Results showed that in terms of mechanical properties of the deposited metal and its appearance, as well as efficiency, these surfacing operations are acceptable for the production conditions at TAP and may considerably extend the interrepair period of critical process equipment. PWI suggested application of automatic arrangement of the deposited beads for surfacing further on. A number of adjustable electrode wire oscillators were developed for this purpose.

Introduction of a series of modular semi-automatic machines of PSh107 type at TAP involved training of a large group of welders and adjusters (35 persons). During training they assimilated theoretical knowledge and skills of setting up and performance of various welding, surfacing and cutting processes. Welders, which included some highly experienced and qualified specialists, readily mastered the new systems. They acquired high skills in mechanized arc processes and gave quite high estimates of the new equipment.

The performed work enabled outlining the plans for further introduction of mechanized arc welding equipment of PSh107 type at TAP, which was designed by the modular principle with a significant increase of the number of semi-automatic machines

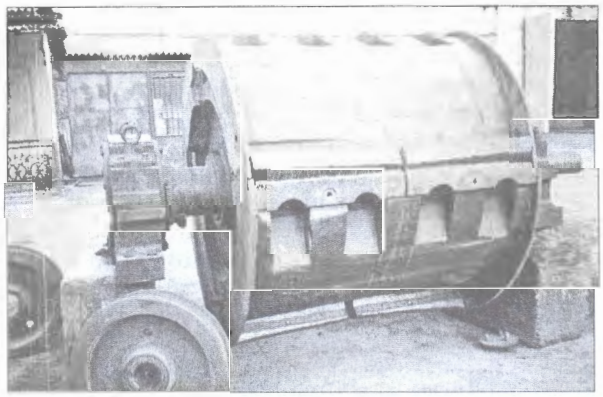

Figure 11. Components and parts for part reconditioning by surfacing

and widening of their range (semi-automatic machines for aluminium welding with electrode wires of 3 mm diameter, semi-automatic machine for fitting small-scale mechanization devices, when they are used for welding and surfacing, etc.). Further on additional activities are planned on welding aluminium busbars in the operating electrolyzers in magnetic fields. For this purpose, in addition to the above measures, it is intended to apply pulsed methods of control of electrode metal transfer into the pool. Effectiveness of application of semi-automatic machines with a pulsed feed of electrode wire was confirmed during performance of experimental work at PWI with simulation of strong magnetic fields. It was determined that welding with a pulsed feed of electrode wire, when applied on electrolyzer current-carrying elements (aluminium buses, steel anode-holders) greatly influences the lowering of transient resistance in the welding location [5].

Experience of a broad integrated introduction of a series of semi-automatic machines of PSh107 type in one plant so as to solve practically the entire range of problems of welding, surfacing and cutting under different conditions, using equipment designs, developed from one basic model, demonstrated that such equipment, its concepts and methods of design, of ensuring its repairability and reliability are justified, cost-effective and rational. This is also confirmed by joint plans and agreement on further wide-scale introduction of modular semi-automatic machines, as well as small-scale mechanization means, based on them, at TAP. Results of the presented integrated introduction of a series of semi-automatic machines of PSh107 type may be useful also for other plants facing similar tasks of implementation of arc processes for various purposes.

1. Lebedev, V.A., Pichak, V.G. (1997) New modular equipment for mechanised consumable-electrode arc welding, surfacing and cutting. *Svarochn. Proizvodstvo*, **7**, 32–36.
2. Lebedev, V.A., Pichak, V.G. (1998) Semi-automatic machines of PSh107 type for welding and surfacing. *Avtomatich. Svarka*, **7**, 38–42.
3. Lebedev, V.A., Pichak, V.G., Rogatkin, A.A. et al. (1997) Semi-automatic machine for consumable-electrode arc welding of aluminium and its alloys. *Ibid.*, **11**, 51–56.
4. Lebedev, V.A. (1999) Mechanised consumable-electrode arc welding. In: *Abstr. of pap. of 1st Ukr. Sci.-Techn. Conf. on Current Technologies and Equipment in Gas-Thermal Processes of Reconditioning and Recycling of Parts of Machinery and Structures*, Kiev, Oct. 27–29, 1999. Kiev: KPI.
5. Paton, B.E., Lobanov, L.M., Grigorenko, G.M. et al. (2001) Energy- and resource-saving technologies and equipment in welding of aluminium busbars in graphitised carbon manufacturing. *Svarochn. Proizvodstvo*, **1**, 1–35.

IMPROVEMENT OF ENERGY EFFICIENCY OF RESONANT WELDING SOURCES BASED ON MODULAR STRUCTURES

A.E. KOROTYNSKY
E.O. Paton Electric Welding Institute, NASU, Kiev, Ukraine

Peculiarities of operation of the resonant-type welding equipment based on a modular principle are considered. It is shown that this approach allows energy consumption to be decreased and also reliability of operation of the equipment to be substantially improved. Simplified calculation of the transition process in module on-off is given and it is shown on its base that the disturbances by current in welding circuit are eliminated as a result of a dynamic mutual compensation.

Keywords: *arc welding, resonant welding unit, energy saving, module, dynamic compensation*

Raw material and energy deficit, the lack of which is experienced even in the industrialized countries, demands from designers of welding equipment for search of effective methods of significant improvement of parameters of material- and energy-saving in the creation of new types of welding arc power sources. The idea of a multichannel conversion of power flow which was studied in works [1–3], is most challenging. As regards to power units, based on high-frequency converters, the algorithms of conversion of power parameters are suggested in [1, 2] using the methods of a quasi-single-sideband modulation. However, their practical realization requires the use of completely controllable power commutators (transistors) and auxiliary filters-transformers that is not always rational from the economical point of view.

Often, the electrical units, which include also the welding equipment, are designed with a parallel connection of similar modules, whose power parameters define the total capacity of the unit as a whole. As regards to the welding equipment, the problems of the modular designing had already been considered in [3, 4], however, the problems of optimum operation from the point of view of a minimum consumption of electric energy within the wide range of adjustment of welding currents were not analyzed. Here, two approaches are possible: first approach, when all the modules, included into the unit structure, are operating under the conditions of a uniform loading; the second approach, when the minimum quantity of modules is loaded, which is defined by a load capacity, while the rest ones are spare. The second condition at definite conditions allows significant improvement in such parameter of the welding equipment as «duty cycle», as there is a feasibility to connect modules periodically from the reserve.

It is known [5] that the welding equipment based on resonant converters, is characterized by high energy properties. Interest is attracted by the problem of investigation of methods of modular organization of structures of welding power sources, as in accordance with the classification [3] the resonant welding modules refer to direct symmetrical converters, where each of them is described by appropriate Y_j-matrix:

$$Y_j = \begin{vmatrix} 0 & Y_{12} \\ -Y_{12} & 0 \end{vmatrix}. \qquad (1)$$

In connection of n of similar modules in parallel in input and output (so-called a parallel-parallel connection) we shall obtain a welding unit, for which it is possible to write

$$\begin{vmatrix} I_1 \\ I_2 \end{vmatrix} = Y_m \begin{vmatrix} U_1 \\ U_2 \end{vmatrix} = \begin{vmatrix} 0 & ny_{12} \\ -ny_{12} & 0 \end{vmatrix} \cdot \begin{vmatrix} U_1 \\ U_2 \end{vmatrix}, \qquad (2)$$

where I_1, I_2 and U_1, U_2 are the input and output current and voltages of the unit, respectively; Y_m is the matrix, presetting the modular design.

Input and output currents are determined by the expressions

$$\begin{aligned} I_1 &= nU_2y_{12}, \\ I_2 &= -nU_1y_{12}. \end{aligned} \qquad (3)$$

Expressions (3) prove that at a parallel-parallel connection of n modules, forming the welding unit, the consumed current I_1 and welding current I_2 are n times increased.

It should be noted that three more variants of modules connection are possible, which could be used in the design of equipment for welding and plasma technologies. This is a parallel-series connection (inputs are connected in parallel, while the outputs are series connected) and also series-parallel and series-series connections.

Let us consider more in detail the variant of a parallel-parallel connection, which schematic diagram is given in Figure 1. A separate module, for example *M1*, is designed on the base of a welding transformer *WT* and capacitance reactor *Cp*[*]. Inputs and outputs of all the modules are commutated by appropriate electronic switches K_{jx} and K_{jy}. Commutation in output circuits of modules is obligatory, as the non-operating resonant circuit will create an additional load. If to use a rectifier in the secondary circuit, then the output switches can be eliminated. The device

[*]It should be noted that these diagrams were investigated for the first time in [6], and in [7] the use of electrolytic capacitors with an inverse-parallel method of connection in them was offered. The latter allowed designing of sufficiently small-sized welding units.

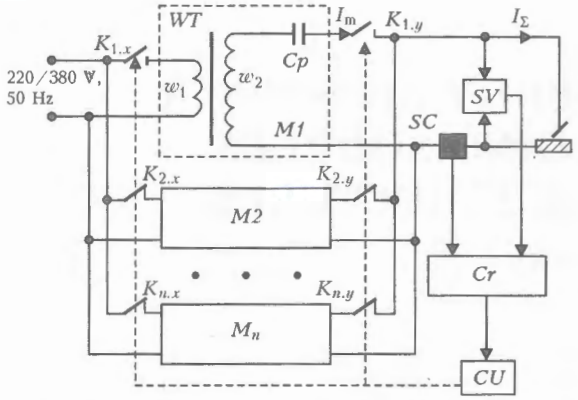

Figure 1. Schematic diagram of resonant power source with a parallel-parallel connection of modules

is furnished with sensors of current *SC* and voltage *SV*, whose outputs are connected to the controller *Cr*. The latter realizes an algorithm of optimum connection of modules using the commutation unit *CU*.

The described design of the welding unit, based on a modular principle, is characterized by one more advantages, except advantages of a feasibility of reserving, an additional resource in duty cycle, and also a sufficiently thorough control of the output capacity, namely improved parameters of energy saving. This will be shown on the example of the following calculations. Let us to preset the welding current $I_w = I_\Sigma$ which is determined by some system of modules. Then, the load on each connected module is $I_m = I_\Sigma/k$ and it should not exceed the maximum allowable load, i.e. $I_m \le I_{al}$. Hence, it is possible to determine the minimum number of modules, capable to provide the required current of welding $k_{min} =]I_\Sigma/I_{al}[$, where the reverse square brackets denote the roundoff values up to the closest integral number.

Let us select the model of losses of electric energy in module in the form of a linear polynomial $P_l(I_m) = P_{no\text{-}load} + \alpha I_m$, where $P_{no\text{-}load}$ are the losses defined by the no-load condition; α is the coefficient characterizing the additional losses in active condition. Using this representation, let us calculate losses in case of a uniform and optimum loading of modules. Here, we shall take into consideration that the welding unit is operating at a load lower than the allowable load. At all modules connected, each of them has the current I_{m0}, and at «k» of modules connected the current is

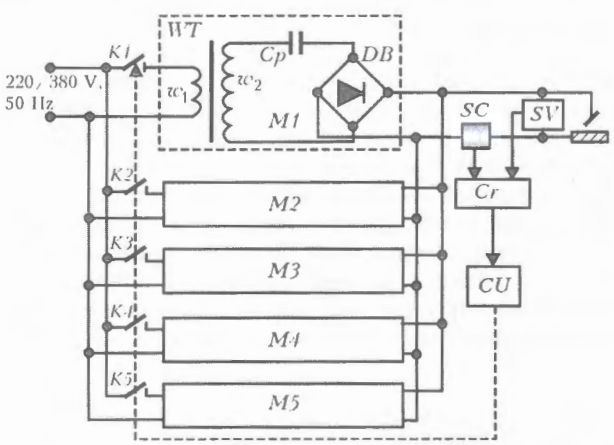

Figure 2. Simplified diagram of five-module resonant welding source made according to parallel-parallel scheme of connection

equal to $I_k = (n/k)I_{m0}$. Consequently, the total losses have a form

$$P_l(n) = nP_{no\text{-}load} + n\alpha I_m, \quad (4)$$

$$P_l(k) = kP_{no\text{-}load} + n\alpha I_m. \quad (5)$$

Difference between (4) and (5) defines the absolute value of advantage by power in case of non-uniform loading of modules and is equal to

$$P_l(n) - P_l(k) = (n - k)P_{no\text{-}load} = mP_{no\text{-}load}, \quad (6)$$

where m is the number of disconnected modules.

Expression (6) proves that at linear model of losses the advantage by power is attained by reducing the no-load losses.

If to preset the quadratic dependence of losses in module on welding current in the form of $P_l(I_m) = P_{no\text{-}load} + \alpha I_m + bI_m^2$, then the expressions for total losses can be presented in the following form:

$$P_l(n) = n(P_{no\text{-}load} + \alpha I_m + bI_m^2), \quad (7)$$

$$P_l(k) = kP_{no\text{-}load} + n\alpha I_m + b(n^2/k)I_m^2. \quad (8)$$

Thus, the reduction in losses in the given case is determined by the first and third summands, i.e.

$$P_l(n) - P_l(k) = (n - k)P_{no\text{-}load} - bn(n/k - 1)I_m^2. \quad (9)$$

To determine the optimum number of modules as a function of a preset current of the welding unit, we shall find the maximum of expression $[P_l(n) - P_l(k)]$. Using the derivative $d[P_l(n) - P_l(k)]/dk$ and, making it equal to zero, we shall obtain

$$k_{opt} = nI_m(b/P_{no\text{-}load})^{0.5}. \quad (10)$$

Using algorithm (10), the controller of welding unit is setting in each definite case the optimum number of operating modules for the selected condition, thus providing the minimum losses of electric power.

As an example, let us consider the case of organizing a modular structure of a resonant welding source (RWS) for 300 A maximum current. As shown in the Table, five variants of their modular organizing is possible: 2M, 3M, 4M, 5M and 6M. Technical characteristics are indicated for each of them. If to dwell on maximum «duty cycle» (i.e. reliability) as a criterion of selection of RWS structure, then the five-module variant is most preferable. The simplified diagram of power source, corresponding to structure 5M, is given in Figure 2. Separate module consists of *WT*, whose secondary current is not more than 60 A, capacitance reactor *Cp*, including 10 capacitors of K50-20 (2000 μF/50 V) and diode bridge *DB* which, as was mentioned, allows elimination of output power

No.	*Structure of RWS*	*Number of capacitors in module*	*Total number of capacitors*	$I_{m\,max}$, *A*	$I_{k\,max}$, *A*	*Duty cycle, %*
1	2M	20	40	150	15	20
2	3M	16	48	100	12.5	30
3	4M	12	60	75	12.5	30
4	5M	10	50	60	12	35
5	6M	8	48	50	12.5	30

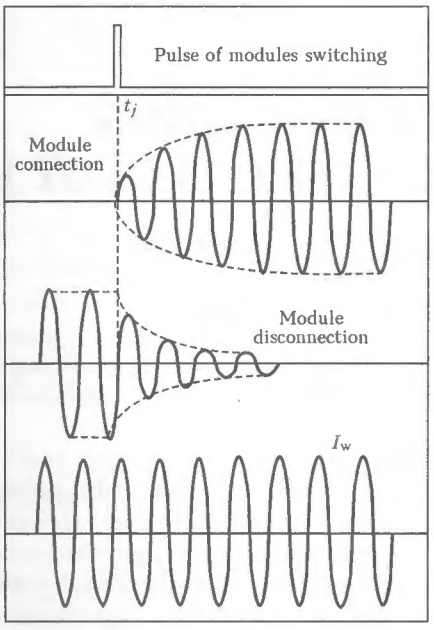

Figure 3. Time diagrams of modules switching

commutators from the diagram. Connection and disconnection of any module M_j, or a group of modules is realized by electronic switches *K1–K5* made on the base of triacs. Control signals for them are preset by a commutation unit *CU*, whose output voltages are defined by an algorithm of the controller operation. The latter is a program-controllable multifunctional generators [8], the frequency of pulses of which is associated functionally with the condition and defined by the controller by the *SC* signal level. As the transition process in connection-disconnection of the module occurs not spontaneously, but at some constant of time, defined by the properties of a series resonant circuit, then it is necessary to be careful using this procedure. It is known from the theory of oscillations [9] that the process of current setting in the series resonant circuit, whose time constant is equal to τ_c, is determined by expression

$$i_1(t) = \{I_m [1 - \exp(-t/\tau_c)]\} \sin \omega t, \qquad (11)$$

where I_m is the current amplitude; ω is the circular frequency of oscillations.

In disconnection of a supply circuit of voltage the process of current drop corresponds to

$$i_2(t) = [I_m \exp(-t/\tau_c)] \sin \omega t. \qquad (12)$$

If to synchronize in time the processes of connection of one module and disconnection of another module and then to sum their currents, then it will occur that total current at the stage of the transition process is not almost changed

$$i_{t.p}(t) = i_1(t) + i_2(t) = I_m \sin \omega t. \qquad (13)$$

To realize practically the relations (13) it is necessary to form only the pulse of modules switching simultaneously with transition of welding current curve through zero. Time diagrams, illustrating the processes of modules switching in accordance with expressions (11)–(13), are given in Figure 3.

Let us estimate quantitatively the dynamic characteristics of a resonant module by using the formula

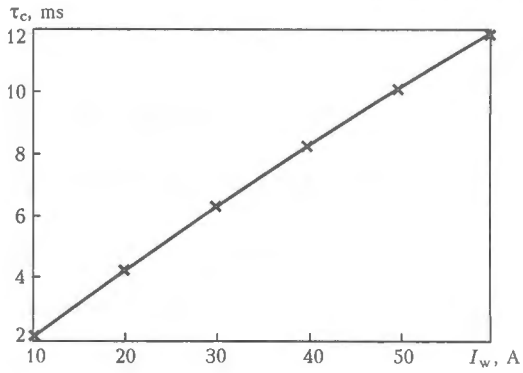

Figure 4. Dependence of time constant of module on welding current

for a constant time of the series circuit [9]: $\tau_c = 2L_c/r_c$. In this case L_c is the leakage inductance and determined by formula $L_c = L_s = 1/(4\pi^2 f^2 C_c)$. As follows from the Table, $C_c = 5 \cdot 10^{-3}$ F for five-module variant at inverse-series connection of capacitors. Consequently, *WT* should be designed so that to provide $L_s = 2.02$ mH. Resistance of circuit losses consists of three components: armature resistance of *WT* r_{wind}, resistance of welding cables r_{cable} and arc resistance r_a. Let us assume that the module is designed so that the components r_{wind} and r_{cable} can be neglected. Then $r_{cable} = r_a = U_a/I_w$. If to use the known expression $U_a = 18 + 0.04I_w$, then the calculation formula for a time constant of module can be presented in the form

$$\tau_c = 2L_s/r_a = 4.04 [I_w/(18 + 0.04I_w)]. \qquad (14)$$

The graphical illustration of expression (14) for 10–60 A range of currents is given in Figure 4. As the data obtained show, the duration of the transition process is increased with the current rise. However, it should be noted that these estimates of the time constant are somewhat overestimated, as the losses in windings and welding cables were not taken into account.

Thus, at a tandem connection-disconnection of modules a dynamic mutual compensation is occurred and resulting current remains almost constant at similar time constants of the circuit. If the time constants of circuits are differed by 10–15 %, then, as the experimental investigations showed, the occurred low disturbances do not almost influence the weld formation.

1. Mytsak, G.S. (1989) *Principles of theory of structural-algorithm synthesis of secondary electric supplies.* Moscow: MEI.
2. Mytsak, G.S., Mikheev, V.V., Fridman, P.M. (1992) Multichannel design of converters with intermediate high-frequency conversion. *Elektrichestvo*, **4**, 22–31.
3. Milyakh, A.N., Volkov, I.V. (1974) *Systems of invariable current on the base of inductance-capacitance converters.* Kiev: Naukova Dumka.
4. Paton, B.E., Korotinskij, A.E. (1999) Wielozadaniowe urzadzenie spawalnicze o przeksztalcalnej strukture. *Biuletyn Instytutu Spawalnictwa w Gliwicach*, **5**, 33–35.
5. Lebedev, W.K., Korotinskij, A.E., Zuk, G.W. (1997) O niektorych wlasnosciach procesu spawania lukowego z wykorzystaniem zrodel zasilania z obwodem resonansowych LC. *Ibid.*, **3**, 34–36.
6. Lebedev, V.K., Naruchkyavichyus, I.R. (1971) Stability of AC arc burning in circuit with capacitor. *Avtomatich. Svarka*, **4**, 3–5.
7. Svirchevsky, A.M., Antosyak, V.G. (1976) *Efficiency of resonance phenomena in arc welding of metals.* Kishinyov: Shtiintsa.
8. Korotynsky, A.E., Kornienko, A.N., Mukhlygin, N.S. (1981) Program-controllable device of time delay formation. *Pribory i Tekhnika Eksperimenta*, **6**, 119–121.
9. Gonorovsky, I.S. (1971) *Radio circuits and signals.* Moscow: Sov. Radio.

AIR-PLASMA CUTTING IN FABRICATION OF LOCOMOTIVE PARTS AT «LUGANSKTEPLOVOZ HC»

G.G. BASOV[1], A.N. TKACHENKO[1], S.A. TKACHENKO[1] and K.A. KORSUNOV[2]
[1]OJSC «Luganskteplovoz Holding Company», Lugansk, Ukraine
[2]V. Dal East-Ukrainian National University, Lugansk, Ukraine

The paper describes the experience of application of air-plasma cutting instead of gas-oxygen process in manufacture of thick parts at a blanking-welding shop of OJSC «Luganskteplovoz Holding Company».

Keywords: *air-plasma cutting, gas-oxygen cutting, part, quality, cost, cost-effectiveness, plasmatron, cathode assembly, nozzle*

Blanking-welding production of «Luganskteplovoz HC» of the area of about 60,000 m^3 has the capacity of fabrication of more than 70,000 t of metal structures annually. Dimensions of the shops, range of equipment and transportation means enable fabrication of assemblies of different steels and alloys of up to 30×5×5 m size and up to 70 t weight. In the plant plasma and gas-oxygen cutting, cold and hot stamping, brazing, assembly, welding and other technologies are used in fabrication of welded structures.

Thermal cutting section consists of integrated-mechanization lines using thermal cutting machines, devices of mechanized loading of rolled metal sheets and loading out of finished parts.

One line was constructed on the basis of four plasma cutting machines TPL-2.5K of OJSC «Zavod Kristal», Ukraine, the second includes three wide-gantry six-cutter machines KT-720 for gas-oxygen cutting of Tanaka Co., Japan. Development of control programs, cutting charts and technological processes for these machines is performed using computing means.

Plasma cutting is applied to make 4 to 30 mm thick parts of approximately one thousand part names, gas-oxygen cutting is used for cutting out parts 14 to 80 mm thick of about 400 part names. Gas-oxygen cutting line is supplied with oxygen from an oxygen unit, located at up to 3,000 m distance from gas-cutting machines. Oxygen under the pressure of 0.5 MPa comes to the cutting location either by the main pipeline or is delivered by a specialized AGU-2M unit with subsequent pumping into the manifold near the thermal cutting section and its feeding to gas-cutting machines.

The plant faced the problem of lowering the cost of gas-oxygen cutting operations, which was due to the following reasons. Oxygen unit K-0.4 of 736 kW power has the capacity of 400 m^3/h, and capacity lowering to just 30 % of the rated value is permitted. Optimum mode of the unit operation is continuous generation of oxygen, and additional starting and stopping significantly increases the energy consumption and lowers the efficiency. Previously (at output of 1200 heat locomotive sections per year) oxygen was generated around the clock and supplied to the cutting location through a pipeline. However, considering the reduced output oxygen requirement currently is much smaller. The above-said leads to the conclusion that making parts by gas-oxygen cutting method using the oxygen generated by K-0.4 unit is not rational.

Looking for ways to lower the product cost and increase the labour productivity with the method of thermal cutting, plant specialists came to the conclusion that gas-oxygen cutting can be replaced by plasma cutting in manufacturing thick parts. In this connection, comparative analysis was performed of the advantages and drawbacks of plasma and gas-oxygen cutting of thick metal for our plant conditions, taking into account the following aspects:

- cost of generation and supply of oxygen to the location of metal cutting;
- possibility of processing various metals by plasma cutting at a high speed (at metal thickness of 50 mm plasma cutting speed v_c = 600 mm/min; for gas-oxygen cutting it is 325 mm/min), this allowing improvement of labour productivity [1–3];
- lowering of thermal deformations and, therefore, improvement of the quality of parts and lowering of labour consumption for their straightening using a more concentrated heat of the plasma jet [1, 2];
- improvement of the quality of edges of the parts being cut, due to a higher accuracy of plasma cutting, compared to oxygen cutting, which permits reducing the allowance and subsequent machining, lowering the labour consumption and shortening the cycle of part manufacture;
- saving of power and cutting tools [1, 2];
- elimination of use of gaseous fuels, etc.

Cost effectiveness of introduction of plasma cutting to replace gas-oxygen cutting is determined by the following formula:

$$E_{GOC} = C_{GOC} - C_{APC}, \text{ UAH.} \quad (1)$$

Effectiveness components are cost of gas-oxygen cutting per 1 runing meter of 50 mm thick metal C_{GOC} (Table 1) and cost of air-plasma cutting of 1 runing meter of 50 mm thick metal C_{APC} (Table 2), respectively:

Table 1. Initial data for calculation of the cost at gas-oxygen cutting of 50 mm thick metal

Initial data	*Units of measurement*	*Values*
Oxygen flow rate	m^3/h	5.71
Cost of 1 m^3 of oxygen	UAH	7.73
Natural gas low rate	m^3	1.93
Cost of 1 m^3 of natural gas	UAH	0.4551
Consumed power	kW	16
Cost of 1 kW·h of power	UAH	0.1837
Cutting cost	m/h	15.9

Table 2. Initial data for calculation of the cost in air-plasma cutting of 50 mm thick metal

Initial data	*Units of measurement*	*Values*
Oxygen flow rate	m^3/h	7.2
Cost of 1 m^3 of oxygen	UAH	0.748
Natural gas low rate	m^3	0.252
Cost of 1 m^3 of natural gas	UAH	1.31
Consumed power	kW	116
Cost of 1 kW·h of power	UAH	0.1837
Cutting cost	m/h	25.2

$$C_{GOC} = \frac{Q_{ox}C_{ox} + Q_gC_g + N_{GOC}C_p}{v_{GOC}}, \text{ UAH}, \qquad (2)$$

$$C_{APC} = \frac{Q_aC_a + Q_lC_l + N_{APC}C_p}{v_{APC}}, \text{ UAH}, \qquad (3)$$

where Q_{ox}, Q_g, Q_a, Q_l are the flow rate of oxygen, natural gas, compressed air and cooling liquid, m^3/h, respectively; C_{ox}, C_g, C_a, C_l is the cost of the above components, UAH/m^3; C_p is the cost of power, UAH/(kW·h); v_{GOC}, v_{APC} is the rate of gas-oxygen and air-plasma cutting and compressed-air cutting, respectively; N_{GOC} and N_{APC} is the power of gas-oxygen cutting machine KT-720, air-plasma cutting machine and compressor, respectively.

Substituting the obtained data of Tables 1 and 2 into formulas (2) and (3), we have

$$C_{GOC} = 3.016 \text{ UAH/run. m};$$
$$C_{APC} = 1.072 \text{ UAH/run. m},$$

then

$$E = 3.016 - 1.072 = 1.944 \text{ UAH/run. m}.$$

This leads to the conclusion that use of air-plasma cutting instead of gas-oxygen cutting in manufacture of thick parts (up to 60 mm thickness) not only significantly reduces the cost of preparatory production, but also improves the quality of part manufacture, and, therefore, also the cost of the finished products.

Plasmatrons of PVR-1 type, used earlier at «Luganskteplovoz HC» did not allow cutting up metal thicker than 30 mm. Therefore, batch-produced VPR-15 plasmatrons were put into operation. These units allow cutting up to 80 mm thick sheets. Comparative characteristics of PVR-1 and VPR-15 plasmatrons are given in Table 3. However, in connection with widening of the product range it became necessary to manufacture parts thicker than 80 mm, for which purpose the engineering services of the Company, in co-operation with specialists of V. Dal East-Ukrainian National University, developed P-24 plasmatron with a hollow copper cathode (Figure) [4].

The plasmatron is an assembly, consisting of cathode and nozzle components, which are separated by a vortex chamber for plasma gas feeding. Cathode

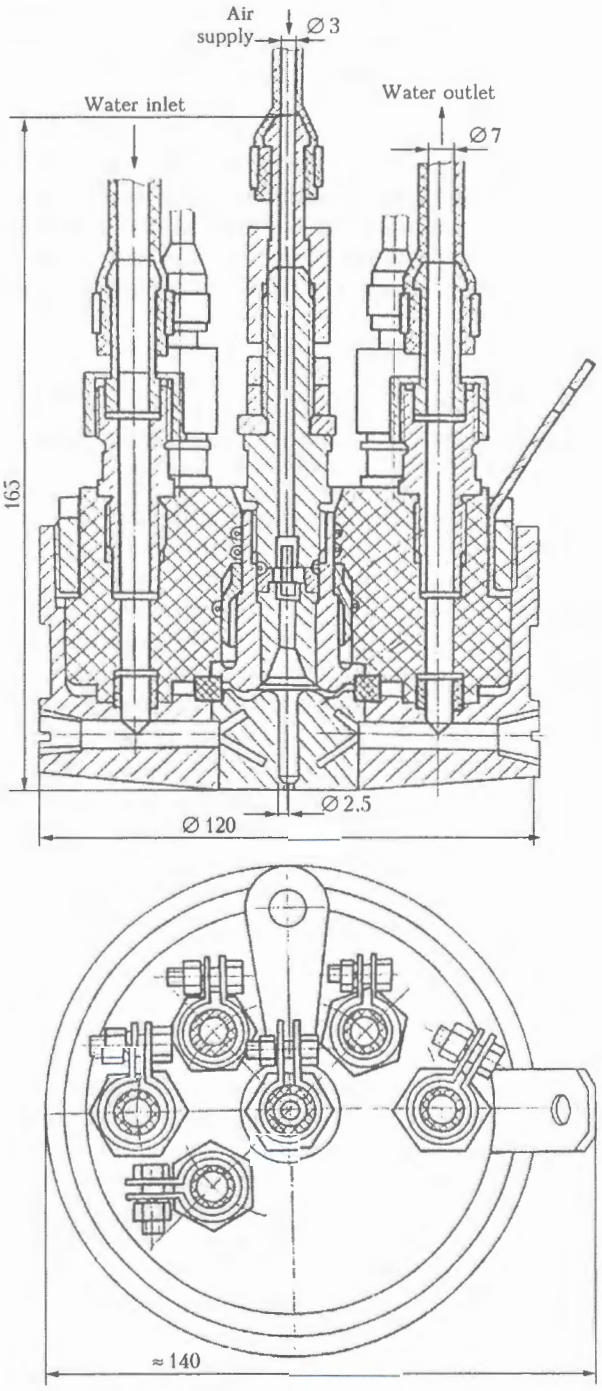

Schematic of P-24 plasmatron with a hollow copper cathode for air-plasma cutting of thick metal

Table 3. Comparative characteristic of the plasmatrons

Parameter	Plasmatron model	
	PVR-1	VPR-15
Plasmatron power, kW	60	80
Working current, A	310	315
Cutting velocity at 20 mm thickness, mm/min	1300	1980
Thickness of cut structural steels, mm	30	80
Operating life, h	3	4

component incorporates a hollow copper cathode, inserted into a water-cooled copper case. Flash chamber of the electrode, made to have a step-like shape with widening of the diameter from 4 to 8 mm in the direction of the arc coming out, has a thread and end face hole for feeding additional gas with 10 % flow rate of the main plasma gas, through a hole at the top of the electrode. Plasmatron nozzle component is a powerful water-cooled section, having a through channel of 5 mm diameter going over to 2.5 mm diameter. Specification of P-24 plasmatron is given below:

Working voltage, V 200–400
Working current, A 200–800
Plasma gas ..... air
Gas pressure, MPa 0.3–0.5
Maximum thickness of cut metal, mm 200

In the plasmatron gas-vortex stabilization of the arc is used, which promotes better thermal and erosion characteristics. When the plasmatron electrode was designed, a model was accepted of a continuously moving spot of tying the arc to the cold electrode surface. Each macrospot consists of microspots, which move in a jump-like fashion within the macrospot and heated electrode surface. Reduction of near-cathode drop of current density in the microspots provides a lowering of specific erosion. Applying a thread on the inner surface of a hollow cathode leads to the flow separation behind each protrusion of the tread, which promotes formation of «stagnant» zones. Any separation zone is a turbulence source, promoting increase of pulsation intensity, equalizing of the temperature field, velocity optimizing and other parameters. Favourable conditions are created for a predominant large-scale shunting. As a result, the base spot of the arc breaks up into several base spots, local heating is prevented, and electrode operating life is extended. Selection of the thread pitch ensures stability of the process of arc splitting.

Compared to other plasma sources, this plasmatron has several advantages:

- provides the required cooling of the parts, subjected to intensive heating;
- increases the plasmatron power and cutting process efficiency by 10–15 %, respectively, as a result of arc voltage rise;
- range of working currents can be increased up to 600 to 1000 A, with improvement of parallelism of the cut side edges;
- operates reliably both with the neutral and oxygen-containing gases, not having any limitation of the number of starting operations;
- has an extended operating life of the nozzle and inner electrode of up to 120–150 h, etc.

CONCLUSIONS

1. Replacement of gas-oxygen cutting by air-plasma cutting with application of new VPR-15 plasmatrons in manufacture of locomotive parts enables:
   - eliminating from the production cycle two wide-gantry six-cutter machines for gas-oxygen cutting;
   - saving fuel-energy resources;
   - lowering the labour consumption in part manufacture.
2. Developed P-24 plasmatron allows cutting out parts of low-carbon and low-alloyed steels up to 200 mm thickness.

1. Lashchenko, G.I. (2003) *Plasma cutting of metals and alloys*. Kiev: Ekotekhnologiya.
2. Shirshov, I.G., Kotikov, V.N. (1987) *Plasma cutting*. Leningrad: Mashinostroenie.
3. Nikiforov, N.I., Neshumova, S.P., Antonov, I.A. (1999) *Reference book of gas welder and gas cutting torch operator*. Moscow: Vysshaya Shkola.
4. Dzyuba, V.L., Tkachenko, A.N., Tkachenko, S.A. (2002) Cutting plasmatron with hollow copper electrode. In: *Vestnik VUNU im. V.I. Dalya*, 53(7), 280–282.

APPLICATION OF SIX-POLE ELECTROMAGNETIC SYSTEM FOR CONTROL OF WELD FORMATION PARAMETERS IN NON-CONSUMABLE ELECTRODE WELDING

R.N. RYZHOV, V.D. KUZNETSOV and A.V. MALYSHEV
NTUU «Kiev Polytechnic Institute», Kiev, Ukraine

Principle of operation and advantages of design of a specialized torch with a six-polar electromagnetic system are described. Using the property of superposition, both axial and transverse resultant magnetic fields were induced in the zone of welding. Results of experimental investigations of the effect of the parameters of welding with electromagnetic actions on the geometrical characteristics are given.

Keywords: *electromagnetic systems, axial and transverse magnetic field, weld depth and width*

Application of external electromagnetic actions (EMA) is one of the most effective methods for increasing and stabilizing the quality indices of the welds in arc welding processes. In implementation of these technologies the control action is applied by an external magnetic field (MF) in the welding zone, which induces body forces in the weld pool melt at interaction with the electric field of welding current. The nature and effectiveness of EMA on the weld pool metal depend on the direction, magnitude and time characteristics of MF induction. In downhand welding the axial MF relative to the pool surface are applied to control its hydrodynamics, which enables effectively acting on the processes of weld solidification [1]. Axial MF are further applied to improve formation of horizontal welds on the vertical plane [2]. Transverse MF, where the magnetic induction vector is parallel to the pool surface plane and normal to its longitudinal axis, are used with success in unsupported downhand welding to compensate for the gravity forces, acting on the weld pool melt, which enables controlling the geometrical features of the reverse side of the weld [3].

Direction of the induction vector of the controlling MF in the welding zone is determined by the design of specialized electromagnetic devices. Predominantly axial MF are induced, using cylindrical electromagnets, located on the case elements of the torches concentrically relative to the electrode [4]. Such designs allow minimizing the transverse component of the MF, which when controlling the pool hydrodynamics, promotes dispersion of the arc as a heat source, this leading to a certain reduction of penetration depth [1]. In its turn, when transverse components of MF are induced, two- and four-pole electromagnetic systems (EMS) are used [3, 5]. Designs of such devices are characterized by location of electromagnet windings on П-shaped cores, placed transversely to the weld, with their poles oriented in the direction of the weld pool. Different polarity of the poles of such cores eliminates the possibility of inducing in the welding zone an axial component of MF induction which allows controlling the pool hydrodynamics. In addition, at control of unsupported weld formation presence of MF axial component in the welding zone is undesirable, as metal flows from the pool head into its tail part induced by this component increase the probability of undercuts appearance from the weld face side [6]. Thus, the known designs of the devices for generation of a controlling MF in the welding zone are highly specialized and designed to solve various tasks.

A tendency has recently emerged of making the welding machines versatile, and widely applying robotic welding processes, allowing all-position welding of various weld types to be performed. Therefore, EMA hardware should have process flexibility, providing in the welding zone MF with the parameters, corresponding to the spatial position of the weld and thermophysical characteristics of the materials being welded.

Operating principle of versatile devices for applying a controlling MF to the welding zone can be based on superposition of MF induced by functionally independent electromagnets, which are EMS elements. Combining the polarities and amplitudes of electromagnet currents provides all the required characteristics of controlling MF in the welding zone. Errors made during manufacture of the elements of MF applying devices can cause distortions of MF parameters in the welding zone. This often leads to unsymmetric shape of the arc column, and, as a result, to deterioration of the processes of weld formation. When the majority of the known processes of MF generation are used, a forced measure to eliminate this negative effect is mechanical fitting of the magnetic core elements with concurrent control of MF parameters. This procedure is labour-consuming and difficult-to-perform. When using MF generation devices, consisting of several independent electromagnets, MF parame-

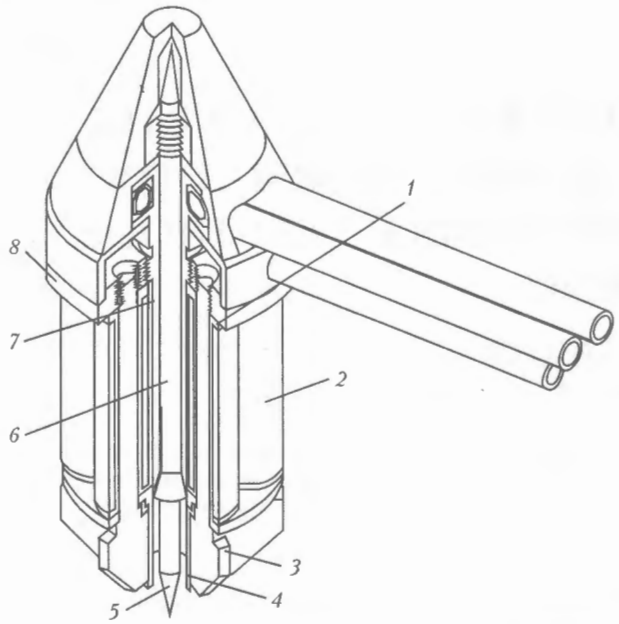

Figure 1. Schematic of a specialized torch with a six-pole electromagnetic system: *1* — frame; *2* — electromagnet winding; *3* — magnet core; *4* — nozzle; *5* — electrode; *6* — collet; *7* — collet-holder; *8* — case

ters can be varied by correction of currents in the respective windings. Thus, process flexibility of EMS completely compensates their somewhat more complicated design, compared to known devices.

When EMS were designed, it was taken into account that the number of electromagnets should be sufficient to ensure the width of the range of induction values of the resultant MF. Moreover, at even number of electromagnets and their identical design features, axial symmetry was used to achieve the distribution of MF induction in the welding zone. The developed EMS consisted of six electromagnets, placed at 60° intervals at the same distance from the longitudinal axis of the torch co-axially with the electrode (Figure 1) [7]. Now, the electromagnets consisted of cylindrical coils, wound on dielectric frames, which contained magnet cores, formed by abutted rod-shaped

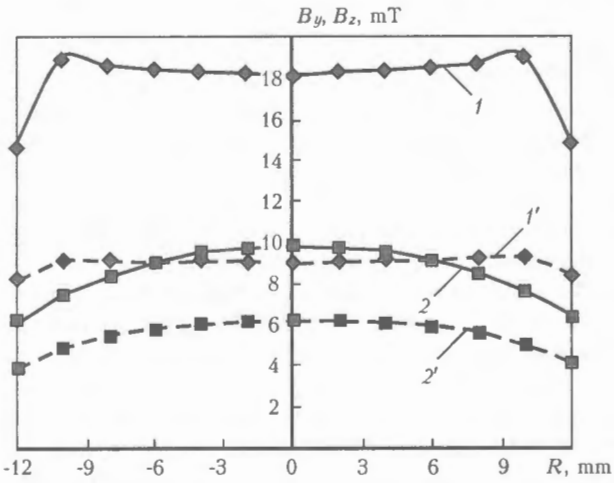

Figure 2. Distribution of induction of a controlling magnetic field along the pool longitudinal axis: *1*, *1′* — B_z; *2*, *2′* — B_y; solid curves — I_{EM} = 4 A; hatched lines — I_{EM} = 2 A; R — distance from EMS longitudinal axis

cores and end pieces. The long sides of the latter were aimed in the electrode direction.

When the developed EMS is used, combining the polarities of currents flowing through each electromagnet, allows creating in the welding zone a wide spectrum of characteristics of the controlling MF. Figure 2 shows experimental curves of distribution of axial B_z and transverse B_y components of MF on the pool longitudinal axis with three electromagnets located on each side of it. The distance from the pool surface plane to the end piece edges was 4.5 mm. It is established that at the same amplitude and polarity of currents in the coils of all the electromagnets (matched connection) B_z varies by a curve with a minimum in the centre and two maximums at 10 mm distance from electrode axis, the presence of which is accounted for by the position of magnet core end pieces. B_z increase from 9 up to 18 mT in the welding zone corresponds to increase of electromagnet coil currents from 2 up to 4 A. In this case B_y = 0 on the pool longitudinal axis, as a result of mutual compensation of MF transverse components in oppositely located electromagnets. It should be noted that in this case a much greater uniformity of MF axial component is achieved than with the use of specialized torches with cylindrical electromagnets. In the case, when current of one polarity was passed through coils, located on one side of the pool longitudinal axis, and current of opposite polarity was flowing through the coils on the other side of the axis (subtractive polarity) component $B_z \approx 0$. In this case, at currents of 2 and 4 A passing through electromagnets, component B_y was 6 and 10 mT on the electrode axis, respectively, and at 12 mm distance from the center it dropped by 34–40 %. Thus, use of the developed EMS allows generation in the welding zone of both the axial and transverse MF, where the induction level is sufficient for controlling the parameters of weld formation.

During experimental determination of the dependencies of the weld geometrical characteristics on controlling MF parameters, plates of stainless steel 12Kh18N10T 6 mm thick were penetrated in the following mode: I_w = 100 A, U_a = 10 V, v_w = 10 m/h. In order to induce a controlling MF in the welding zone, sinusoidal current pulses I_{EM} of 100 Hz frequency of constant value, coming from single-phase EMA control unit, were applied to EMS coils [8]. The induction magnitude was regulated by varying I_{EM} in the range of 1–5 A. Axial MF, required for achieving electromagnetic stirring, were induced at the same polarity of I_{EM} in all the EMS coils. Here, reversible motion of weld pool metal was provided by periodical variation of I_{EM} polarity after time intervals t_r = 0.01–0.06 s.

When transverse MF were induced in the welding zone, not only polarity of I_{EM} flowing through EMS coils, but also pole orientation relative to the weld pool was taken into account. Central angle of the sector of pool head part, α, located in the transverse MF, was changed by changing the electromagnet con-

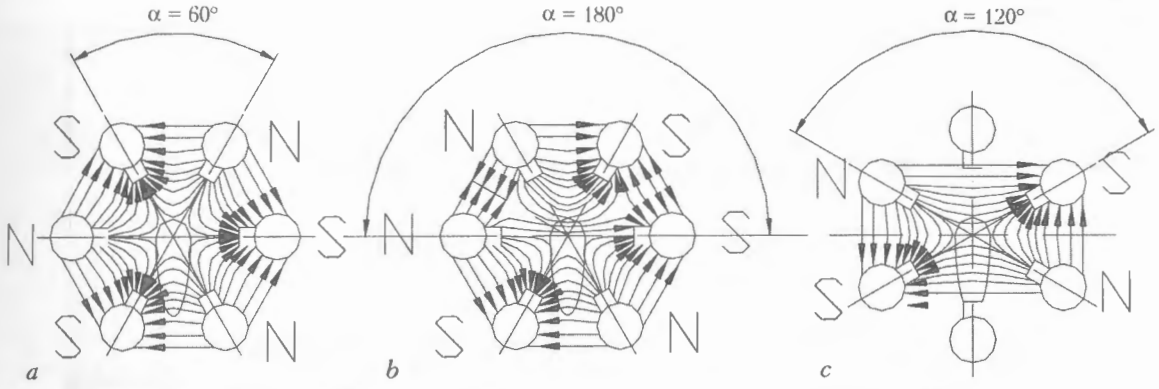

Figure 3. EMS orientation and polarities of currents in the electromagnets at generation of transverse MF

nection circuits. In this case, in all the realizable circuits, I_{EM} value was the same in each electromagnet, and in the poles, opposite relative to the pool longitudinal axis, I_{EM} had equal polarity (Figure 3). Connection circuit, in which three electromagnets are placed on each side of the pool at the same distance from its longitudinal axis, and in the central poles I_{EM} polarity is opposite to the currents of the front and rear poles, is characterized by $\alpha = 60°$ (Figure 3, *a*). At the same polarity of I_{EM} in the central and front pair of poles and opposite polarity of I_{EM} in the rear pair of poles $\alpha = 180°$ (Figure 3, *b*). Quadrupole EMS [6] with $\alpha = 120°$ was realized by orienting an unconnected pair of poles along the pool longitudinal axis (Figure 3, *c*). In this case, electromagnets located along the pool longitudinal axis had opposite I_{EM} polarities. It should be noted that at implementation of all of the above circuits, simultaneous change of I_{EM} polarity in all EMS poles leads to a reversal of the direction of the vector of MF transverse component. In this case the direction of force action on elementary volumes of pool melt is also changed accordingly. Thus, the weld pool was in a force field, directed either vertically upwards or vertically downwards.

In welding with EMA, controlling MF acts simultaneously both on the pool metal and on the arc. Under the conditions of the experiments, when using axial MF the arc shape changed into a conical one. Circuit of connection of EMS coils with $\alpha = 60°$ allowed compensating for the impact of a transverse MF on the arc, this leading to minor changes of its shape. At $\alpha = 120°$ in the case, when the force action on the pool metal is directed upwards, the arc is extended along the weld longitudinal axis towards the pool head and tail part and is compressed in the transverse direction. Change of polarities of I_{EM} in EMS coils, inducing a downwards force action on the metal, is accompanied by arc spreading towards the pool side edges and its constriction in the longitudinal direction. Circuit of EMS coils connection with $\alpha = 180°$ is characterized by an uncompensated action of transverse MF on the arc. Here, change of polarity of I_{EM} of the coils leads to welding being performed with an arc inclined either forward or backward.

It is established that under the conditions of the experiment, in welding with axial MF I_{EM} increase up to 7.3 A was accompanied by 6 to 10 % increase of weld width, which is attributable to «washing out» of the pool side edges by hot flows of the melt (Figure 4). In EMA modes with $t_r = 0.05$–0.06 s and $I_{EM} = 2$ A, characterized by a low intensity of electromagnetic stirring, stabilization of spatial position of the arc led to 10–25 % increase of the penetration depth. Further increase of I_{EM} was accompanied by a significant dispersal of the arc as a heat source, and, consequently, lowering of penetration depth by 25–30 %, compared to the initial conditions of penetration depth. It should be noted that in welding with axial MF used to control the formation parameters, the weld depth and width depend on the magnitude of MF induction to a greater degree. Accordingly, condition of the weld face surface and axial symmetry of the cast zone depend on t_r duration.

In welding in a transverse MF, irrespective of whether the force action on the melt is directed upwards or downwards, in the sector of the pool head part, limited by $\alpha = 60$ and 120°, increase of penetration depth by 50–65 % was recorded at increase of I_{EM} up to 2–3 A (Figure 5, *a*, *b*). Further increase of I_{EM} led to this parameter decreasing to the initial level. At $\alpha = 120°$ weld width did not change significantly. However, at downward-directed force action, beginning from $I_{EM} = 3$ A, a flat shape of the pool bottom was observed, which is characteristic for welding with transverse oscillations of the arc. At $\alpha = 60°$

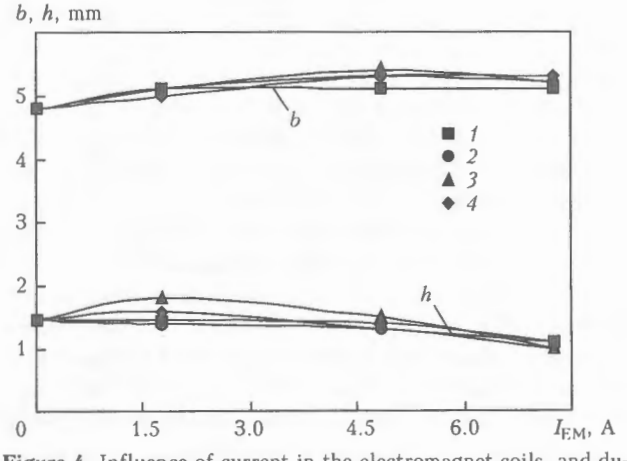

Figure 4. Influence of current in the electromagnet coils, and duration of intervals of reversal of axial MF on penetration depth and weld width: *1* — $t_r = 0.03$; 2 — 0.04; 3 — 0.05; 4 — 0.06 s

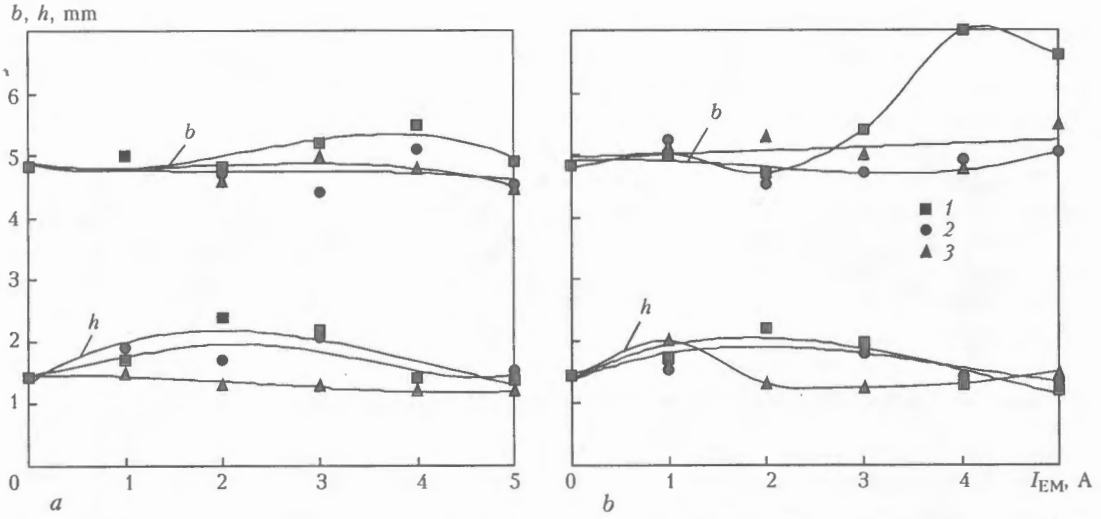

Figure 5. Influence of current in electromagnet coils on penetration depth and weld width at different schematics of generation of transverse MF: *a* — force action is directed upwards; *b* — force action is directed downwards; *1* — α = 60°; *2* — 120°; *3* — 180°

in the case, when the force action is directed downwards, I_{EM} rise above 3 A corresponds to weld width increasing by 35 %. Connection circuit with α = 180° at force action directed upwards, is characterized by a slight decrease of weld width and penetration depth. Change of the direction of force action led to penetration depth increasing by 38 % already at I_{EM} = = 1 A. However, at further increase of I_{EM} a gradual decrease of this parameter was observed.

Shape of the curves, shown in Figure 5, can be explained as follows. In welding at low speeds the penetration depth essentially depends on the thickness of liquid layer of the melt under the arc. As in the pool volume the welding current flows mainly in the direction of pool head part, EMA intensity in this region is much higher than in other regions.

Force action, directed vertically upwards or downwards promotes driving the melt from under the arc with concurrent increase of arc penetrability. However, at excess increase of I_{EM}, and, therefore, also of induction of transverse MF, eddy flows of the melt are formed with its reverse jet directed towards the pool center. In this case, the thickness of liquid layer under the arc is increased, and, as a result, its penetrability is decreased.

Increase of weld width up to 7 mm at α = 60° is due to the fact that with this circuit the pool side edges are «washed out» by the eddy flows of the melt. Transverse MF, induced by the circuit in Figure 5, *b* (α = 180°), are characterized by greater magnitude of induction in the pool head part, because of the same polarity of I_{EM} in the front pairs of poles than in circuits with α = 60 and 120°. This may account for greater penetration depth at lower I_{EM} values. However, in this circuit with I_{EM} increase arc deviation becomes greater, either towards the pool head part, or towards the solidification front, depending on the direction of the vector of induction of transverse MF. Here the effect of variation of penetration depth at eddy motion of the melt is enhanced in the first case, and weakened in the second case.

Thus, performance of non-consumable electrode welding, using a system of specialized equipment consisting of a torch with a multi-pole EMS and a device for EMA control, allows making joints with different requirements to weld formation parameters without replacing the tools. Development of this work may involve integrated use of axial and transverse MF during welding.

CONCLUSIONS

1. It is established that in welding with EMA use of specialized torches with EMS, formed of functionally independent electromagnets, allows inducing in the welding zone both the axial MF, effective for control of pool hydrodynamics, and transverse MF, effective for weld formation control.

2. It is shown that in welding with incomplete penetration use of a six-pole electromagnetic system to control such formation parameters, as weld depth and width, is the most effective with coil connection circuits, where a transverse MF with 6–10 mT induction is generated in the pool head part in a sector, limited by central angle α = 60–120°.

1. Chernysh, V.P., Kuznetsov, V.D., Briskman, A.N. et al. (1983) *Electromagnetic stir welding*. Kiev: Tekhnika.
2. Fujita, Yu., Manabe, Yu., Zenitani, S. et al. (2000) Development of two wires TIG welding with electromagnetically controlled molten pool process. *The Paton Welding J.*, **9/10**, 145–148.
3. Akulov, A.I., Rybachuk, A.M. (1972) Containment of weld pool molten metal by transverse magnetic field. *Svarochn. Proizvodstvo*, **2**, 3–4.
4. Chernysh, V.P., Kukhar, S.N. (1984) *Equipment for electromagnetic stir welding*. Kiev: Vyshcha Shkola.
5. Zvorono, Ya.P., Katler, S.M. (1970) Arc welding with containment of weld pool. *Svarochn. Proizvodstvo*, **5**, 3–4.
6. Akulov, A.I., Rybachuk, A.M., Chernyshev, G.G. (1979) Peculiarities of weld formation during welding in transverse magnetic field. *Ibid.*, **7**, 11–14.
7. Ryzhov, R.M., Malyshev, O.V. *Torch for welding with external electromagnetic actions*. Pat. 42252A Ukraine. Int. Cl. B 23 K 9/08. Publ. 15.10.01.
8. Titov, A.A., Malyshev, O.V., Ryzhov, R.M. *Non-consumable electrode welding method with use of the external control magnetic fields and device for its implementation*. Pat. 50430 Ukraine. Int. Cl. B 23 K 9/08. Publ. 15.10.02.

SURFACING OF DIPPING DRUMS OF GALVANISING UNITS

S.V. SHCHETININ, K.K. STEPANOV and N.G. ZAVARIKA
Priazovsky State Technical University, Mariupol, Ukraine

Technology for strengthening of dipping drums of a galvanising unit by deposition of a chrome-nickel layer ensuring high wear and corrosion resistance of deposited metal is described.

Keywords: *surfacing, dipping drums, galvanising units, corrosion resistance*

The process of continuous hot galvanising is used at cold rolling workshops to ensure consistent deposition of zinc coatings on a cold-rolled strip. Hot galvanising is performed by passing the preliminarily prepared strip through a bath with molten zinc at a temperature of 445–455 °C.

Dipping drums of the galvanising units, made from steel 08kp (rimming), perform the function of a pulling element and operate under conditions of abrasive wear caused by friction with a strip, corrosion effect of the zinc melt and high temperatures. In addition, a dipping drum is affected by convective flows in the molten pool resulting from movement of the strip. Experience of operation of the hot galvanising units shows that the prevailing type of wear of the dipping drums is corrosion. Relative wear in this case amounts to $(125–130)\cdot10^{-7}$ m/t.

State of the surface of a drum providing dipping of a cold-rolled strip into the zinc melt determines to a considerable degree the strength of adhesion of zinc to the strip, formation and regulation of thickness of a zinc coating and, therefore, quality of the Zn-plated metal, zinc consumption and material intensity of the process.

Profile of wear of the dipping drum body affects variations in thickness of the zinc coating, formation of corrugations and dents on it, as well as other defects. To provide strong adhesion of a coating to the strip, the forces of adhesion between zinc and strip should be higher than those with the zinc melt. While dipping the strip into the melt, the drum exerts an extra pressure on zinc, which sums up with the adhesion forces to provide its adhesion to the strip surface. Wear of the drum should be uniform to ensure satisfactory adhesion strength.

In addition to corrosion resistance, an important factor that affects wear of the drum is friction at a point of contact with the strip. This leads to the need to regularly recondition the dipping drums after their two-week operation in a line of the continuous hot galvanising unit at the cold-rolling workshops.

After dismantling and cleaning from zinc by etching in the sulphuric acid solution, the dipping drum is machined by a lathe to restore the required profile of its body and remove traces of corrosion fracture from its surface. This leads to decrease in the active layer on the drum body and, after three or four reconditioning operations, to its complete failure. Therefore, improvement of resistance of the dipping drums is a topical problem, and this study is dedicated to finding a solution to it.

One of the methods for improving resistance of metallurgical equipment is electric arc surfacing [1]. Earlier this method was used to increase wear resistance of dipping drums of the Al–Zn plating line at a cold rolling workshop of the Cherepovets Metallugical Works [2].

Investigations of the effect of chemical composition of welding wires on properties of deposited metal were conducted to determine the type of the deposited metal which would ensure high resistance of the dipping drum under conditions of operation of a galvanising unit. Surfacing was performed on plates of steel 08kp using wires of the type of 08Kh21N10G6, 10Kh9G2MFS, 08Kh19N9F2S2, 12Kh20N16G7T and 12Kh12G12SF, the choice of which was based on the necessity to ensure corrosion and abrasive wear resistance. The investigations were carried out under industrial conditions. Deposited samples were placed into a bath of the galvanising unit. Wear caused by friction of metal on metal was eliminated, as the samples were dipped into the galvanising unit bath with no contact with the strip. The samples were measured after the tests, and a wire for surfacing the dipping drums was selected on this basis.

As found from the investigations conducted, the highest resistance under the dipping drum operation conditions was exhibited by the deposited metal of the type of 08Kh21N10G6 (wt.%: 0.08C, 20.4Cr, 9.8Ni, 5.4Mn, 0.28Si, 0.22Mo, 0.03Ti).

Prior to surfacing, the dipping drums were subjected to machining using a lathe or grinding using a grinding machine to ensure removal of all the surface defects of the type of cracks, cavities, dents, spallings, corrosion crack networks and non-uniform wear. Thickness of the removed layer should be not less than 5 mm to prevent ingress of zinc from the surface of the drum body to the deposited metal and formation of defects of the type of pores, cavities and blowholes.

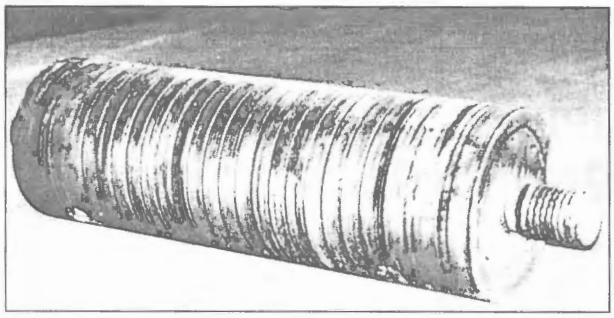

Figure 1. Deposited dipping drum after operation

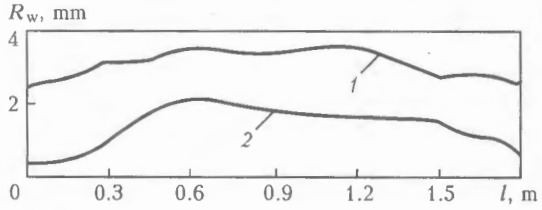

Figure 2. Profilogram of wear along the length of the dipping drum body: *1* — drum of steel 08kp after rolling of 3899.6 t of metal; *2* — deposited drum after rolling of 10621 t of metal; R_w — radial wear of the body

During optimisation of the technology for surfacing of the dipping drums, the investigations were conducted to study the effect of its parameters on formation of the molten pool deposited metal. Finding optimal parameters is especially important because of a relatively small diameter of a dipping drum (600 mm). Otherwise the melt may flow out from the molten pool, and formation of the deposited metal may be violated.

Surfacing of the dipping drums was performed at a direct current of reversed polarity. Rectifier VDU-1202 was used as a power supply. First a sub-layer was deposited using the 4 mm diameter wire Sv-08A or Sv-08GA and the pumice-like flux AN-60 under the following conditions: current 450–500 A, arc voltage 32–34 V and surfacing speed 40 m/h. Then the corrosion-resistant layer was deposited using wire Sv-08Kh21N10G6 and flux AN-26. This deposition was performed under the following conditions: current 400–450 A, arc voltage 30–32 V and surfacing speed 40 m/h.

Surfacing was performed at a pitch of 8–10 mm, which ensured a smooth deposited surface. The number of passes was determined depending upon the initial diameter of the drum body, which provided a corrosion-resistant layer not less than 8 mm thick. In this case the share of base metal in the deposited one was decreased to zero, thus allowing the desirable chemical composition and, therefore, high wear and corrosion resistance to be achieved.

Surfacing was followed by machining, and then the dipping drum was installed in the galvanising

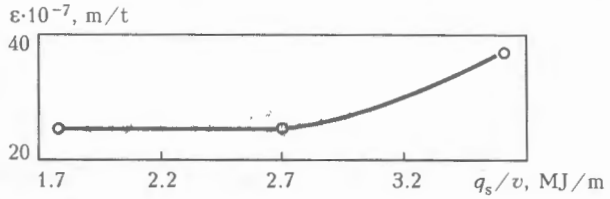

Figure 3. Dependence of relative wear resistance ε upon surfacing energy input q_s/v

unit. Upon completion of service of the deposited dipping drums (Figure 1) in the galvanising unit, diameter along the length of the drum body was measured and a profilogram of the drum surface was plotted (Figure 2).

It was proved that the electric arc deposition of a corrosion-resistant layer made it possible to substantially decrease wear and improve relative wear resistance of the dipping drums. Considering that the main type of wear is caused by corrosion, wear resistance of the dipping drums is determined by their corrosion resistance.

Wear resistance is affected by the energy input. The relative wear resistance increases with decrease in the energy input (Figure 3). This results from increase in the solidification rate and refining of the structure, thus leading to the rise in the level of corrosion and wear resistance of the deposited metal. At the same time, refining of the structure in surfacing performed at an increased speed and low energy input is accompanied by decrease in heat input, welding stresses and sensitivity to formation of solidification and sub-solidus cracks.

In addition, increase in the surfacing speed and decrease in the energy input is accompanied by decrease in the penetration depth and share of the base metal in the deposited one, which also leads to improvement of corrosion and wear resistance of the dipping drums.

Deposition of the corrosion-resistant layer using the developed technology allowed corrosion and wear resistance, as well as service life of the dipping drums used at the cold rolling workshops to be increased more than 4 times.

Increase in wear resistance of the dipping drums provided improvement of the quality and increase in output of the galvanised plates owing to reduction in reconditioning time and downtime of the rolling mill. Surfacing of the dipping drums is applied at the Open Joint Stock Company «Iljich Metallurgical Works in Mariupol».

1. Frumin, I.I. (1961) *Automatic electric arc surfacing*. Moscow: Metallurgiya.
2. Kalensky, V.K., Semenikhin, A.V., Novikova, D.P. (1998) Repair of parts of a unit for aluminium-zinc plating of coiled steel by surfacing. *Avtomatich. Svarka*, **2**, 38–44.

ABOUT CONTINUOUS MONITORING OF LIQUID AMMONIA STORAGES

A.Ya. NEDOSEKA[1], S.A. NEDOSEKA[1], M.A. YAREMENKO[1], A.A. ELKIN[2], Yu.F. KURBATOV[2] and A.S. VASILIEV[2]
[1]E.O. Paton Electric Welding Institute, NASU, Kiev, Ukraine
[2]Odessa In-port Plant, Odessa, Ukraine

Brief information on the development and successful application of diagnostic acoustic-emission system for continuous monitoring of welded structures is presented.

Keywords: *welded structures, safe service, monitoring, acoustic-emission systems*

Over the recent 35 years the works are carried out at the E.O. Paton Electric Welding Institute on the creation of methods and equipment for evaluation of condition and assurance of safety of welded structures. These are gas-, oil- and ammonia pipelines, high-pressure vessels, large storages for different products and others. 12 years ago these works were finalized in collaboration with Hungarian company «Videoton» by the development of a basic diagnostic equipment for evaluating the condition of structures and constructions, including powerful network systems of a continuous monitoring of structures, observing the current condition of structures. To solve this problem, an acoustic-emission (AE) technology was used, which is based on record of elastic waves, emitted by material being deformed. This technology together with other characteristics of fracture makes it possible to form a group of parameters defining the load-carrying capacity of material of structures in each moment of time. 10 years of successful industrial service of mobile diagnostic systems in a basic version (tested more than 800 objects in Ukraine, Russia and Poland) confirmed the right selection of the trend.

Equipment, used for control, was certified metrologically by Gosstandart of Ukraine, instructions on its application are coordinated with Gosnadzorokhrantrud of Ukraine. In collaboration with the latter, the systematic training and attestation of specialists as regards to application of the technology developed, are carried out. By the present moment, more than 1500 specialists, working successfully in industry for the inspection of condition of structures and constructions, have been trained.

A large attention at present is paid to a continuous monitoring of critical objects, whose failure may lead to the serious ecological losses. Thus, the continuous monitoring of oil tanks with a degree of safety by I class VBN V.2.2 -58.2–94 of Ukraine is recommended. It envisages the prediction of reliability of the tank with a determination of a residual life of its operation in the current period of service (short-term prediction) and the probability of failure-free operation during the preset period of its next service (long-term service).

The construction of these systems represents a complex scientific-technical and engineering problem, that requires the combination of the recent achievements in the field of technical diagnostics, monitoring engineering, computer technologies with requirements to the technology of evaluating the condition of structures and its prediction for the preset designed interval of time.

Teams of scientists and specialists of the E.O. Paton Electric Welding Institute, enterprises of Indprom and Hungarian company «Videoton» have developed the EMA-3M system of diagnostic monitoring. The first part of this system EMA-3S (stationary system of continuous monitoring) was manufactured by the order of Odessa In-Port plant and put into the scheduled service in March, 2003 for a continuous control of 34,000 m^3 storages of liquid ammonia.

The Figure shows the general view of the storage, the arrow indicates the place of mounting the monitoring part of the system. AE transducers are mounted on the storage casing before the deposition of a protective isothermal coating.

The diagnostic system makes it possible to produce the pattern of AE activity at different areas of the cylindrical surface of the storage tank. The concen-

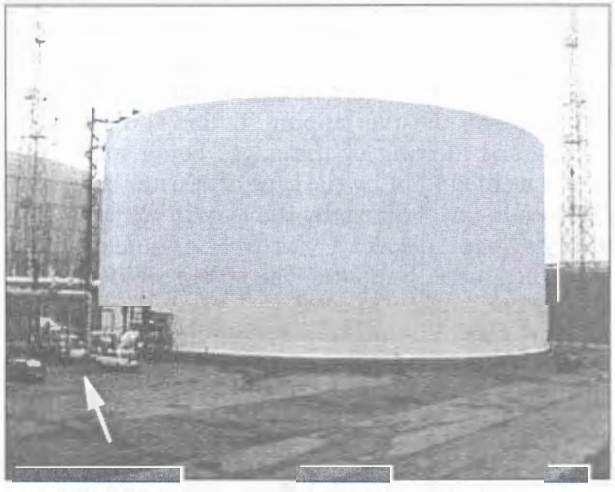

Isothermal storage of ammonia

tration of AE low-energy signals was observed in the area of fastening brackets supporting the technological pipelines. The high sensitivity of the equipment allowing recording of very low AE signals occurring in the tank wall material in the area of welding-on of brackets should be noted. It was also established that some concentration of AE signals is observed around defects, revealed earlier by the ultrasonic control, however, their effect on service characteristics of the tank shell is negligible.

It can be noted in conclusion that owing to the AE system, put into service, it is possible to detect the initiating defects over the entire surface of the structure. It is interesting to note the fact that the priority zones with propagating defects became not those defects which were earlier of attention of the inspectors, but quite new ones which did not cause earlier any hazard in selection of place of inspection from the point of view of their performance.

AUTOMATED UNIT FOR MAGNETIC-PULSE WELDING

E.L. STRIZHAKOV, N.A. KHAKHIN, M.Yu. BATSEMAKIN and **D.S. KHOKHLOV**
Donskoj State Technical University, Rostov-on-Don, Russia

The paper describes the block-diagram of a three-channel unit for magnetic-pulse welding of shell sheet structures. Advantages are demonstrated compared to a single-channel unit.

Keywords: *magnetic-pulse welding, shell structures, multi-channel units, operating cyclogram, advantages*

It is rational to make complex-shaped shell structures of sheet materials as stamp-welded structures. The authors of [1] studied the process of magnetic-pulse welding of overlap joints by induced currents, which allows applying a thermal and force impact to the mating surfaces at discharge of the capacitor storage to the working tool — the inductor.

The combined process essentially consists in the following. A flat sheet blank, first cut out to shape, is rolled up with an overlap and mounted into a matrix, having the shape of the future item. The operating tool, i.e. the inductor, is located in the processing zone. During discharge of the capacitor bank, current pulse I_d runs through the inductor turns, and its variable magnetic flux induces currents I_{in} in the blank. On the other hand, interaction of the inductor magnetic field with the eddy current in the blank creates magnetic pressure P_m over its entire surface. When induced current passes through the overlap joint, Joule heat evolves in the contact. Joint action of pressure on the overlapping section and of heating with partial melting of the edges being joined produces a welded joint by the type of resistance welding [2]. Forming of the item by the matrix configuration, proceeds simultaneously with welding under the impact of magnetic pressure. The stamp-welded part is made in one cycle.

The versatile magnetic-pulse welding unit used for welding and forming has a charging device, consisting of a high-voltage transformer and rectifier, high-voltage capacitor bank, connected to the discharge channel, which incorporates a switching device and inductor. The switching device has two main and one auxiliary (firing) electrodes. When a firing pulse is applied to the auxiliary electrode the capacitor bank is discharged to the operating tool — the inductor. A magnetic-pulse impact is applied [3].

This device performs the full cycle of magnetic-pulse processing of one part. In order to process the next part, it is necessary to switch off the high voltage, remove the component or part from the inductor working zone and install a new part. The cycle is repeated. At frequent discharges the inductor is overheated, which leads to its failing quickly. The need to cool the latter and time losses for idle running lower the equipment efficiency, and the charging unit and the capacitor storage are underloaded.

Initial introduction of the technology of producing stamp-welded cases of electric connectors into pilot production of space systems demonstrated that the versatile magnetic-pulse equipment cannot meet the requirements of batch-production of cables of onboard and ground instruments. Multi-channel equipment should be developed, which has several working positions, in order to achieve higher efficiency of the equipment and wear resistance of the inductor.

Higher efficiency is achieved by mounting in the equipment the discharge channels, operating in parallel with a phase shift, thus permitting a more uniform loading of the charging device and capacitor storage, and providing natural cooling of the inductors. This improves the resistance of the operating tool, allows combining the idle running at loading-unloading of the parts.

Figure 1 shows the block-diagram of a three-channel unit for magnetic-pulse processing of metals. The unit incorporates charging device *1*, including high-voltage transformer *3* and rectifier *4*, high-voltage capacitor bank *2*, to which first *5*, second *6* and third *7* discharge channels with three-electrode switching

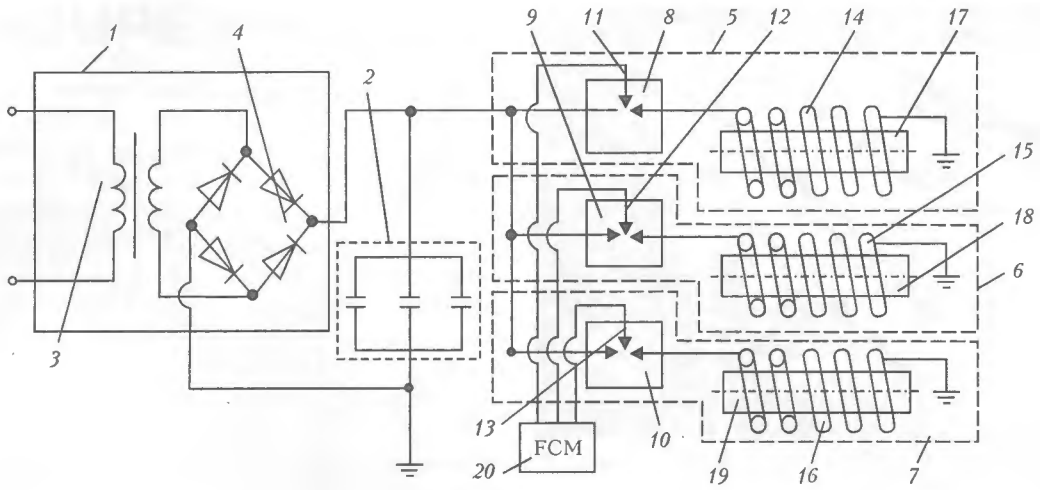

Figure 1. Block-diagram of a three-channel unit for magnetic-pulse processing of metals (for designations see the text)

devices *8, 9, 10* are connected, inductors *14, 15, 16*, processed parts *17, 18, 19*, three-channel firing control module *20*, where the taps are connected to auxiliary electrodes *11, 12, 13* of switching devices *8, 9, 10*.

The unit operates as follows. Three blanks are loaded into the inductor working zone. Charging device is switched on and energy is stored in the capacitor bank. After the required energy level has been achieved, charging is stopped. FCM applies a firing pulse to the auxiliary electrode of the switching device of the first discharge channel. Capacitor bank is discharged to the first inductor, which results in a magnetic-pulse impact on the item. Then a command is again issued for charging of the capacitor bank. Capacitor storage is charged up to the required energy (it may differ from the initial one). Charging is stopped. FCM applies a firing pulse to the auxiliary electrode of the switching device of the second discharge channel. Capacitor storage is discharged to the inductor, and magnetic-pulse impact is applied to the second item. Then magnetic-pulse processing of the third item by the required energy pulse proceeds. After that the high voltage is switched off, and finished parts are unloaded. New blanks are loaded into the inductor working zone, and the cycle of alternative magnetic-pulse processing is repeated. This equipment allows processing various items in one cycle. Operating cyclogram of the unit is given in the Table.

General view of a pilot sample of specialized automated magnetic-pulse process equipment is given in Figure 2.

Capacitor storage consists of two capacitors IK 25-12, total capacity of the banks is 24 μF. Ignitron discharge units IRT-6 are used as switching devices. Magnetic-pulse welding-forming of aluminium cases (0.2 mm thick) of electric connectors of different dimensions is performed.

Operating cyclogram of the three-channel unit

Step No.	Step description	Used device	Full cycle of processing three parts
1	Unloading of finished parts, blank loading in, fastening the tools and fixtures	Process module	t_l 15 30 45 s
2	Setting up the processing mode	Control panel	t_{set}
3	Charge of capacitor storage of energy	Capacitor storage of energy	t_c t_{ch}
4	Magnetic-pulse impact	Inductor	t_{MPI}

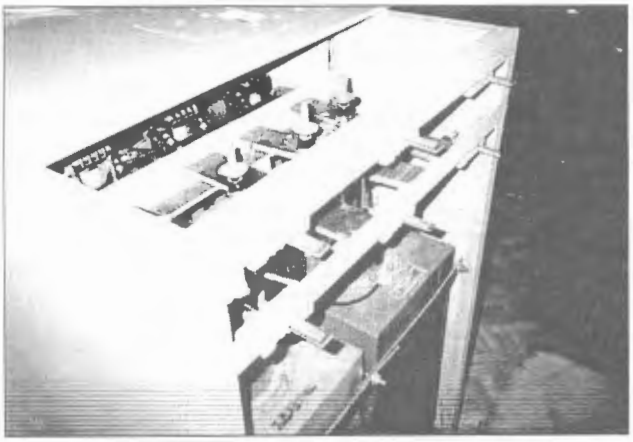

Figure 2. General view of a pilot sample of specialized magnetic-pulse process equipment

A case of 48 mm diameter and 30 mm length is loaded into the working zone of the first 16 turn inductor. A case of 32 mm diameter, 24 mm length is loaded into the working zone of the second 14 turn inductor. A case of 24 mm diameter and 20 mm length is loaded into the working zone of the third 12 turn inductor.

At discharge to the first inductor the storage was charged up to voltage $U_1 = 4.8$ kV (energy stored in the capacitor bank is $W = 276$ J), voltage $U_2 = 3.6$ kV ($W = 155$ J) is required for processing the second part, and $U_3 = 2.4$ kV ($W = 69$ J) for the third part. Maximum amplitude of the discharge current pulse varied in the range of 18–22 kA, pulse time was 40–60 μs. Resistance magnetic-pulse welding-forming was conducted without collision of the part edges [1, 2].

Three typical parts of different overall dimensions were made in a full cycle of the unit operation, which is very convenient in a multi-type versatile production.

Compared to commercially produced single-channel unit of «Impuls 2-1» type, described in [4], equipment efficiency rose from 120 up to 250 pcs/h. Wear resistance of the inductors rose from 20,000 to 40,000 discharges of the capacitor storage on average. This improvement, despite an increase of material content and cost of the unit, allowed covering the cost of development and introduction of automated equipment within six months.

Initial introduction of a three-channel unit for magnetic-pulse processing has been performed in cable production at aerospace plant of M.V. Khrunichev GKNPTs.

1. Strizhakov, E.L., Glinberg, A.D., Karandashev, A.N. (2000) Magnetic-pulse resistance welding-forming of shell structures. *Svarochn. Proizvodstvo*, **11**, 37–39.
2. Strizhakov, E.L., Karandashev, A.N., Plotnikov, V.V. et al. (2002) Magnetic-pulse stamping-welding of shell structures. *Kuzn.-Shtamp. Proizvodstvo*, **3**, 12–14.
3. Dudin, A.A. (1979) *Magnetic-pulse welding of metals*. Moscow: Energiya.
4. Krutin, A.F., Karandashev, N.A., Glinberg, A.D. *Method to produce welded joints of sheet metallic materials*. Pat. 2110381 Russia. Publ. 1998.